INFORMATION TO USERS

This manuscript has been reproduced from the microfilm master. UMI films the text directly from the original or copy submitted. Thus, some thesis and dissertation copies are in typewriter face, while others may be from any type of computer printer.

The quality of this reproduction is dependent upon the quality of the copy submitted. Broken or indistinct print, colored or poor quality illustrations and photographs, print bleedthrough, substandard margins, and improper alignment can adversely affect reproduction.

In the unlikely event that the author did not send UMI a complete manuscript and there are missing pages, these will be noted. Also, if unauthorized copyright material had to be removed, a note will indicate the deletion.

Oversize materials (e.g., maps, drawings, charts) are reproduced by sectioning the original, beginning at the upper left-hand corner and continuing from left to right in equal sections with small overlaps.

Photographs included in the original manuscript have been reproduced xerographically in this copy. Higher quality 6" x 9" black and white photographic prints are available for any photographs or illustrations appearing in this copy for an additional charge. Contact UMI directly to order.

ProQuest Information and Learning
300 North Zeeb Road, Ann Arbor, MI 48106-1346 USA
800-521-0600

RESONANT SPECTRUM METHOD

TO CHARACTERIZE PIEZOELECTRIC FILMS

IN COMPOSITE RESONATORS

Yuxing Zhang

A Thesis

in

The Department of Physics

Presented in Partial Fulfillment of the requirements

For the degree of Doctor of Philosophy at

Concordia University

Montreal, Quebec, Canada

February 2002

ABSTRACT

Resonant Spectrum Method to Characterize Piezoelectric Films in Composite Resonators

Yuxing Zhang, Ph. D.

Concordia University, 2002

Resonant Spectrum Method, a direct method to characterize a piezoelectric film which is deposited on a substrate to form a composite resonator (also known as over-moded resonator), has been developed. Based on the parallel and series resonant frequency spectra of a composite resonator, with the calculation of the spacing of the parallel resonant frequencies and the effective coupling coefficient, the electromechanical coupling factor, the density, and the elastic constant of the piezoelectric film can be evaluated directly. Experimental results on samples consisted of ZnO films on fused quartz substrates with different thicknesses are presented. They show good agreement with numerical simulations. The effects of the electrode thickness, the mechanical loss and the contact/electrode resistance on the accuracy of this method have also been investigated and it is found that the electrode thickness manifestly affects the accuracy of the method. The mechanical loss of the piezoelectric film has no significant impact. The contact/electrode resistance has some effect but this can be corrected. Applications of the method in piezoelectric film characterization and resonator filter design have been described.

ACKNOWLEDGEMENT

I would like to express my deep appreciation to Dr. J. D. N. Cheeke for his guidance, supervision and support throughout this study. His generosity for allowing me to finish the thesis part time is very important for my life and career. Special appreciation is extended to him for his time and invaluable comments in reviewing this thesis.

I would also express my deep appreciation to Prof. Z. Wang for his active help, guidance and encourage. His contribution to the development of the *Resonant Spectrum Method* and knowledge in acoustics are invaluable for this research.

I greatly appreciate Dr. F. S. Hickernell from Motorola for providing the ZnO/Fused quartz resonator samples and Dr. Xing Li from Nortel Networks for providing a high frequency network analyzer to measure the samples. Their assistance made the experiment possible.

I'm deeply grateful to my friends, Daniel Drolet and Kevin Shannon for reviewing the thesis.

My sincere thanks go to my colleagues at Concordia University, including Manas Dan, Kevin Shannon, Julien Banchet and Xing Li, and other faculty and non-faculty members of the Physics Department, Dr. Mariana Frank, Ms. Gloria Thompson and Ms. Lynn Chapmann for their help and cooperation during my study.

I wish to thank my wife for her encouragement, love, sacrifice and patience. I also wish to acknowledge the years of help and encouragement given by my parents, parents-in-law and the rest of my family.

This research is supported by NSERC (National Science and Engineering Research Council of Canada). The financial support provided by the Graduate School and Physics Department of Concordia University in the forms of *Graduate Fellowship*, *International Student Fee Remission Award* and teaching assistantship is gratefully acknowledged.

CONTENTS

Nomenclature

c^D Piezoelectrically stiffened elastic constant

F Mechanical force

f_p Parallel resonant frequency

f_s Series resonant frequency

I Electric current

k_{eff}^2 Effective coupling coefficient

k_t^2 Electromechanical coupling coefficient of a resonator

l Thickness of a piezoelectric film, or thickness of another media when combined with a subscript

m_N+1 The resonant mode order at the first normal region center

m_T+1 The resonant mode order at the first transition region center

Q Quality factor of a material or a resonator

R The ratio of the resonant frequency of the free film to that of the free substrate

R_c Contact resistance between a probe and a resonator

SPRF The spacing of parallel resonant frequencies

- Δf_p *SPRF* of a composite resonator
- Δf_0 *SPRF* of a bare substrate
- Δf_N *SPRF* at the center of the first normal region
- Δf_T *SPRF* at the center of the first transition region

U Mechanical displacement

V Electric voltage

v Acoustic wave velocity of a piezoelectric film, or velocity of another media when combined with a subscript

Y_{in} Electric input admittance of a resonator

Z Acoustic impedance of a piezoelectric film, or such an impedance of a media when combined with a subscript

z Normalized acoustic impedance of a piezoelectric film, or such a impedance of a media when combined with a subscript

Z_{in} Electric input impedance of a resonator

γ Acoustic wave phase delay of a piezoelectric film, or phase delay of another media when combined with a subscript

ρ Density of a piezoelectric film, or density of another media when combined with a subscript

LIST OF FIGURES

LIST OF TABLES

CHAPTER 1. INTRODUCTION

Piezoelectricity is a linear property of certain materials that manifest itself by an onset of electrical polarization when the material is subjected to mechanical stress, and by the onset of deformation in the material subjected to an electric field [1].

Piezoelectric films are an important class of piezoelectric materials which are deposited in thin films on various substrates using different technologies. They have been widely used in high frequency bulk acoustic wave (BAW) and surface acoustic wave (SAW) devices, such as filters, resonators, transducers, actuators and sensors [2]~[10]. Although single crystal materials are dominant in most of these applications, piezoelectric films attract many interests for their particular acoustic properties, such as high acoustic velocity (ZnO/diamond on silicon [6], AlN on SiO_2/silicon [11], $LiNbO_3$ on diamond/silicon [12]), smaller temperature coefficient (ZnO on Quartz [13], SiO_2 on $LiNbO_3$ or $LiTaO_3$ [14][15]) and large electromechanical coupling coefficient ($LiNbO_3$ [12] and $KnbO_3$ [16]). They also have the potential to be integrated in microelectronics integrated circuits [17].

The characterization methods of piezoelectric films have been studied for decades. Among the parameters of the piezoelectric film, the electromechanical coupling coefficient k_t^2, which is a measure of the strength of the piezoelectricity of the material, is one of the most important parameters, but also most difficult to measure. In this chapter, we will review some characterization techniques on k_t^2 of piezoelectric films.

1.1 Single piezoelectric film

For self-supported single piezoelectric films, such as the piezoelectric film in FBAR (Film Bulk Acoustic wave Resonator)[18][19], some measurement techniques developed to characterize piezoelectric thin plates can be applied directly [20] [21]. Basically, a self-supported piezoelectric film and a piezoelectric thin plate have the same physical configuration.

In the case that the piezoelectric film forms a thickness extension mode resonator, which means only a longitudinal wave along the direction normal to the resonator surface exists in the resonator (the z direction in Fig.1.1) and there is no motion in the directions transverse to the z direction, there are three relevant material constants involved to represent the intensity of piezoelectricity. They are an elastic constant in c^E, a piezoelectric constant e, and a dielectric constant ε^S. IEEE Standard on Piezoelectricity [21] defined the electromechanical coupling coefficient k_t^2 in term of these constants as

$$\frac{k_t^2}{1-k_t^2} = \frac{e^2}{\varepsilon^S c^E} = \frac{\text{Stored electric energy}}{\text{Stored elastic energy}} \tag{1.1}$$

Thus, the electromechanical coupling coefficient k_t^2 gives a measure of the efficiency of conversion of stored electric energy to the total stored energy and vice versa.

By introducing the piezoelectrically stiffened elastic constant [1]

$$c^D = c^E/(1-k_t^2) \tag{1.2}$$

which is the elastic constant when the electric displacement in the z direction is zero, Eq. (1.1) can be re-written as

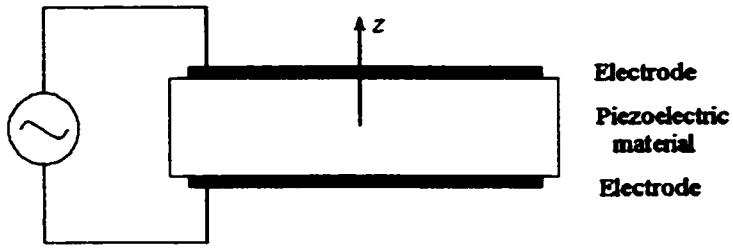

Fig.1.1 *A single-plate piezoelectric resonator*

$$k_t^2 = \frac{e^2}{\varepsilon^S c^D} \tag{1.3}$$

The electrical impedance of such a resonator is given by

$$Z_{in}(\omega) = \frac{l}{j\omega\varepsilon^S S}\left[1 - k_t^2 \frac{\tan(\omega/4f_p)}{(\omega/4f_p)}\right] \tag{1.4}$$

where l is the thickness of the piezoelectric film, S is the area of the electrodes of the resonator and ω is the angular frequency. The parallel resonant frequency f_p is related to the elastic constant of the film by

$$c^D = 4\rho f_p^2 l^2 \tag{1.5}$$

where ρ is the density of the piezoelectric film. Notice that in the z direction, the velocity of the longitudinal acoustic wave in the piezoelectric film is

$$v = \sqrt{c^D/\rho} \tag{1.6}$$

The parallel resonant frequency f_p is simply determined by the longitudinal wave velocity and half thickness of the piezoelectric film

$$f_p = \frac{v}{2l} \tag{1.7}$$

From Eq. (1.4) one finds that the electromechanical coupling coefficient can be determined from two resonant frequencies f_s and f_p.

$$k_t^2 = \frac{\pi}{2}\frac{f_s}{f_p}\tan\left(\frac{\pi}{2}\frac{f_p - f_s}{f_p}\right) \tag{1.8}$$

where f_s is the series resonant frequency at which $Z(\omega) = 0$. In a lossless resonator, which means the mechanical and the electrical dissipations of the resonator material have been ignored, the series resonant frequency corresponds to the maximum (infinite) admittance and the parallel frequency corresponds to the maximum (infinite) impedance. When k_t^2 is small, Eq. (1.8) approximates to

$$k_t^2 = \frac{\pi^2}{4}\frac{f_s}{f_p}\cdot\frac{f_p - f_s}{f_p} \tag{1.9}$$

In a real material, however, dissipation is present and it obscures the definition of the resonant frequencies. When there is dissipation in a piezoelectric material, IEEE Standard on Piezoelectricity [21] defined the series resonant frequency f_s as the frequency at the maximum conductance and the parallel resonant frequency f_p as the frequency at the maximum resistance. The standard also states that the critical frequencies of a lossy resonator must correspond to the critical frequencies of an ideal resonator made from a lossless material having the same electroelastic constants. Thus, k_t^2, which is only determined by the resonant frequencies, should not be affected by the loss of the material. In practice, the resonant frequencies in lossy material differ from those defined in lossless material by a small amount. Consequently, k_t^2 of lossy material calculated from Eq. (1.8) also differs from that defined in lossless material. For the evaluation of material constants, it is always sufficient to use an experimental value of f_s in Eq. (1.8). But f_p can be used

within the experimental error only for low loss material, or high Q material, where Q is the quality factor of the piezoelectric film. The difference of f_p between lossless and lossy materials is about $1/Q^2$.

1.2 Piezoelectric film on a thick substrate

Most piezoelectric films used as high frequency acoustic wave devices are not self-supported. These include piezoelectric ceramic films created by sol-gel techniques such as PZT films on metal substrates [9], and crystal films created by evaporating or sputtering techniques such as zinc oxide films on fused quartz [8] [22] and AlN films on silicon [23]. Usually these techniques produce a collection of crystallites more or less randomly oriented around a preferential direction rather than a true single crystal layer. The final properties of the piezoelectric films are no longer the same as those determined from measurement of bulk samples at low frequency and depend on the properties of the substrate. Therefore, the characterization methods recommended by the IEEE Standard [21] are not available and new techniques have been developed.

In the case of thin films deposited on very thick substrates, which are used as high frequency transducers, some characterization techniques have been developed [24][25]. For example, such a structure can be viewed as a one-port delay line with the piezoelectric film acting as a transducer. By putting an identical transducer at the other side of the delay line as a receiver and measuring the insertion loss of the delay line, the electromechanical coupling coefficient k_t^2 can be extracted by fitting the frequency response. The

determination of k_t^2 from the loss measurement is critically dependent on knowing the amount of energy lost from the acoustic wave when it travels through the substrate. The exact value of this transmission loss is often difficult to ascertain because of diffraction effects, misalignment of crystalline axes, etc. Bahr and Court [24] developed a method to determine the coupling coefficient from measuring the transducer input admittance. From the equivalent circuit of a thin-film thickness-mode transducer, the authors derived the input admittance of such a device, Y_{IN}, as a function of angular frequency ω, clamped capacity of the piezoelectric film C_0, electromechanical coupling coefficient k_t^2 and series resistance associated with the electrodes r_s,

$$Y_{IN} = Y_{IN}(\omega, C_0, k_t^2, r_s) \tag{1.10}$$

At the frequency far away from resonance, the admittance is basically a capacitor

$$Y_{IN} = j\omega C_0 \tag{1.11}$$

Thus, C_0 can be obtained with fairly good accuracy from the gradient of a straight line drawn through the measured input susceptance. k_t^2 and r_s can be determined by choosing their values to make the theoretical conductance *vs.* frequency curve to best fit the measured data. By using pulse measurement instead of conventional continuous wave measurement, an infinitely long delay line is simulated, and thus the propagation characteristics of an acoustic wave in the substrate will not affect the measured values of the input admittance. Since the variation in the conductance *vs.* frequency curve produced by a change in the value of k_t^2 is quite different from that produced by the change of r_s, this method leads to a very good accuracy. Taking into account all the possible sources of

experimental error, a ±6.5% accuracy was achieved for the electromechanical coupling coefficient.

Meitzler and Sittig [25] improved the method by taking the effects of electrode and interconnection layers into account to characterize high frequency piezoelectric transducer which is either a piezoelectric film deposited on a substrate or a thin piezoelectric plate bonded on a substrate. The conductance of the transducer or the insertion loss of an acoustic delay line composed of two identical transducers were measured carefully and then compared with families of calculated curves for conductance *vs.* frequency or insertion loss *vs.* frequency where k_t^2 is one of the dominant variables. Curve fitting the measurement data with the conductance or the insertion loss formulae can achieve more accurate results.

Admittance measurements have the advantage that only one transducer is needed. When k_t^2 is large, this method yields good accuracy. When k_t^2 is small, however, the admittance measurement is inaccurate because a small conductance has to be measured in the presence of a large suspectance, and the effects of spurious circuit elements in the interconnection is substantial. In this situation, insertion loss is sufficiently high that additional losses caused by absorption and diffraction are a small part of the total loss. In this case, the insertion loss measurement method is preferable to the admittance measurement.

No matter which measurement is used, since the value of k_t^2 is determined by the magnitude of the frequency response of the device, a complicated measurement system and very accurate calibration of the system is necessary.

1.3 Piezoelectric film on a thin substrate

In the case of a piezoelectric film being deposited on a thin substrate to form a thickness extension mode composite resonator (over-moded resonator) [3][22][23], the behavior of the resonator is quite different from that of a self-supported single piezoelectric film or a piezoelectric film on a thick substrate. In a composite resonator, the acoustic wave generated by the piezoelectric film will resonate in the substrate and cause multi-mode resonances. The resonances are dominated by the substrate, but modulated by the piezoelectric film. Therefore, the properties of the substrate have primary importance on the resonance and the properties of the piezoelectric film have only a secondary importance. This brings to the characterization of piezoelectric films more difficulties and more uncertainties.

Hickernell [22] and Naik, *et al* [23] developed methods to determine k_t^2 by fitting the electrical impedance and admittance data with the equivalent circuit analysis results on multi-mode resonances of a composite resonator.

A typical four-layer composite resonator is shown in Fig. 1.2, where l_{e1}, l, l_{e2} and l_{sb} are the thickness of the top electrode, piezoelectric film, middle electrode and isotropic substrate, respectively; ρ_{e1}, ρ, ρ_{e2} and ρ_{sb} are the density of the top electrode, piezoelectric film, middle electrode and isotropic substrate, respectively; v_{e1}, v, v_{e2} and v_{sb} are the longitudinal velocity of the top electrode, piezoelectric film, middle electrode and isotropic substrate, respectively, and k^2 is the electromechanical coupling coefficient of the piezoelectric film.

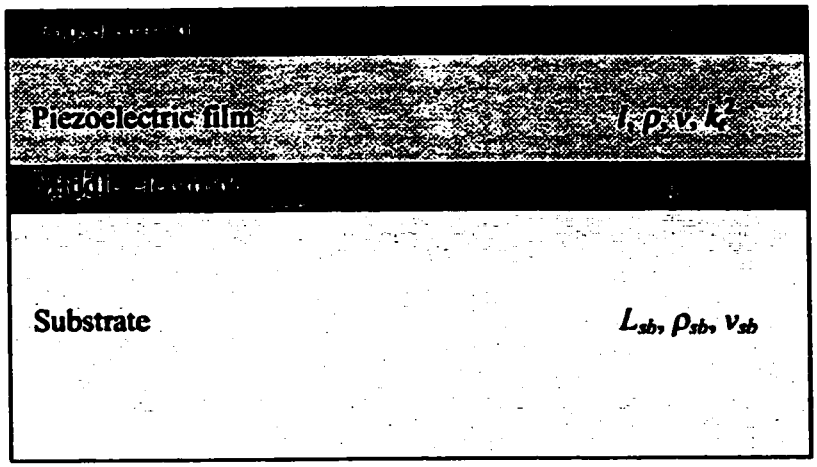

Fig.1.2 *A four layer composite resonator*

By solving the linear equation of piezoelectric elasticity for the one-dimensional case with suitable boundary conditions, Lakin derived the electric impedance of such a composite resonator measured from two electrodes [3] as,

$$Z_{in} = \frac{1}{j\omega C}\left[1 - k_t^2 \frac{\tan\phi}{\phi} \cdot \frac{(z_1 + z_2)\cos^2\phi + j\sin 2\phi}{(z_1 + z_2)\cos 2\phi + j(1 + z_1 z_2)\sin 2\phi}\right] \qquad (1.12)$$

where z_1 and z_2 denote mechanical load impedances on the top and bottom of the piezoelectric film normalized by the acoustic impedance of the piezoelectric film, and $2\phi = \frac{\omega}{v} l$ is the phase delay in the piezoelectric film.

Hickernell [22] explored several measurement techniques for evaluating piezoelectric thin films. One powerful method to characterize a piezoelectric film on a thin substrate is to measure the impedance or return loss of the composite resonator. Fig.1.3 shows an example of the impedance measurement on a composite resonator

composed of a zinc oxide film on fused quartz substrate. The finite thickness of the fused quartz substrate causes resonances to occur which register as circular areas on a Smith chart. Over a broad frequency range, there are multiple circles such as those shown in Fig.1.3a, corresponding to multiple resonance modes. The predicted response by using the acoustic and geometrical properties of the resonator and electrode gives a similar response (Fig. 1.3b) with an optimized value of k_t. Thus, the electromechanical coupling coefficient of the piezoelectric film on a composite resonator is evaluated by a single electrical impedance measurement. But from Fig. 1.3, we can see that the theoretical prediction doesn't fit the experimental response perfectly. The accuracy of this method is not reported.

Naik, *etc.* developed a curve fitting method based on the Butterworth Van-Dyke (BVD) model of a simple piezoelectric resonator and the theoretical electric impedance of a composite resonator [23]. The BVD model describes a simple piezoelectric resonator with an equivalent electric circuit shown in Fig.1.4. The electric impedance of such a resonator is expressed as

$$Z = \frac{1}{j\omega(C1+C2)} \frac{1-\left(\frac{f}{f_s}\right)^2 + \frac{j}{Q}\left(\frac{f}{f_s}\right)^2}{1-\left(\frac{f}{f_p}\right)^2 + \frac{j}{Q}\left(\frac{f}{f_p}\right)^2} \tag{1.13}$$

where

$$f_s = \frac{1}{2\pi}\sqrt{\frac{1}{LC_1}} \tag{1.14}$$

$$f_p = \frac{1}{2\pi}\sqrt{\frac{C_1+C_2}{LC_1C_2}} \tag{1.15}$$

$$Q|_{f,BVD} = \frac{2\pi fL}{R} \tag{1.16}$$

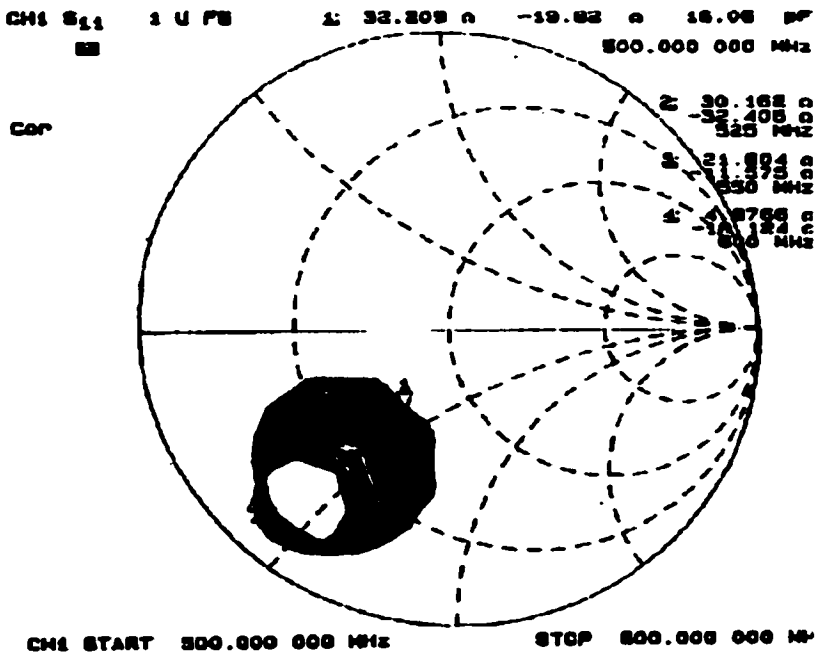

a. Measured

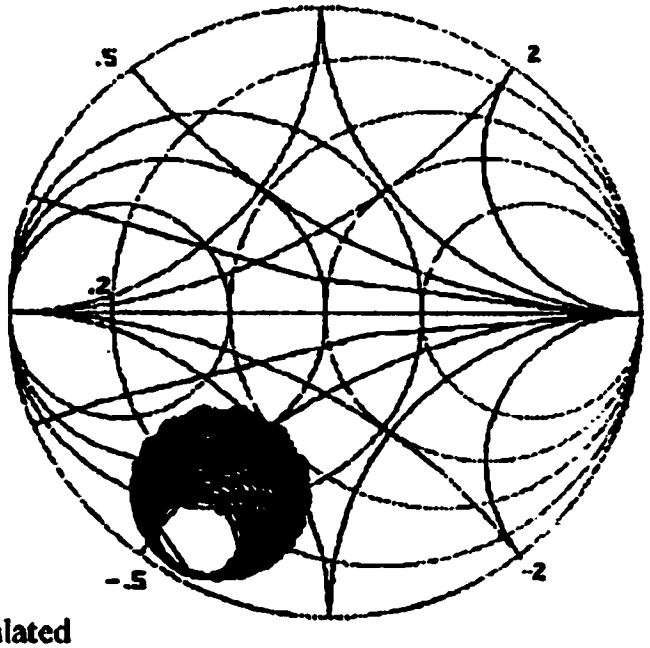

b. Calculated

Fig.1.3 *Impedance of a ZnO/quartz composite resonator on a Smith Chart*

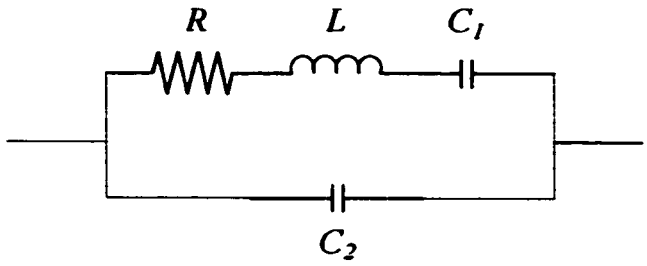

Fig.1.4 *BVD model of a simple piezoelectric resonator*

It has to be noted that in this method, f_s and f_p do not correspond to the minimum and maximum of the impedance because of the finite Q of the resonator, which are the common definitions for f_s and f_p.

For a composite resonator, each resonance can be quantified by two figures of merit k_{eff}^2 and Q, where k_{eff}^2 is the effective coupling coefficient and Q the quality factor. The quantity k_{eff}^2 is defined as

$$k_{eff}^2 = \frac{\varphi}{\tan\varphi}, \qquad \varphi = \frac{\pi}{2}\frac{f_s}{f_p} \tag{1.17}$$

and Q is defined from the slope of the phase response

$$Q|_{\text{slope}} = \frac{f_s}{2}\frac{\partial \angle Z}{\partial f}\Big|_{f_s} \tag{1.18}$$

where $\angle Z$ is the impedance phase response.

To extract f_s and f_p, a narrow window is defined around the phase or amplitude response of each resonance of a composite resonator, and the BVD model is fitted to the response using Levenberg-Marquardt nonlinear regression algorithm. The effective coupling factor k_{eff}^2 and quality factor Q are calculated using (1.17) and (1.18) with the

optimized values for f_s and f_p, respectively. By repeating this procedure for each resonance, curves of k^2_{eff} and Q *vs.* f_s can be obtained. In practice, the measured k^2_{eff} and Q curves and the simulated k^2_{eff} and Q curves using Eqs. (1.17) and (1.18) are compared to extract the best electromechanical coupling coefficient k^2 of the piezoelectric film and acoustic viscosity η of the substrate. The extraction procedure is shown in Fig. 1.5.

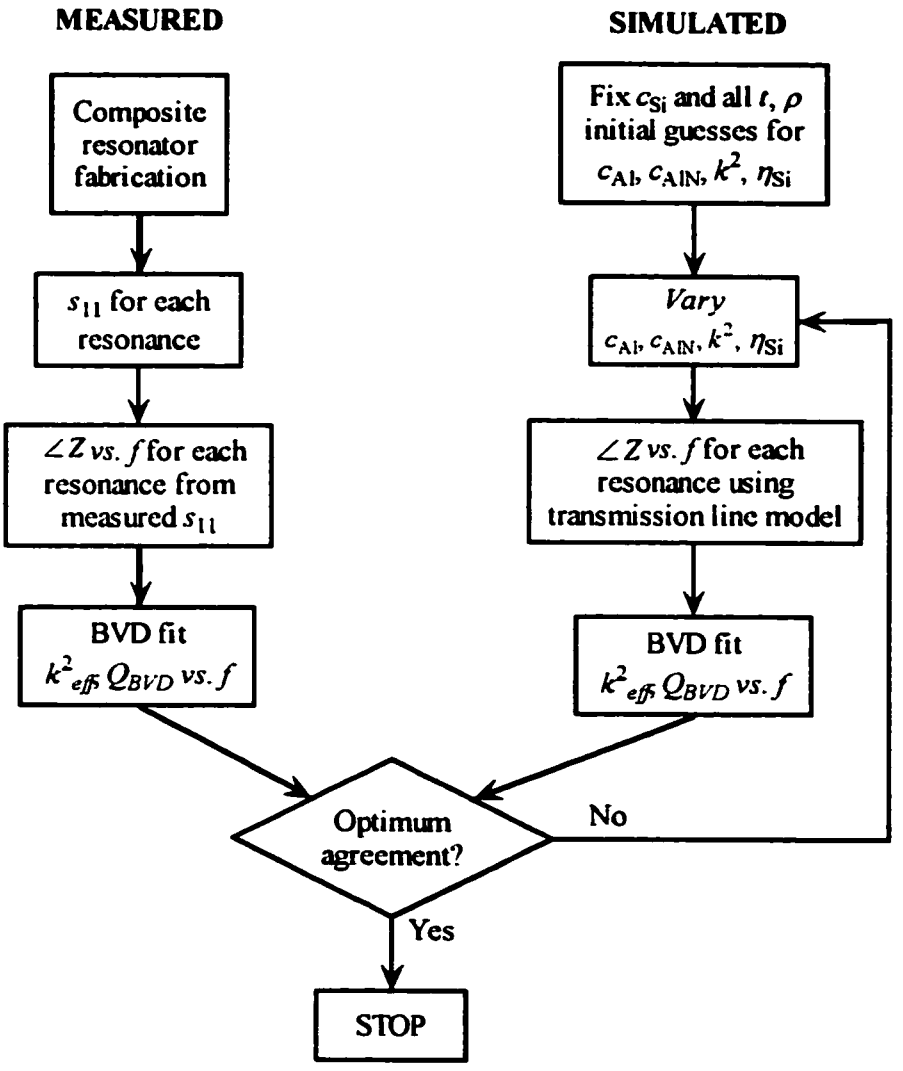

Fig. 1.5 *Flow chart showing the extraction procedure for* k^2 *and* η_{Si}*[23]*

1.4 The *Resonant Spectrum Method*

All the characterization methods introduced above are based on curve-fitting techniques, either to fit the impedance/admittance response of a composite resonator, or to fit the frequency response of an acoustic delay line with two identical piezoelectric transducers. These techniques are also referred to as "inverse problem" techniques. The approach needs an accurate knowledge on all the material parameters other than the variables to be extracted. The variables to be extracted must have independent contributions to the response. Besides, sometimes the initial values of the variables are so critical that different initial values will cause the problem of convergence to different

critical that different initial values will cause the problem of convergence to different results. Since in the inverse problem, there are no explicit expressions to relate the variables and the response, the curve fitting techniques cannot give a clear physical relationship between the material properties and the response. Also the dependence of impedance amplitude requires accurate calibration and measurement.

We have published a series of papers on the *Resonant Spectrum Method*, a "direct" method to characterize a piezoelectric film coated on an isotropic substrate to form a composite resonator [26]~[30]. From a knowledge of the parallel and series resonant spectra of a composite resonator, three parameters of the piezoelectric film, *i.e.*, the electro-mechanical coupling coefficient, the density, and the elastic constant can be calculated directly with a set of explicit formulae.

The *Resonant Spectrum Method* was first developed for a simplified two layer composite resonator. The validity of the method was demonstrated with simulations when

electrodes were ignored. For high frequency devices, however, the electrode effect cannot necessarily be ignored. Thus the *Resonant Spectrum Method* was extended to the case of four layer composite resonators where the electrodes were taken into account. The validity and the feasibility of the method have been proved by experiment and simulations.

In this thesis, derivation of the *Resonant Spectrum Method*, experimental verification and numerical simulation are presented. Chapter 2 will give the derivation of the method for two layer composite resonators and in Chapter 3, this principle will be extended to four layer composite resonators, which includes two electrodes. The experimental results will be presented in Chapter 4. The impact on the accuracy of the method caused by electrodes, material mechanical losses and probe contact resistance/electrode resistance will be discussed in Chapter 5. Chapter 6 will describe some applications of the *Resonant Spectrum Method* on piezoelectric film characterization and composite resonator design.

CHAPTER 2. *RESONANT SPECTRUM METHOD* FOR A TWO LAYER COMPOSITE RESONATOR

In this chapter we will derive the *Resonant Spectrum Method* for a composite resonator which consists of only a piezoelectric layer and a non-piezoelectric substrate [26][27]. The metal electrodes usually existing on both sides of the piezoelectric film are ignored. The *Resonant Spectrum Method* for two layer composite resonator not only is the first step in our development of the *Resonant Spectrum Method*, but also has a clear physical interpretation. In fact all of the basic physics of the method is contained in the present chapter, the treatment is then extended to include the effects of the electrodes in Chapter 3.

2.1 The input impedance of a two layer composite resonator

There are many approaches to derive the input impedance of a composite resonator. One can derive it by solving the linear equation of piezoelectric elasticity for the one-dimensional case with suitable boundary conditions [3][31], or by analyzing the equivalent circuit of the composite resonator [24]. Here we are going to use the transfer matrix approach [25][32][33], which is simply matrix operations and can be easily extended to arbitrary number of layers.

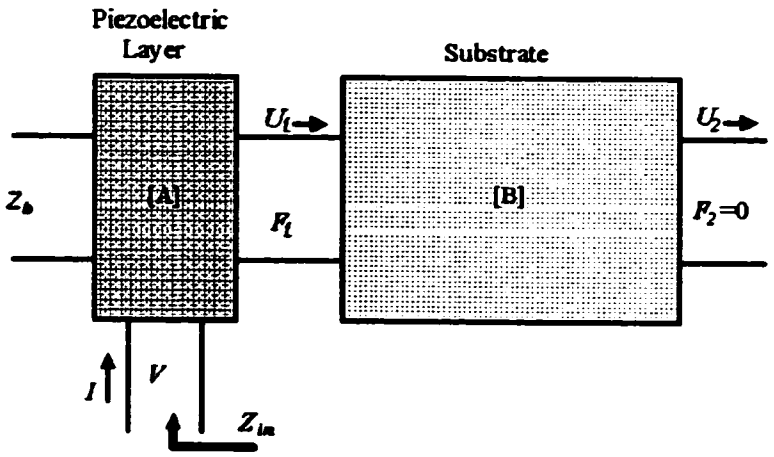

Fig.2.1 *Matrix presentation of two layer composite resonator*

A matrix model for a 2-layer composite resonator is shown in Fig. 2.1. The piezoelectric layer can be presented as a three-port component. One port is the electrical terminal pair, voltage V and current I. The other two are back and front acoustic ports presented by the forces F and the displacement U. If the acoustic backing port is terminated with an acoustic impedance Z_b, the electric pair can be expressed as

$$\begin{bmatrix} V \\ I \end{bmatrix} = [A] \cdot \begin{bmatrix} F_1 \\ U_1 \end{bmatrix} \tag{2.1}$$

The transfer function [A] of a piezoelectric film can be obtained from equivalent circuit analysis of Mason's in-line model,

$$[A] = \frac{1}{\phi H} \begin{bmatrix} 1 & j\phi^2/\omega C_0 \\ j\omega C_0 & 0 \end{bmatrix} \cdot \begin{bmatrix} \cos\gamma + jz_b \sin\gamma & Z_0(z_b \cos\gamma + jz_b \sin\gamma) \\ j\sin\gamma / Z_0 & 2(\cos\gamma - 1) + jz_b \sin\gamma \end{bmatrix} \tag{2.2}$$

where $\phi = \left(k_t^2 C_0 Z_0 l / v\right)$ is the transformer ratio in the Mason's equivalent circuit,

l is the thickness of the piezoelectric layer,

v is the longitudinal acoustic wave velocity in piezoelectric layer along the direction normal to the resonator surface,

$C_0 = \varepsilon S/l$ is the clamped capacitor of the resonator with area S,

$Z_0 = S\rho v$ is the acoustic impedance of the piezoelectric layer with density ρ,

$H = \cos\gamma - 1 + jz_b \sin\gamma$, where $\gamma = \omega/lv$ is the phase delay of the acoustic wave in the piezoelectric film and $\omega \equiv 2\pi f$ is the angular frequency, and

$z_b = Z_b / Z_0$ is the normalized acoustic impedance of the backing material where Z_b is the acoustic impedance of the backing material. In this scenario Z_b is zero since there is no backing layer.

An isotropic substrate can be presented as a device with two acoustic ports,

$$\begin{bmatrix} F_1 \\ U_1 \end{bmatrix} = [B] \cdot \begin{bmatrix} F_2 \\ U_2 \end{bmatrix} \tag{2.3}$$

where [B] is the transfer matrix for a piezoelectric inert media,

$$[B] = \begin{bmatrix} \cos\gamma_{sb} & jZ_{sb}\sin\gamma_{sb} \\ j\sin\gamma_{sb}/Z_{sb} & \cos\gamma_{sb} \end{bmatrix} \tag{2.4}$$

where $\gamma_{sb} = \omega l_{sb}/v_{sb}$ is the phase delay of the acoustic wave in the substrate with thickness l_{sb} and longitudinal velocity v_{sb}. $Z_{sb} = S\rho_{sb}v_{sb}$ is the acoustic impedance of the substrate with density ρ_{sb}.

For the substrate in a two layer composite resonator, one side is in contact with the piezoelectric film, the other side is force-free, $F_2 = 0$. Substitute (2.2) ~ (2.4) into (2.1), we obtained the electric impedance of such a two layer composite resonator.

$$Z_{in} = \frac{V}{I} = \frac{1}{j\omega C_0}\left[1 - \frac{k_t^2}{\gamma} \cdot \frac{2\tan(\gamma/2) + z_{sb}\tan\gamma_{sb}}{1 + z_{sb}\tan\gamma_{sb}/\tan\gamma}\right] \tag{2.5}$$

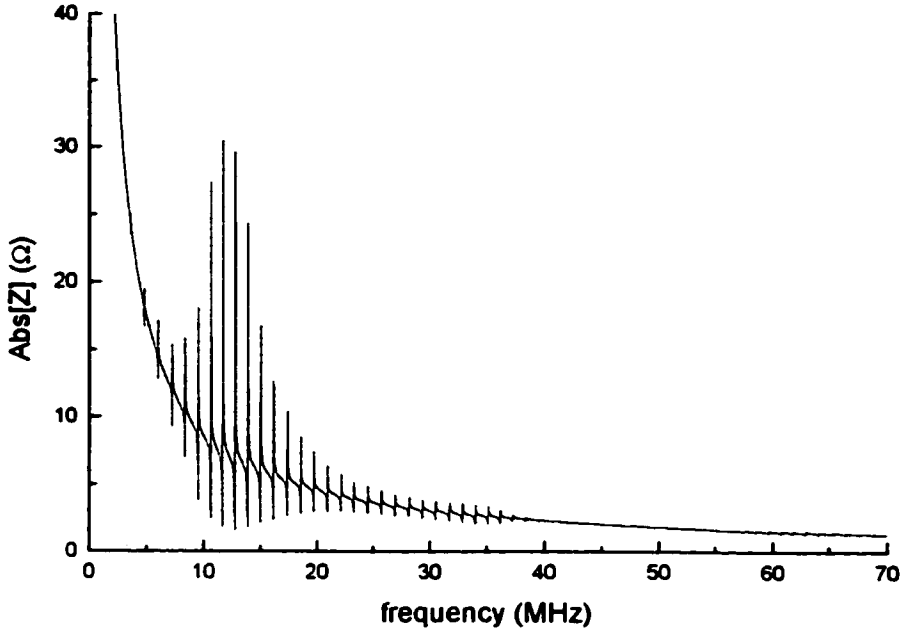

(a)

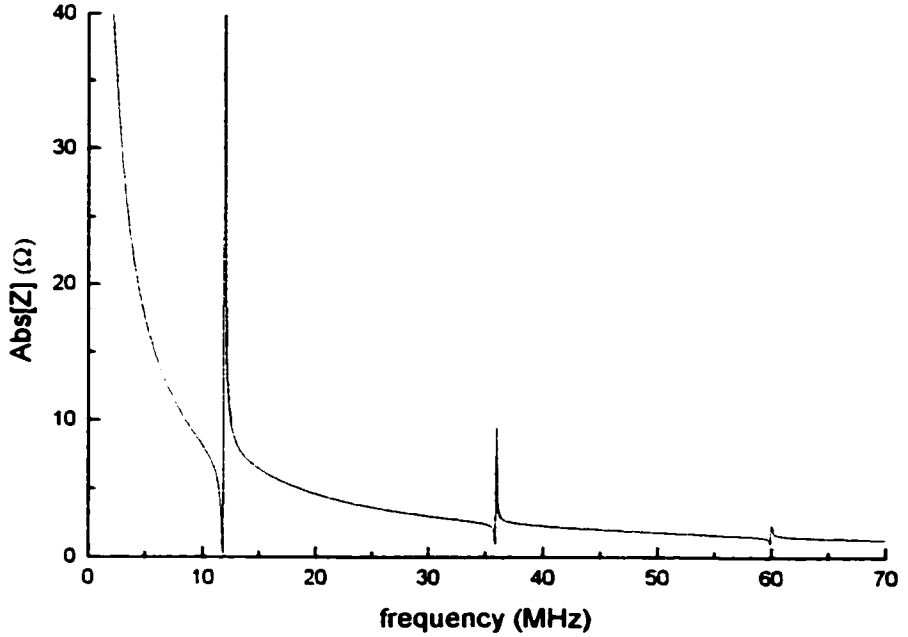

(b)

Fig.2.2 *The impedance of (a) a PZT/Stainless steel composite resonator*

(b) PZT film resonator

Figure 2.2 shows the impedance of a two layer composite resonator consisting of a PZT film deposited on a stainless steel substrate. As a comparison, the impedance of the corresponding PZT film resonator is also shown. In the calculation, a small imaginary part is added to the velocities of both the film and substrate to avoid singularities.

The characterization of the electric impedance of a composite resonator is clearly shown in this figure. Generally, the impedance follows a hyperbolic decrease which is the presentation of the static capacitance C_0 of the piezoelectric film. If the film is a non-piezoelectric film, $k_t^2 = 0$, then Z_{in} degrades to the impedance of a capacitor. This leads to the conclusion that the static capacitance C_0 is only related to the shape of the impedance curve, not with the resonance. On the hyperbolic response, there are multiple sharp peaks which are the resonant "modes". The envelope of the resonant modes is determined by the bandwidth of the free piezoelectric film resonator.

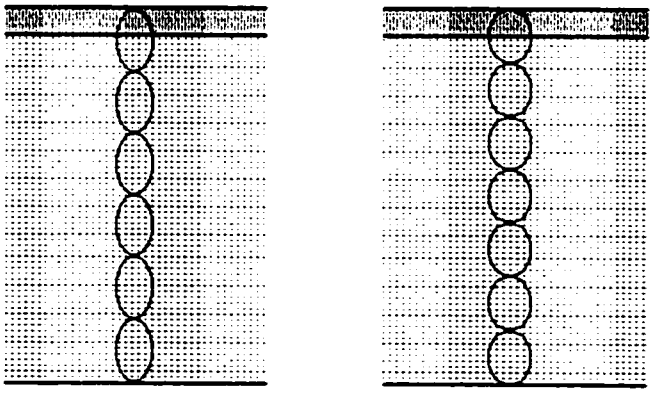

Fig.2.3 *Standing wave patterns in a composite resonator*

At a resonant mode, a standing wave is established in the thickness direction of the composite resonator. Since the substrate is usually much thicker than the piezoelectric film, the modal frequency is mainly determined by the acoustic properties and geometric parameters of the substrate, but will be modulated by the film. Fig. 2.3 shows the standing wave patterns of two neighboring resonant modes. Raising the frequency will add one more cycle into the standing wave in the resonator.

The multiple resonant modes have their maximum magnitude at a certain frequency which is determined mainly by the piezoelectric film and also by the acoustic impedance ratio of the piezoelectric film and the substrate. It will be shown in Chapter 5 that when the acoustic impedance of the piezoelectric layer is smaller than that of the substrate, referred to as a "hard substrate", such as PZT on stainless steel, the maximum magnitude is located in the first transition region. When the acoustic impedance of the piezoelectric layer is greater than that of the substrate, referred to as a "soft substrate", such as ZnO on quartz, the maximum magnitude is located in the first normal region. In the following sections, we will derive the relations between the resonant frequencies of the modes and the piezoelectric film parameters. Since the film parameters can be determined by the distribution of the resonant frequencies, we name this method as the *Resonant Spectrum Method.*

2.2 Spacing of parallel resonant frequencies (*SPRF*) and effective coupling coefficient $k_{eff}^2(m)$

According to the definition in the IEEE standard [21], the parallel resonant frequency of a single piezoelectric plate corresponds to the maximum resistance, which is the real part of the impedance of the resonator. Applying this definition to a composite resonator, the parallel resonant frequencies correspond to the maxima of the real part of the impedance in each resonant mode. When the resonator materials are lossless, the impedance at parallel resonant frequency will approach infinity and thus the parallel resonant frequencies can be calculated from the impedance equation (2.5) by setting the denominator to zero.

$$\tan\gamma + z_{sb}\tan\gamma_{sb} = 0 \tag{2.6}$$

The series resonant frequencies correspond to the minima of the resistance, or say the maxima of the conductance, which is the real part of $Y_{in} = 1/Z_{in}$. The series resonant frequencies can be calculated from the impedance equation (2.5) for lossless material by setting the numerator to zero.

$$\tan\gamma + z_{sb}\tan\gamma_{sb} = \frac{k_t^2}{\gamma}\cdot\left[2\tan(\gamma/2) + z_{sb}\tan\gamma_{sb}\right]\cdot\tan\gamma \tag{2.7}$$

Comparing with Eqs. (1.7) and (1.8) for the single piezoelectric plate case, where f_p is simply determined by the thickness and longitudinal acoustic wave velocity of the piezoelectric plate and k_t^2 was directly calculated from the series resonant frequency

equations of the fundamental mode, the two resonant frequency equations for a composite resonator become much more complicated and there exist multiple modes.

It is noted that Eq. (2.6) has the same form as the cut-off frequency equation of the longitudinal components of Lamb waves in a two-layer composite structure [34]~[37]. It has been proved that the spacing of the cut off frequencies, which is defined as

$$\Delta f_{cut-off}(m) = f_{cut-off}(m) - f_{cut-off}(m-1) \tag{2.10}$$

relies only on the mechanical properties of the two layers, and two material constants, *e.g.* ρ and C_{33}^{D} can be determined from the distribution of the spacing. We believe this principle should also apply to a composite resonator, meaning that the distribution of the spacing of the resonant frequencies only relies on the mechanical properties of the piezoelectric film and the substrate. This can be seen from the parallel resonant frequency equation (2.6) where only mechanical parameters are involved. Fig. 2.4 shows the solutions for equation (2.6). In this figure, the solid line is the first term in Eq. (2.6), which is the contribution of the film and has resonance at $\gamma = \pi/2$, $3\pi/2$, $5\pi/2$, etc. The dash line is the second term in Eq. (2.6), which is the contribution of the substrate and has a series of equally spaced resonances. The crossings of these two lines are the solutions, *i.e.* the parallel resonant frequencies. Because of the existence of the film, the solutions are no longer equally spaced. Similar to Eq.(2.8), we define the spacing of the parallel resonant frequencies (*SPRF*) as the difference between two adjacent parallel resonant frequencies,

$$\Delta f_p(m) = f_p(m) - f_p(m-1) \tag{2.9}$$

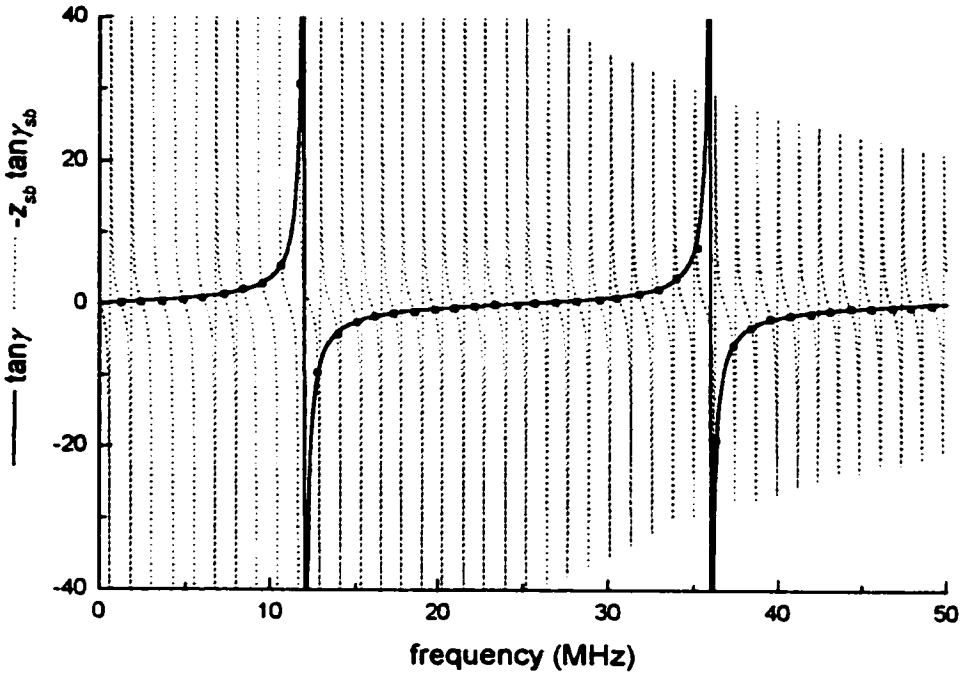

Fig.2.4 *The solutions of the parallel resonant frequency equation*

In analogy to the formula for the coupling coefficient of a single plate piezoelectric resonator Eq. (1.8), an effective coupling coefficient is introduced [23], which represents the electromechanical coupling intensity of a specific resonant mode of a composite resonator,

$$k_{eff}^2(m) = \frac{\pi}{2}\frac{f_s(m)}{f_p(m)}\tan\left(\frac{\pi}{2}\frac{f_p(m)-f_s(m)}{f_p(m)}\right) \tag{2.10}$$

When $k_{eff}^2(m)$ is small (this is usually true for a composite resonator at high order mode), the above equation can be simplified as

$$k_{eff}^2(m) = \frac{\pi^2}{4} \cdot \frac{f_s(m)}{f_p(m)} \cdot \frac{f_p(m) - f_s(m)}{f_p(m)} \tag{2.11}$$

As an indicator of the intensity of the piezoelectricity, it is natural to believe that the effective coupling coefficient $k_{eff}^2(m)$ is strongly ties to the coupling coefficient k_t^2 of the piezoelectric film.

Fig. 2.5 shows the *SPRF* and k_{eff}^2 distributions *vs.* frequency of a composite resonator with the same parameters as in Fig. 2.2. Since the thickness of the substrate is much larger than that of the film, the value of the *SPRF* is dominated by the substrate and is close to the *SPRF* of the bare substrate plate Δf_0, but the distribution shape is dominated by the film. The period of the *SPRF* can be obtained by letting $\tan\gamma = 0$ or $\tan\gamma \to \infty$. The regions corresponding to $\tan\gamma = 0$ *i.e.* $\gamma \approx n\pi$, are referred to as the "normal regions" and the regions where $\tan\gamma \to \infty$, i.e., $\gamma \approx (n + 1/2) \cdot \pi$, are referred to as the "transition regions". The k_{eff}^2 has its maximum in the first transition region for this sample.

In the following sections, we will derive the relations between the effective coupling coefficient k_{eff}^2 and *SPRF* and the piezoelectric film parameters.

2.3 The first normal region

The normal regions are the areas where γ is close to an integral multiple of π. The first normal region is where $\gamma \approx \pi$, and therefore

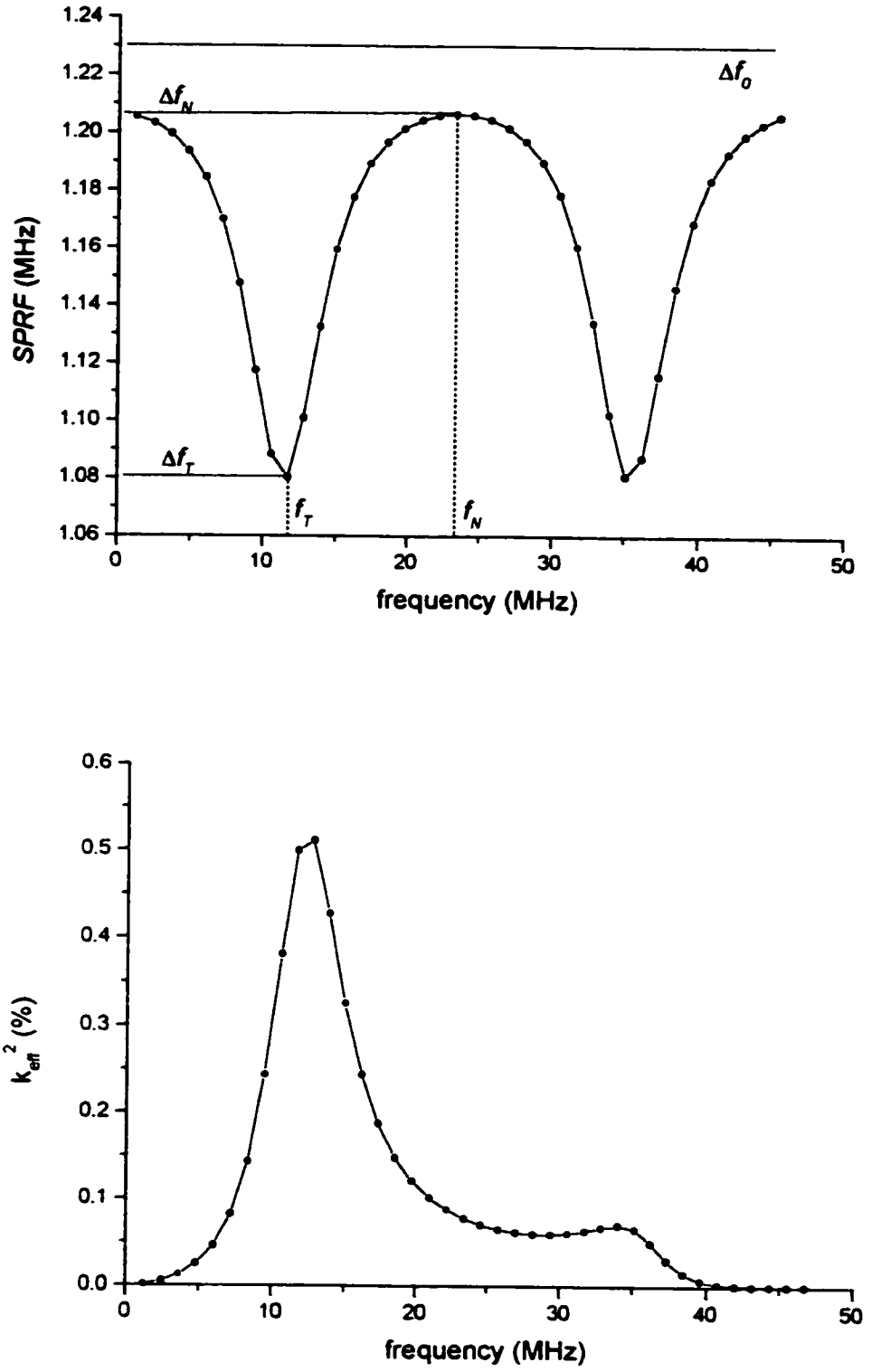

Fig. 2.3 *The SPRF and k_{eff}^2 distributions of a composite resonator*

$$\tan\gamma \approx 0 \tag{2.12}$$

Since the first term in the parallel resonant frequency equation (2.6) is near zero, in order for Eq. (2.6) to be satisfied, the second term also has to be near zero,

$$\tan\gamma_{sb} \approx 0 \tag{2.13}$$

By introducing the following approximate expressions

$$\begin{aligned} \gamma &= \pi + \varepsilon \\ \gamma_{sb} &= m_N \cdot \pi + \delta \end{aligned} \tag{2.14}$$

where m_N is the mode order of the bare substrate plate resonator at the center of the first normal region, and ε and δ are small quantities, we get

$$\begin{aligned} \tan\gamma &= \tan(\pi + \varepsilon) \approx \varepsilon \\ \tan\gamma_{sb} &= \tan(m_N\pi + \delta) \approx \delta \end{aligned} \tag{2.15}$$

Therefore, in the first normal region, Eq. (2.6) can be written as

$$\varepsilon + z_{sb} \cdot \delta = 0 \tag{2.16}$$

Substituting

$$\begin{aligned} \varepsilon &= \gamma - \pi = \frac{2\pi f_p(N)}{v} \cdot l - \pi \\ \delta &= \gamma - m_N\pi = \frac{2\pi f_p(N)}{v_{sb}} \cdot l_{sb} - m_N\pi \end{aligned} \tag{2.17}$$

into (2.16), we obtain the parallel resonant frequency of the composite resonator in the first normal region

$$f_p(N) = \frac{1 + m_N \cdot z_{sb}}{2l/v + z_{sb} \cdot 2l_{sb}/v_{sb}} \tag{2.18}$$

where $N = m_N + 1$ is the mode order of the composite resonator at the center of the first normal region. We define R to be the ratio of the resonant frequency of the free film f_c to that of the free substrate plate f_0,

$$R = \frac{f_c}{f_0} = \frac{v/2l}{v_{sb}/2l_{sb}} \tag{2.19}$$

Then m_N is the round integer of R.

$$m_N = \text{round}\ (R) \tag{2.20}$$

It should be noted that the mode order of the composite resonator at the center of the first normal region, is $m_N + 1$, rather than m_N.

The spacing of the parallel resonant frequencies in the first normal region is

$$\begin{aligned} \Delta f_N &= \frac{z_{sb}}{2l/v + z_{sb} \cdot 2l_{sb}/v_{sb}} \\ &= \Delta f_0 \cdot \left(1 + \frac{\rho l}{\rho_{sb} l_{sb}}\right)^{-1} \end{aligned} \tag{2.21}$$

where

$$\Delta f_0 = \frac{v_{sb}}{2l_{sb}} \tag{2.22}$$

is the resonant frequency spacing of the bare substrate plate, which is a constant.

On the other hand, the series resonant frequency in the first normal region can be derived with a similar procedure. When k_{eff}^2 is small (which is usually true), $f_s(N) \approx f_p(N)$, and we have similar approximate expressions for the phase delays

$$\begin{aligned} \gamma &= \pi + \varepsilon' \\ \gamma_{sb} &= m_N \cdot \pi + \delta' \end{aligned} \tag{2.23}$$

where ε' and δ' are also small quantities.

Substituting them into (2.7) with the frequency being the series resonant frequency and using the approximation

$$\tan\frac{\gamma}{2} = \tan\left(\frac{\pi}{2} + \frac{\varepsilon'}{2}\right) \approx -\frac{2}{\varepsilon'} \tag{2.24}$$

we obtain

$$k_t^2 = \gamma \cdot \frac{\tan(\gamma) + z_{sb} \cdot \tan(\gamma_{sb})}{\left[2 \cdot \tan(\gamma/2) + z_{sb} \cdot \tan\gamma_{sb}\right] \cdot \tan\gamma}$$

$$= \gamma \cdot \frac{\varepsilon' + z_{sb} \cdot \delta'}{-4 + z_{sb}\varepsilon'\delta'} \tag{2.25}$$

Ignoring the second order small quantity $\varepsilon'\delta'$ *i.e.* taking $(1 - z_{sb} \cdot \varepsilon' \cdot \delta'/4) \approx 1$, we get

$$k_t^2 \approx -\frac{\gamma}{4}(\varepsilon' + z_{sb}\delta)$$

$$= -\frac{\gamma}{4}\left[(\gamma - \pi) + z_{sb}(\gamma_{sb} - m_N\pi)\right]$$

$$= \frac{\pi^2}{4} \cdot \frac{2l}{v} \cdot f_s(N) \cdot \left[\left(1 + z_{sb} \cdot m_N\right) - \left(2l/v + z_{sb} \cdot 2l_{sb}/v_{sb}\right) \cdot f_s(N)\right] \tag{2.26}$$

From Eq.(2.18), we have

$$1 + m_N \cdot z_{sb} = \left(2l/v + z_{sb} \cdot 2l_{sb}/v_{sb}\right) \cdot f_p(N) \tag{2.27}$$

and

$$\frac{v}{2l} = \frac{1 + \rho_{sb}l_{sb}/\rho l}{1 + m_N \cdot z_{sb}} \cdot f_p(N) \tag{2.28}$$

Substituting them into (2.26), we obtain a formula for the electromechanical coupling coefficient in the first normal region

$$k_t^2 = \frac{\pi^2}{4} \cdot \frac{1 + z_{sb} \cdot m_N}{1 + \rho_{sb} l_{sb} / \rho l} \cdot \frac{f_s(N)}{f_p(N)} \cdot \frac{1 + z_{sb} \cdot m_N}{f_p(N)} \left[f_p(N) - f_s(N) \right]$$
$$= \frac{(1 + z_{sb} \cdot m_N)^2}{1 + \rho_{sb} l_{sb} / \rho l} k_{eff}^2(N) \tag{2.29}$$

where

$$k_{eff}^2(N) = \frac{\pi^2}{4} \cdot \frac{f_s(N)}{f_p(N)} \cdot \frac{f_p(N) - f_s(N)}{f_p(N)} \tag{2.30}$$

is the effective coupling coefficient of the N order mode.

In the case that R is an integer, which means that $f_p(N)$ is exactly at the center of the first normal region,

$$m_N = R = \frac{v / l}{v_{sb} / l_{sb}} \tag{2.31}$$

$$1 + m_N \cdot z_{sb} = 1 + \frac{\rho_{sb} l_{sb}}{\rho l} \tag{2.32}$$

Then (2.29) can be simplified to

$$k_t^2 = \left(1 + \frac{\rho_{sb} l_{sb}}{\rho l} \right) \cdot k_{eff}^2(N) \tag{2.33}$$

If the ratio R is large enough that its fraction can be ignored, (2.31) is satisfied approximately and therefore (2.33) is also tenable and the error is

$$Error = 1 - \frac{\text{round}(R)}{R} \tag{2.34}$$

It is obvious that when $R > 50$, the error is less than 1%.

The physical interpretation of the *Resonant Spectrum Method* in the first normal region is very clear. Eq. (2. 22) shows that the *SPRF* at this region, Δf_N, is the *SPRF* of the bare substrate plate modified by the mass ratio of the piezoelectric film to the substrate

plate. Eq. (2.33) shows the electromechanical coupling coefficient of the piezoelectric film relates to the effective coupling coefficient of the composite resonator in the first normal region by a factor of the mass ratio of the whole resonator to the piezoelectric film.

2.4 The first transition region

The transition regions are the areas where γ is close to a half integer multiple of π. The first transition region refers to $\gamma \approx \pi/2$. Since for a resonator the total phase delay of the acoustic wave from one side to the other has to be an integer multiple of π in order to make the round trip phase delay an integer multiple of 2π, the phase delay in the substrate has to yield another $\pi/2$.

Since at the center of the first transition region,

$$\tan\gamma \to \infty \tag{2.35}$$

we can rewrite the parallel resonant frequency equation (2.6) in a more convenient form

$$\cot\gamma_{sb} + z_{sb} \cdot \cot\gamma = 0 \tag{2.36}$$

and the series resonant frequency equation (2.7) in the form of

$$\cot\gamma_{sb} + z_{sb} \cdot \cot\gamma = \frac{k_t^2}{\gamma} \cdot \left[2 \cdot \tan\frac{\gamma}{2} \cdot \cot\gamma_{sb} + z_{sb} \right] \tag{2.37}$$

Since the second term in the Eq. (2.36) is near zero, the first term also has to be near zero. Thus by introducing approximate expressions

$$\gamma = \pi/2 + \varepsilon$$
$$\gamma_{sb} = (m_T + 1/2)\cdot\pi + \delta \tag{2.38}$$

where m_T is an integer which is the mode order of the bare substrate plate resonator near the center of the first transition region, ε and δ are small quantities, we get

$$\cot\gamma = \cot(\pi/2 + \varepsilon) \approx \varepsilon$$
$$\cot\gamma_{sb} = \cot[(m_T + 1/2)\pi + \delta] \approx \delta \tag{2.39}$$

Therefore, in the first transition region, the parallel resonant frequencies satisfy

$$\delta + z_{sb}\cdot\varepsilon = 0; \tag{2.40}$$

Substitute

$$\varepsilon = \gamma - \pi/2 = \frac{2\pi f_p(M)}{v}\cdot l - \frac{\pi}{2}$$
$$\delta = \gamma - m_T\pi = \frac{2\pi f_p(M)}{v_{sb}}\cdot l_{sb} - \left(m_T + \frac{1}{2}\right)\pi \tag{2.41}$$

into (2.40), we obtain the parallel resonant frequency of the composite resonator in the first transition region

$$f_p(M) = \frac{m_T + (1 + z_{sb})/2}{2l_{sb}/v_{sb} + z_{sb}\cdot 2l/v} \tag{2.42}$$

where $M = m_T + 1$ is the mode order of the composite resonator at the center of the first transition region, m_T is an integer, which is approximately a half of m_N. From (2.38) one can find that

$$m_T = \text{round}\left[\frac{1}{2}\left(\frac{v}{l}\Big/\frac{v_{sb}}{l_{sb}} - 1\right)\right]$$
$$= \text{round}\left[\frac{R-1}{2}\right] \tag{2.43}$$

The spacing of the parallel resonant frequency in the first transition region is

$$\Delta f_T = \frac{1}{2l_{sb}/v_{sb} + z_{sb}\cdot 2l/v}$$

$$= \Delta f_0 \left(1 + \frac{\rho_{sb} v_{sb}^2}{\rho v^2}\frac{l}{l_{sb}}\right)^{-1} \tag{2.44}$$

Similar to the approximation equations (2.23) in the first normal region, at the series resonant frequency of the M order resonant mode we introduce two approximation expressions

$$\gamma = \frac{2\pi l}{v} f_s(M) = \pi/2 + \varepsilon'$$
$$\gamma_{sb} = \frac{2\pi l_{sb}}{v_{sb}} f_s(M) = (m_T + 1/2)\cdot\pi + \delta' \tag{2.45}$$

Substitute the approximations

$$\cot\gamma = \cot(\pi/2 + \varepsilon') \approx -\varepsilon'$$
$$\cot\gamma_{sb} = \cot[(m_T + 1/2)\cdot\pi + \delta'] \approx \delta' \tag{2.46}$$

and

$$\tan(\gamma/2) \approx 1 + \varepsilon' \tag{2.47}$$

into (2.37), we get

$$k_t^2 = \gamma \cdot \frac{\cot\gamma_{sb} + z_{sb}\cdot\cot\gamma}{2\cdot\tan(\gamma/2)\cdot\cot\gamma_{sb} + z_{sb}}$$

$$= \gamma \cdot \frac{-(\delta' + z_{sb}\cdot\varepsilon')}{-2(1+\varepsilon')\cdot\delta' + z_{sb}} \tag{2.48}$$

By introducing a correction factor Γ which is in the order of unity

$$\Gamma = 1 - 2(1+\varepsilon')\delta'/z_{sb}$$

$$= 1 + \frac{2\rho v}{\rho_{sb} v_{sb}} \left[1 + \frac{2\pi l}{v} f_s(M) - \frac{\pi}{2} \right] \left[(m_T + 1/2)\pi - \frac{2\pi l_{sb}}{v_{sb}} f_s(M) \right] \qquad (2.49)$$

we get

$$k_t^2 = \gamma \cdot \frac{\delta' + z_{sb} \cdot \varepsilon'}{z_{sb} \Gamma}$$

$$= \frac{2\pi f_s(M) l}{z_{sb} v} \cdot \left[2\pi f_s(M) \left(\frac{2l_{sb}}{v_{sb}} + z_{sb} \cdot \frac{2l}{v} \right) - \pi \left(m_T + \frac{1 + z_{sb}}{2} \right) \right] \frac{1}{\Gamma} \qquad (2.50)$$

From (2.43) we have

$$m_T + \frac{z_{sb} + 1}{2} = \left(z_{sb} \frac{2l}{v} + \frac{2l_{sb}}{v_{sb}} \right) f_p(M) \qquad (2.51)$$

and

$$\frac{v}{2l} = \frac{z_{sb} + v l_{sb} / (v_{sb} l)}{m_T + (z_{sb} + 1)/2} f_p(M) \qquad (2.52)$$

By the substitutions of the equations (2.51) and (2.52) into (2.50), the electromechanical coupling coefficient of the piezoelectric film k_t^2 can be calculated from the effective coupling coefficient in the first transition region,

$$k_t^2 = \pi^2 \cdot \frac{2l}{v} \cdot \left(\frac{2l_{sb}}{v_{sb}} + z_{sb} \cdot \frac{2l}{v} \right) \cdot \frac{f_s(M)}{z_{sb}} \cdot \frac{f_p(M) - f_s(M)}{\Gamma}$$

$$= \frac{\left[(2m_T + 1)/z_{sb} + 1 \right]^2}{\left(1 + \frac{l_{sb}}{l} \cdot \frac{\rho v^2}{\rho_{sb} v_{sb}^2} \right)} \cdot \frac{1}{\Gamma} \cdot k_{eff}^2(M) \qquad (2.53)$$

where

$$k_{eff}^2(M) = \frac{\pi^2}{4} \cdot \frac{f_s(M)}{f_p(M)} \cdot \frac{f_p(M) - f_s(M)}{f_p(M)} \qquad (2.54)$$

is the effective coupling factor of the M order mode.

If $R = 2 \cdot m_T + 1$, *i.e.* it is an odd integer, M = (R+1)/2 is an integer, the M order parallel resonant frequency, $f_p(M)$, is exactly at the center of the first transition region, *i.e.*, $\varepsilon = 0$, $\delta = 0$. Then we have the relation

$$m_T = \frac{R-1}{2} = \frac{1}{2}\left(\frac{l_{sb}}{v_{sb}} \cdot \frac{v}{l} - 1\right) \tag{2.55}$$

and then

$$1 + \frac{(2m_T + 1)}{z_{sb}} = 1 + \frac{l_{sb}}{l} \cdot \frac{\rho v^2}{\rho_{sb} v_{sb}^2}; \tag{2.56}$$

Thus the expression for k_t^2 in the first transition region can be simplified to

$$k_t^2 = \left(1 + \frac{\rho v^2}{\rho_{sb} v_{sb}^2} \cdot \frac{l_{sb}}{l}\right) \cdot \frac{k_{eff}^2(M)}{\Gamma} \tag{2.57}$$

If the ratio R is large enough that its fraction can be ignored, (2.55) is satisfied approximately and therefore (2.57) is also tenable and the error is

$$Error = 1 - \frac{\text{round}[(R-1)/2]}{(R-1)/2} \tag{2.58}$$

Again when $R > 100$, the error is less than 1%.

The correction factor Γ is caused by the fact that the series resonance is not exactly at the center of the first transition region. The term in the first bracket of Eq.(2.49) represents the deviation of the Mth order series resonant frequency from the center of the first transition region. The term in the second bracket represents the deviation of phase delay in the substrate at the Mth order series resonant frequency from a half integer multiple of π. Since the first bracket is close to unity, second order small quantity can be ignored, the correction factor can be simplified as

$$\Gamma = 1 + \frac{2\rho v}{\rho_{sb} v_{sb}} \left[(m_T + 1/2)\pi - \frac{2\pi l_{sb}}{v_{sb}} f_s(M) \right]$$

$$+ \frac{2\rho v}{\rho_{sb} v_{sb}} \left[\frac{2\pi l}{v} f_s(M) - \frac{\pi}{2} \right] \left[(m_T + 1/2)\pi - \frac{2\pi l_{sb}}{v_{sb}} f_s(M) \right]$$

$$\approx 1 + \frac{2\rho v}{\rho_{sb} v_{sb}} \left[(m_T + 1/2)\pi - \frac{2\pi l_{sb}}{v_{sb}} f_s(M) \right] \qquad (2.59)$$

The correction factor is not necessarily near unity, especially for a soft substrate case where $\frac{\rho v}{\rho_{sb} v_{sb}} > 1$. Fortunately, for a soft substrate case, the maximum of k_{eff}^2 is located in the first normal region and the equation of k_t^2 in the first normal region (2.29) is recommended. For the hard substrate case where the maximum of k_{eff}^2 is located in the first transition region, $\frac{\rho v}{\rho_{sb} v_{sb}} < 1$ and the correction factor is within an order of several percents from unity.

For example, in the PZT/stainless steel composite resonator shown in Fig.2.2, the parameters used in the calculation are

v = 2400m/s, ρ = 7000kg/m^3, l = 50μm;

v_{sb} = 5900m/s, ρ_{sb} = 7800kg/m^3, l_{sb} = 2400μm.

At the center of the first transition region, the 10th series resonant frequency $fs(10)$ =11.693MHz. The correction factor Γ = 0.97.

2.5 Summary

In this chapter, we derived the *Resonant Spectrum Method* for a two layer composite resonator. The method gives six formulas

1. In the first normal region, the *SPRF* is given by

$$\Delta f_N = \Delta f_0 \cdot \left(1 + \frac{\rho l}{\rho_{sb} l_{sb}}\right)^{-1} \tag{2.60}$$

2. In the first transition region, the *SPRF* is given by

$$\Delta f_T = \Delta f_0 \left(1 + \frac{\rho_{sb} v_{sb}^2}{\rho v^2} \frac{l}{l_{sb}}\right)^{-1} \tag{2.61}$$

3. The electromechanical coupling coefficient in the first normal region is given by

$$k_t^2 = \frac{(1 + z_{sb} \cdot m_N)^2}{1 + \rho_{sb} l_{sb} / \rho l} k_{eff}^2(N) \tag{2.62}$$

where $N=m_N+1$, or the approximate expression when R is an integer or R is large enough

$$k_t^2 = \left(1 + \frac{\rho_{sb} l_{sb}}{\rho l}\right) \cdot k_{eff}^2(N) \tag{2.63}$$

4. The electromechanical coupling coefficient in the first normal region is given by

$$k_t^2 = \frac{\left[(2m_T + 1)/z_{sb} + 1\right]^2}{\left(1 + \frac{l_{sb}}{l} \cdot \frac{\rho v^2}{\rho_{sb} v_{sb}^2}\right)} \cdot \frac{1}{\Gamma} \cdot k_{eff}^2(M) \tag{2.64}$$

where $M = m_T+1$, or the approximate expression when R is an odd integer or R is large enough

$$k_t^2 = \left(1 + \frac{\rho v^2}{\rho_{sb} v_{sb}^2} \cdot \frac{l_{sb}}{l}\right) \cdot \frac{k_{eff}^2(M)}{\Gamma} \tag{2.65}$$

From a knowledge of Δf_N and Δf_T of *SPRF*, we can solve Eqs.(2.60) and (2.61) to obtain ρ and v, assuming other parameters are known. Simulation or measurement of k_{eff}^2 near the maximum in the first normal region or the first transition region yields k_t^2 by Eqs. (2.62) ~ (2.65). Thus with a few simple explicit equations, we can determine three parameters, ρ, v and k_t^2 for the piezoelectric film. This method is much simpler and more direct than solving the inverse problem by curve fittings.

The principles used in this chapter for a two layer composite resonator are also valid when the effects of the electrodes are included in next chapter, although the mathematical description becomes consequently more complicated.

CHAPTER 3. *RESONANT SPECTRUM METHOD* FOR A FOUR LAYER COMPOSITE RESONATOR

In the previous chapter, we have developed the *Resonant Spectrum Method* for a composite resonator where the electrodes are ignored. For very high frequency devices in the GHz range, however, the electrodes usually have some significant percentage thickness of the piezoelectric film and their existence will disturb the resonant condition of the composite resonator. Therefore, the electrode effect can not necessarily be ignored. In this chapter, we will develop the *Resonant Spectrum Method* while taking two electrodes into account [28]~[30].

3.1 The impedance of a 4 layer composite resonator

We still use the transfer matrix approach [25][32][33] to derive the impedance of a 4 layer composite resonator. The symbols used in the derivation are shown in Fig.3.1.

The top electrode is a two acoustic port device, its transfer matrix is

$$\begin{bmatrix} F_0 \\ U_0 \end{bmatrix} = \begin{bmatrix} \cos\gamma_{el} & jZ_{el}\sin\gamma_{el} \\ j\sin\gamma_{el}/Z_{el} & \cos\gamma_{el} \end{bmatrix} \begin{bmatrix} F_1' \\ U_1' \end{bmatrix} \tag{3.1}$$

where F and U represent force and displacement velocity, respectively. $Z_{el}=S\rho_{el}v_{el}$ is the acoustic impedance of the top electrode, $\gamma_{el}=\omega l_{el}/v_{el}$ is the phase delay of the acoustic wave in the top electrode.

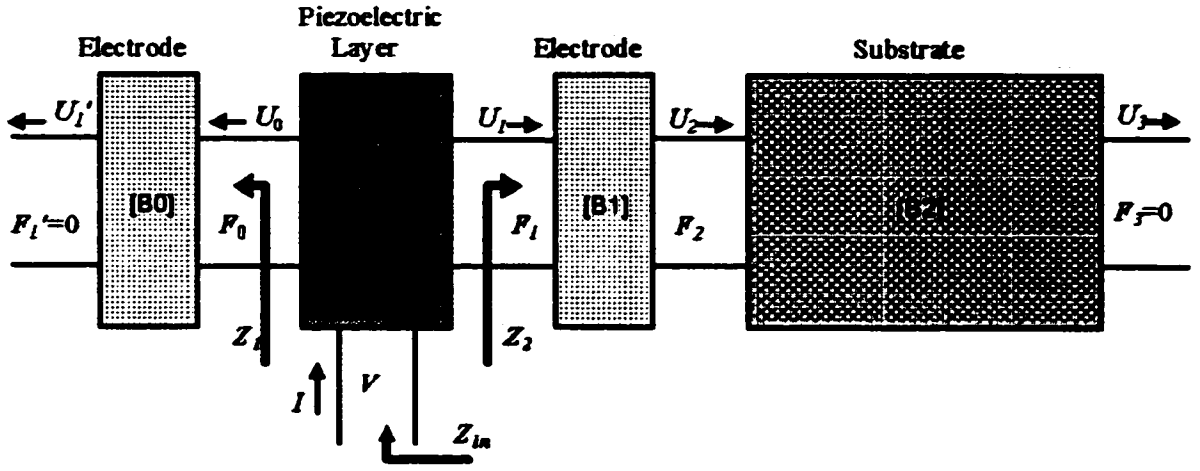

Fig.3.1 *Transfer matrix representation of a 4 layer composite resonator*

Since the left side of the top electrode is a free surface, $F_1' = 0$. Thus, the acoustic impedance of the top electrode, presenting at the left side of the piezoelectric layer, can be deduced by solving the Eq. (3.1)

$$Z_1 = \frac{F_0}{U_0} = jZ_{e1}\tan\gamma_{e1} \tag{3.2}$$

The middle electrode has the same form transfer matrix as the top electrode, since we have defined opposite direction for displacement velocity U at each side of the piezoelectric layer.

$$\begin{bmatrix} F_2 \\ U_2 \end{bmatrix} = \begin{bmatrix} \cos\gamma_{e2} & jZ_{e2}\sin\gamma_{e2} \\ j\sin\gamma_{e2}/Z_{e2} & \cos\gamma_{e2} \end{bmatrix} \begin{bmatrix} F_3 \\ U_3 \end{bmatrix} \tag{3.3}$$

where $Z_{e2}=S\rho_{e2}v_{e2}$ is the acoustic impedance of the middle electrode, $\gamma_{e2}=\omega l_{e2}/v_{e2}$ is the phase delay of the acoustic wave in the middle electrode. The substrate plate also has the same form transfer matrix,

$$\begin{bmatrix} F_3 \\ U_3 \end{bmatrix} = \begin{bmatrix} \cos\gamma_{sb} & jZ_{sb}\sin\gamma_{sb} \\ j\sin\gamma_{sb}/Z_{sb} & \cos\gamma_{sb} \end{bmatrix} \begin{bmatrix} F_4 \\ U_4 \end{bmatrix} \tag{3.4}$$

where $Z_{sb}=S\rho_{sb}v_{sb}$ is the acoustic impedance of the top electrode, $\gamma_{sb}=\omega l_{sb}/v_{sb}$ is the phase delay in the substrate plate. Put Eq. (3.3) and (3.4) together,

$$\begin{bmatrix} F_2 \\ U_2 \end{bmatrix} = \begin{bmatrix} \cos\gamma_{e2} & jZ_{e2}\sin\gamma_{e2} \\ j\sin\gamma_{e2}/Z_{e2} & \cos\gamma_{e2} \end{bmatrix} \cdot \begin{bmatrix} \cos\gamma_{sb} & jZ_{sb}\sin\gamma_{sb} \\ j\sin\gamma_{sb}/Z_{sb} & \cos\gamma_{sb} \end{bmatrix} \begin{bmatrix} F_4 \\ U_4 \end{bmatrix} \tag{3.5}$$

Since the right side of the substrate is also a free surface, $F_4 = 0$. By solving Eq (3.5) we get the acoustic impedance of the middle electrode and the substrate, presenting at the right side of the piezoelectric layer,

$$Z_2 = \frac{F_2}{U_2} = j\frac{Z_{sb}\tan\gamma_{sb} + Z_{e2}\tan\gamma_{e2}}{1-(Z_{sb}/Z_{e2})\tan\gamma_{e2}\tan\gamma_{sb}} \tag{3.6}$$

The transfer matrix of the piezoelectric film is given by

$$\begin{bmatrix} V \\ I \end{bmatrix} = [A] \cdot \begin{bmatrix} F_2 \\ U_2 \end{bmatrix} \tag{3.7}$$

where $[A]$ is the same as defined in Eq. (2.2). The electric input impedance of such a four layer composite resonator is given by

$$Z_{in} = \frac{V}{I} = \frac{1}{j\omega C_0} \cdot \left[1 - \frac{k_t^2}{\gamma} \cdot \frac{(z_1+z_2)\cdot\sin\gamma + j\cdot 2(1-\cos\gamma)}{(z_1+z_2)\cdot\cos\gamma + j\cdot(1+z_1z_2)\cdot\sin\gamma}\right] \tag{3.8}$$

where $z_1 = Z_1/Z_0$ and $z_2 = Z_2/Z_0$ are the normalized acoustic impedance of the top electrode layer and the middle electrode/substrate combination.

3.2 The first normal region, Δf_N and k_t^2

The parallel resonances of a composite resonator correspond to infinite impedance $Z_{in} \to \infty$ when the materials are lossless. This gives a determination equation for the parallel resonant frequencies by setting the denominator of Eq. (3.8) to zero.

$$(z_1 + z_2)\cdot\cos\gamma + j\cdot(1 + z_1 z_2)\cdot\sin\gamma = 0 \tag{3.9}$$

Assuming the electrodes are much thinner than the piezoelectric film, at the center of the first normal region, the m_N+1 order resonant mode corresponds to

$$\gamma \approx \pi, \qquad \gamma_{sb} \approx m_N\pi \tag{3.10}$$

where m_N is the mode order of the bare substrate plate resonator at the center of the first normal region. By using the same approximate expressions as in the two layer case,

$$\gamma = \pi + \varepsilon, \qquad \gamma_{sb} = m_N\cdot\pi + \delta \tag{3.11}$$

we get

$$\begin{aligned} &\tan\gamma = \tan(\pi + \varepsilon) \approx \varepsilon \\ &\tan\gamma_{sb} = \tan(m_N\pi + \delta) \approx \delta \end{aligned} \tag{3.12}$$

Since the electrodes are assumed much thinner than the piezoelectric film, this means $\gamma_{e1} << 1$ and $\gamma_{e2} << 1$ in the first normal region. Thus, we have following approximate equations:

$$\tan\gamma_{e1} \approx \gamma_{e1}, \qquad \tan\gamma_{e2} \approx \gamma_{e2} \tag{3.13}$$

Therefore,

$$z_1 = \frac{Z_1}{Z_0} \approx j\frac{Z_{e1}}{Z_0}\gamma_{e1} = jz_{e1}\gamma_{e1} \tag{3.14}$$

and

$$Z_2 \approx j \cdot \frac{z_{sb}\delta + z_{e2} \cdot \gamma_{e2}}{1-(z_{sb}/z_{e2})\delta\gamma_{e2}} \tag{3.15}$$

Ignore the second order small quantity $\delta\gamma_{e2}$

$$z_2 = \frac{Z_2}{Z_0} \approx j \cdot (z_{sb} \cdot \delta + z_{e2} \cdot \gamma_{e2}) \tag{3.16}$$

If the acoustic impedances of the electrodes are comparable with the acoustic impedance of the piezoelectric layer, z_{e1} and z_{e2} are in the order of unit, then z_1 and z_2 are first order small quantities in the first normal region. Substitute approximations (3.13) ~ (3.16) into parallel resonant frequency equation (3.9), we get

$$[jz_{e1}\gamma_{e1} + j \cdot (z_{sb} \cdot \delta + z_{e2} \cdot \gamma_{e2})] + j \cdot [1 + jz_{e1}\gamma_{e1} \cdot j \cdot (z_{sb} \cdot \delta + z_{e2} \cdot \gamma_{e2})] \cdot \varepsilon = 0 \tag{3.17}$$

Replace δ, ε with equations (3.11)

$$\begin{aligned}
&(jz_{e1}\gamma_{e1} + j \cdot [z_{sb} \cdot (\gamma - m_N\pi) + z_{e2} \cdot \gamma_{e2}]) \\
&\qquad + j(1 + jz_{e1}\gamma_{e1} \cdot j \cdot [z_{sb} \cdot (\gamma - m_N\pi) + z_{e2} \cdot \gamma_{e2}]) \cdot (\gamma - \pi) = 0 \\
&j\left[z_{e1} \cdot \frac{2\pi f l_{e1}}{v_{e1}} + z_{sb}\left(\frac{2\pi f l_{sb}}{v_{sb}} - m_N\pi\right) + z_{e2}\frac{2\pi f l_{e2}}{v_{e2}} \right] \\
&\qquad + j\left\{ 1 - z_{e1} \cdot \frac{2\pi f l_{e1}}{v_{e1}} \cdot \left[z_{sb}\left(\frac{2\pi f l_{sb}}{v_{sb}} - m_N\pi\right) + z_{e2}\frac{2\pi f l_{e2}}{v_{e2}} \right] \right\} \left(\frac{2\pi f l}{v_0} - \pi \right) = 0
\end{aligned} \tag{3.18}$$

The m_N+1 order parallel resonant frequency of such a four-layer composite resonator is

$$f_p(m_N + 1) = \frac{(m_N z_{sb} + 1)}{2\left(\frac{z_{e1}l_{e1}}{v_{e1}} + \frac{z_{sb}l_{sb}}{v_{sb}} + \frac{z_{e2}l_{e2}}{v_{e2}} + \frac{l}{v} \right)} \tag{3.19}$$

The spacing of two parallel resonant frequencies in the first normal region is

$$\Delta f_N = f_p(m_N + 1) - f_p(m_N)$$

$$= \frac{1}{2} \frac{z_{sb}}{\frac{z_{e1} l_{e1}}{v_{e1}} + \frac{z_{sb} l_{sb}}{v_{sb}} + \frac{z_{e2} l_{e2}}{v_{e2}} + \frac{l}{v}}$$

$$= \frac{1}{2} \frac{\rho_{sb} v_{sb}}{\rho_{e1} l_{e1} + \rho_{sb} l_{sb} + \rho_{e2} l_{e2} + \rho l}$$

$$= \Delta f_0 \left(1 + \frac{\rho_{e1} l_{e1} + \rho_{e2} l_{e2} + \rho l}{\rho_{sb} l_{sb}} \right)^{-1} \tag{3.20}$$

where $\Delta f_0 = \frac{v_{sb}}{2 l_{sb}}$ is the parallel resonance frequency spacing of the bare substrate plate.

On the other hand, by setting the numerator of Eq. (3.8) to zero, we get the determination equation for the series resonant frequencies of a lossless four layer composite resonator.

$$[(z_1 + z_2) \cdot \cos\gamma + j \cdot (1 + z_1 z_2) \cdot \sin\gamma] - \frac{k_t^2}{\gamma} \cdot [(z_1 + z_2) \cdot \sin\gamma + j \cdot 2(1 - \cos\gamma)] = 0 \tag{3.21}$$

This gives an expression for k_t^2

$$k_t^2 = \frac{\gamma[(z_1 + z_2) + j(1 + z_1 z_2)\tan\gamma]}{(z_1 + z_2)\tan\gamma + 2j(\sec\gamma - 1)} \tag{3.22}$$

As proved before, both z_1 and z_2 are first order small quantities in the first normal region, therefore $z_1 z_2$ and $(z_1 + z_2)\tan\gamma$ are second order small quantities. Ignore these small terms and use the approximation

$$\sec\gamma = \sec(\pi + \varepsilon) \approx -1 \tag{3.23}$$

we get an approximate expression for k_t^2 :

$$k_t^2 = \frac{\gamma}{-4j}\left[(z_1 + z_2) + j(\gamma - \pi)\right]$$

$$= \frac{1}{-4j}\frac{2\pi f_s l}{v}\left[j2\pi f_s z_{e1}\frac{l_{e1}}{v_{e1}} + jz_{sb}(2\pi f_s \frac{l_{sb}}{v_{sb}} - m\pi) + j2\pi f_s z_{e2}\frac{l_{e2}}{v_{e2}} + j(j2\pi f_s \frac{l}{v} - \pi)\right]$$

$$= \frac{1}{-4}\frac{2\pi f_s l}{v}\left[2\pi f_s (z_{e1}\frac{l_{e1}}{v_{e1}} + z_{sb}\frac{l_{sb}}{v_{sb}} + z_{e2}\frac{l_{e2}}{v_{e2}} + \frac{l}{v}) - (z_{sb}m_N + 1)\pi)\right] \qquad (3.24)$$

Substitute (3.19) into above equation,

$$k_t^2 = \frac{\pi^2 l}{v} f_s (f_p - f_s)\left(z_{e1}\frac{l_{e1}}{v_{e1}} + z_{sb}\frac{l_{sb}}{v_{sb}} + z_{e2}\frac{l_{e2}}{v_{e2}} + \frac{l}{v}\right)$$

$$= \frac{\pi^2}{4}\frac{f_s}{f_p}\frac{f_p - f_s}{f_p}\frac{(1 + m_N z_{sb})^2}{\left(1 + \frac{\rho_{e1}l_{e1} + \rho_{e2}l_{e2} + \rho_{sb}l_{sb}}{\rho l}\right)}$$

$$= \frac{(1 + m_N z_{sb})^2}{\left(1 + \frac{\rho_{e1}l_{e1} + \rho_{e2}l_{e2} + \rho_{sb}l_{sb}}{\rho l}\right)} \cdot k_{eff}^2(N) \qquad (3.25)$$

where the effective coupling coefficient k_{eff}^2 has the same definition as Eq. (2.25)

As in the two layer case, the k_t^2 equation can be further simplified. As shown in equation (3.10), m_N is the resonant mode order of the substrate plate at the center of the first normal region. For the case of a four layer composite resonator, the composite resonator can be considered to be a top resonator composed of the piezoelectric film, the top electrode and part of the middle electrode deposited on a composite substrate composed of the other part of the middle electrode and the substrate plate. As an approximation, we split half of the middle electrode into the top resonator and the other half into the composite substrate (Fig.3.2).

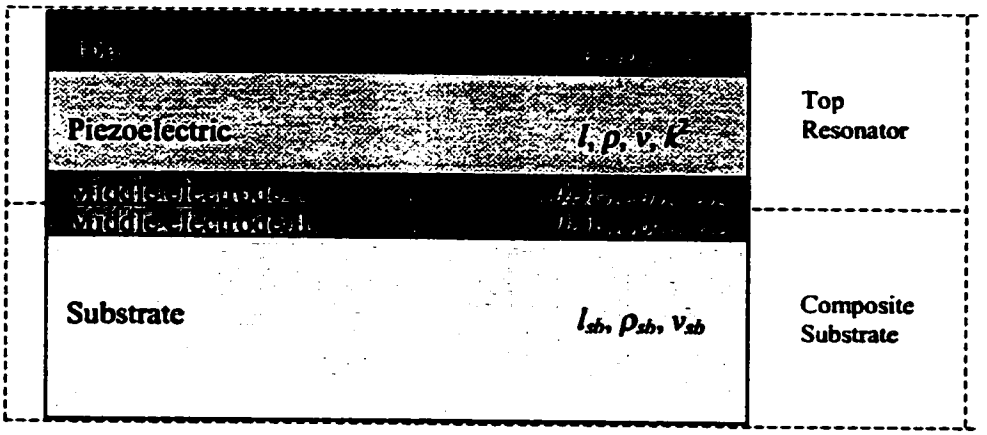

Fig.3.2 *Split of middle electrode*

The center frequency of the first normal region corresponds to the resonant frequency of the top resonator, which can be derived from (3.9) by setting $z_2 = 0.5jz_{e2}\gamma_{e2}$. Ignore the second order small quantity $z_1 z_2$ for thin electrode assumption, we get

$$(jz_{e1}\gamma_{e1} + 0.5jz_{e2}\gamma_{e2}) + j\tan\gamma = 0 \tag{3.26}$$

Using approximation $\tan\gamma = \pi - \gamma$,

$$z_{e1}\gamma_{e1} + 0.5jz_{e2}\gamma_{e2} + \gamma = \pi \tag{3.27}$$

The resonant frequency of the top resonator then can be derived as

$$f_c = \frac{v}{2(l + \rho_{e1}l_{e1}/\rho + 0.5\rho_{e2}l_{e2}/\rho)} \tag{3.28}$$

Similarly, the fundamental resonant frequency of the composite substrate is

$$f_{sb} = \frac{v_{sb}}{(l_{sb} + 0.5\rho_{e2}l_{e2}/\rho_{sb})} \tag{3.29}$$

Thus the ratio R is

$$R = \frac{f_c}{f_{sb}} = \frac{v(l_{sb} + 0.5\rho_{e2}l_{e2}/\rho_{sb})}{v_{sb}(l + \rho_{e1}l_{e1}/\rho + 0.5\rho_{e2}l_{e2}/\rho)} \tag{3.30}$$

m_N is the round integer of R

$$m_N = \text{round}(R) \tag{3.31}$$

If R is close to an integer, or is large enough that the fraction part can be ignored, $m_N \approx R$.

$$1 + m_N z_{sb} = \frac{\rho\, l + \rho_{e1}l_{e1} + \rho_{e2}l_{e2} + \rho_{sb}l_{sb}}{\rho\, l + \rho_{e1}l_{e1} + 0.5\rho_{e2}l_{e2}} \tag{3.32}$$

Substitute Eq.(3.32) into (3.25), we get a simplified expression for the electromechanical coupling coefficient.

$$k_t^2 = \frac{\rho l \cdot (\rho l + \rho_{e1}l_{e1} + \rho_{e2}l_{e2} + \rho_{sb}l_{sb})}{(\rho l + \rho_{e1}l_{e1} + 0.5\rho_{e2}l_{e2})^2} \cdot k_{eff}^2 (m_N + 1) \tag{3.33}$$

3.3 The first transition region, Δf_T and k_t^2

The first transition region is the area where $\gamma \approx \pi/2$. We assume that

$$\gamma = \pi/2 + \varepsilon', \qquad \gamma_{sb} = (m_T + 1/2)\pi + \delta' \tag{3.34}$$

where m_T is the mode order of the bare substrate plate near the center of the first transition region. Therefore, we get approximate expressions in the first transition region as

$$\sin\gamma \approx 1, \qquad \cos\gamma \approx -\varepsilon', \qquad \tan\gamma_{sb} \approx -1/\delta'. \tag{3.35}$$

By taking these approximations into the expression of Z_2, Eq. (3.6), we get

$$z_2 = \frac{j}{Z_0} \cdot \frac{Z_{sb} \cdot \tan\gamma_{sb} + Z_{e2} \cdot \tan\gamma_{e2}}{1 - (Z_{sb}/Z_{e2}) \cdot \tan\gamma_{sb} \tan\gamma_{e2}}$$

$$\approx j \cdot \frac{z_{sb} \frac{1}{-\delta'} + z_{e2}\gamma_{e2}}{1 + \frac{z_{sb}}{z_{e2}} \cdot \frac{\gamma_{e2}}{\delta'}}$$

$$= j \cdot \frac{-z_{sb} + z_{e2}\delta'\gamma_{e2}}{\delta' + \frac{z_{sb}}{z_{e2}} \cdot \gamma_{e2}} \tag{3.36}$$

Ignore the second order small item $\delta'\gamma_{e2}$

$$z_2 \approx -j \cdot \left(\frac{\delta'}{z_{sb}} + \frac{\gamma_{e2}}{z_{e2}} \right)^{-1} \tag{3.37}$$

We can see here that in the first transition region, z_2 is a first order large quantity. Substituting the approximations (3.14), (3.35) and (3.37) into the parallel resonance frequency equation (3.9), we get

$$\left[jz_{e1}\gamma_{e1} - j \cdot \left(\frac{\delta'}{z_{sb}} + \frac{\gamma_{e2}}{z_{e2}} \right)^{-1} \right] \cdot (-\varepsilon') + j \cdot \left[1 - j \cdot (jz_{e1}\gamma_{e1}) \left(\frac{\delta'}{z_{sb}} + \frac{\gamma_{e2}}{z_{e2}} \right)^{-1} \right] \cdot 1 = 0 \tag{3.38}$$

In the first bracket, the first term is a small quantity and the second term is a large quantity, as an approximation, we ignore the first term and get

$$\frac{j\varepsilon'}{\frac{\delta'}{z_{sb}} + \frac{\gamma_{e2}}{z_{e2}}} + j \frac{\frac{\delta'}{z_{sb}} + \frac{\gamma_{e2}}{z_{e2}} + z_{e1}\gamma_{e1}}{\frac{\delta'}{z_{sb}} + \frac{\gamma_{e2}}{z_{e2}}} = 0$$

$$\varepsilon' + \frac{\delta'}{z_{sb}} + \frac{\gamma_{e2}}{z_{e2}} + z_{e1}\gamma_{e1} = 0$$

$$(\gamma - \frac{\pi}{2}) + \frac{\gamma_{sb} - (m_T + 1/2)\pi}{z_{sb}} + \frac{\gamma_{e2}}{z_{e2}} + z_{e1}\gamma_{e1} = 0$$

$$2\pi f_p\left(\frac{l}{v}+\frac{l_{sb}}{z_{sb}v_{sb}}+\frac{l_{e2}}{z_{e2}v_{e2}}+z_{e1}\frac{l_{e1}}{v_{e1}}\right)=\frac{\pi}{2}+\frac{(m_T+1/2)\pi}{z_{sb}} \tag{3.39}$$

Thus, we get the parallel resonant frequency in the first transition region

$$f_p=\frac{1}{2z_{sb}}\frac{m_T+1/2+z_{sb}/2}{\left(\frac{l}{v}+\frac{l_{sb}}{z_{sb}v_{sb}}+\frac{l_{e2}}{z_{e2}v_{e2}}+z_{e1}\frac{l_{e1}}{v_{e1}}\right)} \tag{3.40}$$

The spacing of the parallel resonance frequencies *SPRR* in the first transition region is

$$\begin{aligned}\Delta f_T&=\frac{1}{2z_{sb}}\frac{1}{\left(\frac{l}{v}+\frac{l_{sb}}{z_{sb}v_{sb}}+\frac{l_{e2}}{z_{e2}v_{e2}}+z_{e1}\frac{l_{e1}}{v_{e1}}\right)}\\&=\frac{v_{sb}}{2l_{sb}}\frac{1}{\left(1+z_{sb}\frac{v_{sb}l}{v\,l_{sb}}+\frac{z_{sb}v_{sb}l_{e2}}{z_{e2}v_{e2}l_{sb}}+z_{sb}z_{e1}\frac{v_{sb}l_{e1}}{v_{e1}l_{sb}}\right)}\\&=\Delta f_0\left(1+\frac{\rho_{sb}v_{sb}^2}{\rho v^2}\frac{l}{l_{sb}}+\frac{\rho_{sb}v_{sb}^2}{\rho_{e2}v_{e2}^2}\frac{l_{e2}}{l_{sb}}+\frac{\rho_{sb}\rho_{e1}v_{sb}^2}{\rho^2v^2}\frac{l_{e1}}{l_{sb}}\right)^{-1}\end{aligned} \tag{3.41}$$

As in the first normal region, the series resonance frequencies in the first transition region are determined by (3.21). Since

$$z_2\approx -j\cdot\left(\frac{\delta}{z_{sb}}+\frac{\gamma_{e2}}{z_{e2}}\right)^{-1}>>1,\ z_1=jz_{e1}\gamma_{e1}<<1 \tag{3.42}$$

we ignore z_1 in the term of z_1+z_2 in Eq.(3.21). Also use the approximation of Eq. (3.35), Eq. (3.21) can be simplified in the first transition region as

$$z_2(-\varepsilon')+j\cdot(1+z_1z_2)=\frac{k_t^2}{\gamma}\cdot[z_2+j\cdot 2(1+\varepsilon')] \tag{3.43}$$

Therefore k_t^2 can be expressed as

$$k_t^2 = \gamma \frac{z_2(-\varepsilon') + j\cdot(1 + z_1 z_2)}{[z_2 + j\cdot 2(1+\varepsilon')]}$$

$$= \gamma \frac{z_2(-\varepsilon') + j\cdot(1 + z_1 z_2)}{z_2 \Gamma}$$

$$= \gamma \frac{-\varepsilon' + j\cdot(1/z_2 + z_1)}{\Gamma}$$

$$= \frac{\gamma}{\Gamma}\left[-\varepsilon' + j\cdot\left(\left(-j\cdot\frac{1}{\frac{\delta'}{z_{sb}} + \frac{\gamma_{e2}}{z_{e2}}}\right)^{-1} + jz_{e1}\gamma_{e1}\right)\right]$$

$$= \frac{-\gamma}{\Gamma}\left[\varepsilon' + \frac{\delta'}{z_{sb}} + \frac{\gamma_{e2}}{z_{e2}} + z_{e1}\gamma_{e1}\right]$$

$$= \frac{-\gamma}{\Gamma}\left[\gamma - \frac{\pi}{2} + \frac{\gamma_{sb} - (m_T + 1/2)\pi}{z_{sb}} + \frac{\gamma_{e2}}{z_{e2}} + z_{e1}\gamma_{e1}\right]$$

$$= \frac{-\gamma}{\Gamma}\left[\left(\gamma + \frac{\gamma_{sb}}{z_{sb}} + \frac{\gamma_{e2}}{z_{e2}} + z_{e1}\gamma_{e1}\right) - \left(1 + \frac{2m_T + 1}{z_{sb}}\right)\frac{\pi}{2}\right] \qquad (3.44)$$

Substitute Eq.(3.40) into above equation, we get

$$k_t^2 = \frac{-2\pi f_s l}{\Gamma v}\left[2\pi f_s\left(\frac{l}{v} + \frac{l_{sb}}{z_{sb}v_{sb}} + \frac{l_{e2}}{z_{e2}v_{e2}} + z_{e1}\frac{l_{e1}}{v_{e1}}\right) - 2\pi f_p\left(\frac{l}{v} + \frac{l_{sb}}{z_{sb}v_{sb}} + \frac{l_{e2}}{z_{e2}v_{e2}} + z_{e1}\frac{l_{e1}}{v_{e1}}\right)\right]$$

$$= \frac{4\pi^2 l}{\Gamma v}\left(\frac{l}{v} + \frac{l_{sb}}{z_{sb}v_{sb}} + \frac{l_{e2}}{z_{e2}v_{e2}} + z_{e1}\frac{l_{e1}}{v_{e1}}\right) f_s(f_p - f_s)$$

$$= \frac{4\pi^2 l}{\Gamma v}\left(\frac{l}{v} + \frac{l_{sb}}{z_{sb}v_{sb}} + \frac{l_{e2}}{z_{e2}v_{e2}} + z_{e1}\frac{l_{e1}}{v_{e1}}\right) f_p^2 \cdot \frac{f_s}{f_p}\frac{f_p - f_s}{f_p}$$

$$= \frac{l}{v}\frac{(2m_T + 1 + z_{sb})^2}{\left(\frac{l}{v} + \frac{l_{sb}}{z_{sb}v_{sb}} + \frac{l_{e2}}{z_{e2}v_{e2}} + z_{e1}\frac{l_{e1}}{v_{e1}}\right)}\frac{k_{eff}^2}{\Gamma}$$

$$= \frac{[(2m_T+1)/z_{sb}+1]^2}{\left(1+\frac{\rho v^2}{\rho_{sb}v_{sb}^2}\frac{l_{sb}}{l}+\frac{\rho v^2}{\rho_{e2}v_{e2}^2}\frac{l_{e2}}{l}+\frac{\rho}{\rho_{e1}}\frac{l_{e1}}{l}\right)}\frac{k_{eff}^2}{\Gamma} \tag{3.45}$$

Γ is a correction factor with the value at the order of unity:

$$\Gamma = 1+2j\frac{(1+\varepsilon')}{z_2}$$

$$= 1-2(1+\varepsilon')\left(\frac{\delta'}{z_{sb}}+\frac{\gamma_{e2}}{z_{e2}}\right)$$

$$= 1-2\left(1+\gamma-\frac{\pi}{2}\right)\cdot\left(\frac{\gamma_{sb}-(m_T+1/2)\pi}{z_{sb}}+\frac{\gamma_{e2}}{z_{e2}}\right)$$

$$= 1-2\frac{\rho v}{\rho_{sb}v_{sb}}\left(1+\frac{2\pi f_s l}{v}-\frac{\pi}{2}\right)\cdot\left(2\pi f_s\left(\frac{l_{sb}}{v_{sb}}+\frac{\rho_{sb}v_{sb}l_{e2}}{\rho_{e2}v_{e2}^2}\right)-(m_T+1/2)\pi\right) \tag{3.46}$$

This correction factor has the same interpretation as the correction factor for the 2 layer case, stands for the difference between the first transition region center and the (m_T+1) mode series resonance frequency. But here there is a little modification by the middle electrode.

When R is close to an odd integer or is large enough, $m_T \approx \frac{R-1}{2}$,

$$1+(2m_T+1)/z_{sb} \approx 1+R/z_{sb}$$

$$= \frac{\rho l\left[1+\frac{\rho_{e1}l_{e1}}{\rho l}+\frac{\rho v^2}{\rho_{sb}v_{sb}^2}\frac{l_{sb}}{l}+\frac{1}{2}\left(\frac{\rho^2v^2}{\rho_{sb}^2v_{sb}^2}+1\right)\frac{\rho_{e2}l_{e2}}{\rho l}\right]}{\rho l+\rho_{e1}l_{e1}+0.5\rho_{e2}l_{e2}} \tag{3.47}$$

Since the electrodes are usually much thinner than the substrate, we assume that

$$\frac{1+\frac{\rho_{e1}l_{e1}}{\rho l}+\frac{\rho v^2}{\rho_{sb}v_{sb}^2}\frac{l_{sb}}{l}+\frac{1}{2}\left(\frac{\rho^2v^2}{\rho_{sb}^2v_{sb}^2}+1\right)\frac{\rho_{e2}l_{e2}}{\rho l}}{1+\frac{\rho_{e1}l_{e1}}{\rho l}+\frac{\rho v^2}{\rho_{sb}v_{sb}^2}\frac{l_{sb}}{l}+\frac{\rho_{e2}l_{e2}}{\rho l}}\approx 1 \tag{3.48}$$

Bring Eq. (3.47) and (3.48) into (3.45), we get the simplified electromechanical coupling coefficient expression in the first transition region

$$k_t^2=\frac{1+\frac{\rho_{e1}l_{e1}}{\rho l}+\frac{\rho v^2}{\rho_{sb}v_{sb}^2}\frac{l_{sb}}{l}+\frac{1}{2}\left(\frac{\rho^2v^2}{\rho_{sb}^2v_{sb}^2}+1\right)\frac{\rho_{e2}l_{e2}}{\rho l}}{\left(1+\frac{\rho_{e1}l_{e1}}{\rho l}+\frac{1}{2}\frac{\rho_{e2}l_{e2}}{\rho l}\right)^2}\frac{k_{eff}^2(m_T+1)}{\Gamma} \tag{3.49}$$

3.4 Summary

In this chapter, we derived the *Resonant Spectrum Method* for a 4 layer composite resonator when the electrodes are taken into account, which gives six modified formulas.

1. In the first normal region, the *SPRF* is given by

$$\Delta f_N=\Delta f_0\left(1+\frac{\rho_{e1}l_{e1}+\rho_{e2}l_{e2}+\rho l}{\rho_{sb}l_{sb}}\right)^{-1} \tag{3.50}$$

2. In the first transition region, the *SPRF* is given by

$$\Delta f_T=\Delta f_0\left(1+\frac{\rho_{sb}v_{sb}^2}{\rho v^2}\frac{l}{l_{sb}}+\frac{\rho_{sb}v_{sb}^2}{\rho_{e2}v_{e2}^2}\frac{l_{e2}}{l_{sb}}+\frac{\rho_{sb}\rho_{e1}v_{sb}^2}{\rho^2v^2}\frac{l_{e1}}{l_{sb}}\right)^{-1} \tag{3.51}$$

3. The electromechanical coupling coefficient in the first normal region is given by

$$k_t^2 = \frac{(1+m_N z_{sb})^2}{\left(1+\dfrac{\rho_{e1}l_{e1}+\rho_{e2}l_{e2}+\rho_{sb}l_{sb}}{\rho\, l}\right)} \cdot k_{eff}^2(N) \tag{3.52}$$

or the approximate expression when R is an integer or R is large enough

$$k_t^2 = \frac{\rho l \cdot (\rho l + \rho_{e1}l_{e1} + \rho_{e2}l_{e2} + \rho_{sb}l_{sb})}{(\rho l + \rho_{e1}l_{e1} + 0.5\rho_{e2}l_{e2})^2} \cdot k_{eff}^2(m_N + 1) \tag{3.53}$$

4. The electromechanical coupling coefficient in the first transition region is given by

$$k_t^2 = \frac{[(2m_T+1)/z_{sb}+1]^2}{\left(1+\dfrac{\rho v^2}{\rho_{sb}v_{sb}^2}\dfrac{l_{sb}}{l}+\dfrac{\rho v^2}{\rho_{e2}v_{e2}^2}\dfrac{l_{e2}}{l}+\dfrac{\rho}{\rho_{e1}}\dfrac{l_{e1}}{l}\right)} \frac{k_{eff}^2}{\Gamma} \tag{3.54}$$

or the approximate expression when R is an odd integer or R is large enough

$$k_t^2 = \frac{1+\dfrac{\rho_{e1}l_{e1}}{\rho l}+\dfrac{\rho v^2}{\rho_{sb}v_{sb}^2}\dfrac{l_{sb}}{l}+\dfrac{1}{2}\left(\dfrac{\rho^2 v^2}{\rho_{sb}^2 v_{sb}^2}+1\right)\dfrac{\rho_{e2}l_{e2}}{\rho l}}{\left(1+\dfrac{\rho_{e1}l_{e1}}{\rho l}+\dfrac{1}{2}\dfrac{\rho_{e2}l_{e2}}{\rho l}\right)^2} \frac{k_{eff}^2(m_T+1)}{\Gamma} \tag{3.55}$$

For a low frequency composite resonator, usually l_{e1}, $l_{e2} << l$. These formulae revert to that corresponding to simple 2 layer composite resonator of Chapter 2.

CHAPTER 4. MEASUREMENT ON ZNO/SIO_2 COMPOSITE RESONATORS

In order to demonstrate the feasibility of the *Resonant Spectrum Method*, a few composite resonator samples have been measured and the acoustic properties of the piezoelectric film in the resonators have been evaluated with the *Resonant Spectrum Method* derived in the last chapter.

4.1 The samples and the experiment setup

The resonator samples are composed of ZnO films which are sandwiched between two aluminum electrodes and deposited on fused quartz substrates with different thickness. The thickness of the ZnO films is around 5 μm and the thicknesses of the fused quartz substrates are around 62mil and 92mil, respectively. A circular ground electrode of aluminum approximately 0.4μm thick is underlying the ZnO film, and 4 small circular electrodes of 0.4μm aluminum with a diameter of about 1mm are coated on the top of ZnO film, forming 4 composite resonators (Fig. 4.1) on each substrate plate. The samples are provided by Dr. F.S. Hickernell from Motorola [38].

The resonators were measured in a home-made test fixture. The resonators were placed on a support which contacts the substrate's lower surface only at the four corners so that the resonators can vibrate freely. A pogo probe, which has two pogo pins on the

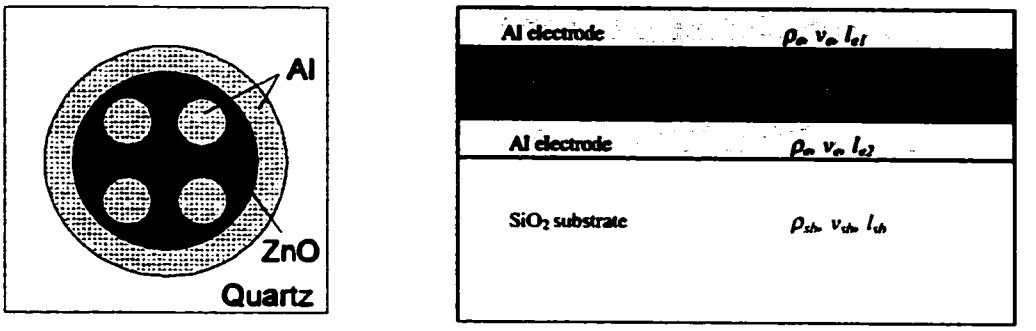

Fig.4.1 *The composite resonators used in the experiment*

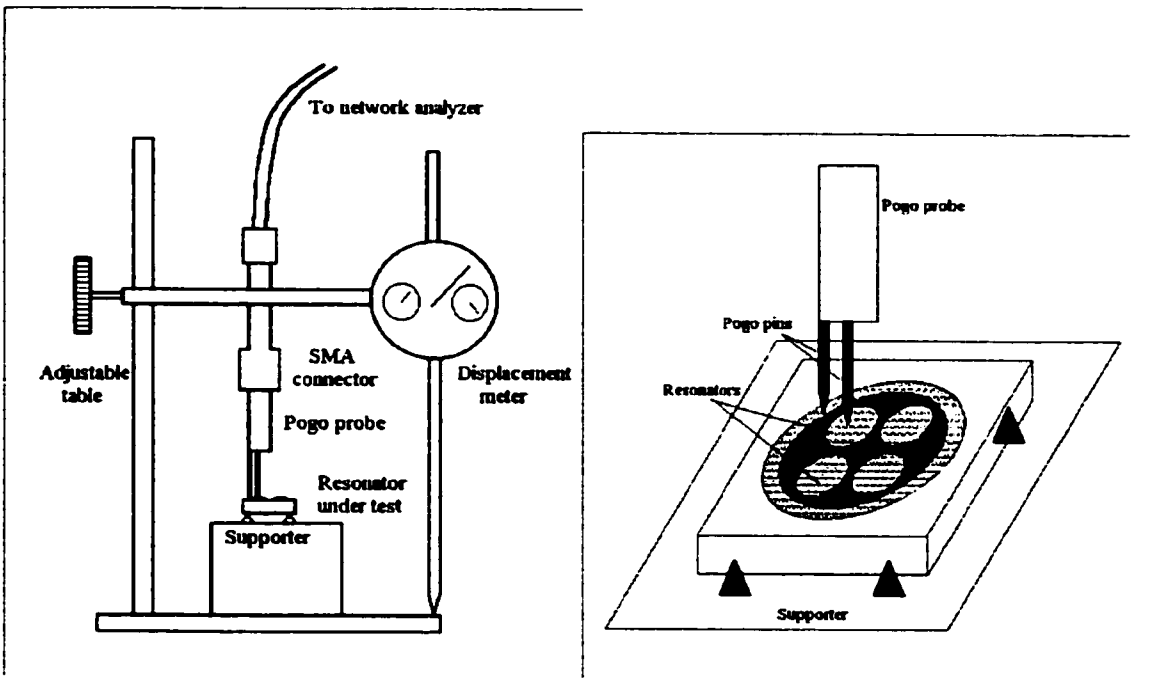

Fig.4.2 *The measurement setup*

tip, was used to make the electric contact with the resonators. The other end of the pogo probe was connected to a network analyzer through a cable. The probe was mounted on an adjustable table. While the probe was moving down to the sample, from the network analyzer it could be seen when the probe touched the sample. After the first touch, the probe continued moving down a certain distance for better contact. A displacement meter was used to monitor the displacement of the probe, ensuring that in each measurement, the pogo probe moved the same distance after the first touch. By this way, the probe contacted the samples with the same pressure, and hence, it is assumed the same contact resistance. Since the calibration could take the contact resistance into account, its effect was ignored in our calculation. For the case where accurate calibration is difficult to implement, the effect of the contact resistance will be discussed in Chapter 5. A schematic diagram of the text fixture is shown in Fig. 4.2.

The reflection coefficients s_{11} of the resonators were measured with an HP8753D network analyzer from 100MHz to 800MHz. Since the maximum number of measurement points of an HP8753D is only 1601 and we want an ultrahigh resolution response to extract resonant spectrum, the whole frequency span of 700MHz was divided into tens of narrow sub-spans, 10MHz each for 62mil thickness samples and 8MHz each for 92mil thickness samples.

The network analyzer was calibrated only once for 700MHz span, and an interpolated calibration was used for each sub-span measurement. The calibration was implemented by applying standards at the tips of the pogo probe, therefore, the propagation delay and contact resistance of the pogo probe are calibrated out. The standard of 50Ω is self-made with an Elite jig (a ceramic plate with 50 transmission lines)

and a 50Ω resistor. The short is a small piece of Al coated substrate. During the calibration procedure, the pogo probe contacts the standards in the same manner as the resonator samples, implying the same contact pressure was applied on the standards and the resonators under test, and therefore the same contact resistances in both cases. Because the electrodes on the Elite jig are made of gold and the electrode on the resonator are aluminum, the contact resistance must have a little difference and the electrode resistance can't be taken into account either. But in fact, the contact resistance and electrode resistance is very small in our experiment. This can be seen from the impedance response of the resonator which will be shown later. For the case that the contact resistors are not the same in calibration and test, Chapter 5 will show its impact on the *Resonant Spectrum Method* and a method to correct the impact.

A LabWindow program running on a PC was used to control the network analyzer for setting the central frequency and span, running the measurement and downloading the measured data to the computer. Thus, high-resolution frequency responses for the whole span were acquired.

4.2 The Control program and the data fitting program

A *LabWindows* program was developed to control an HP8753D network analyzer through GPIB interface to automatically measure the resonators under test. The first motivation of writing this program was to develop a complete program which includes all the functions required by the *Resonant Spectrum Method*. But unfortunately only the part

to control the network analyzer has been completed. Other functions have to be implemented with other software, like *Mathematica*.

The control program includes a setup step and a measurement step. In the setup step, the program will first initialize the network analyzer to a suitable condition, *e.g.* check the connection with the network analyzer, set the network analyzer to listen mode, set the number of measurement point to 1601, set the measurement to s11 configuration and the format to magnitude. Second, the program will ask the user to set the measurement frequency range by setting the start frequency and stop frequency as well as the sub-span for each measurement. Then the program will remind the user to calibrate the analyzer at open, short and load conditions. The measurement step is implemented by clicking a single "Measure" button on the graphic user interface, and the program will automatically setup the network analyzer for each sub-span measurement, download the s_{11} data from the network analyzer, show the data on the graphic window and also save them into the local computer. A new GUI will pop up as the SAVE AS window of standard Windows program. The user will enter a file name and the program will save the s_{11} data for each sub-span measurement in a file name started with the file name input by the user and followed by a series number starting from 000. All the files have an extension name of ".dat". The setup information for the frequency range and sub-span will be saved in the file with the input file name plus extension ".dat". The user can also click the "Cancel" button in the new GUI which will cancel the measurement. The "Load" function is to load the saved s_{11} data into the program and to show them in the graphic window. It gives the user the convenience to check the saved data. The flow chart of this program is shown in Fig.4.3.

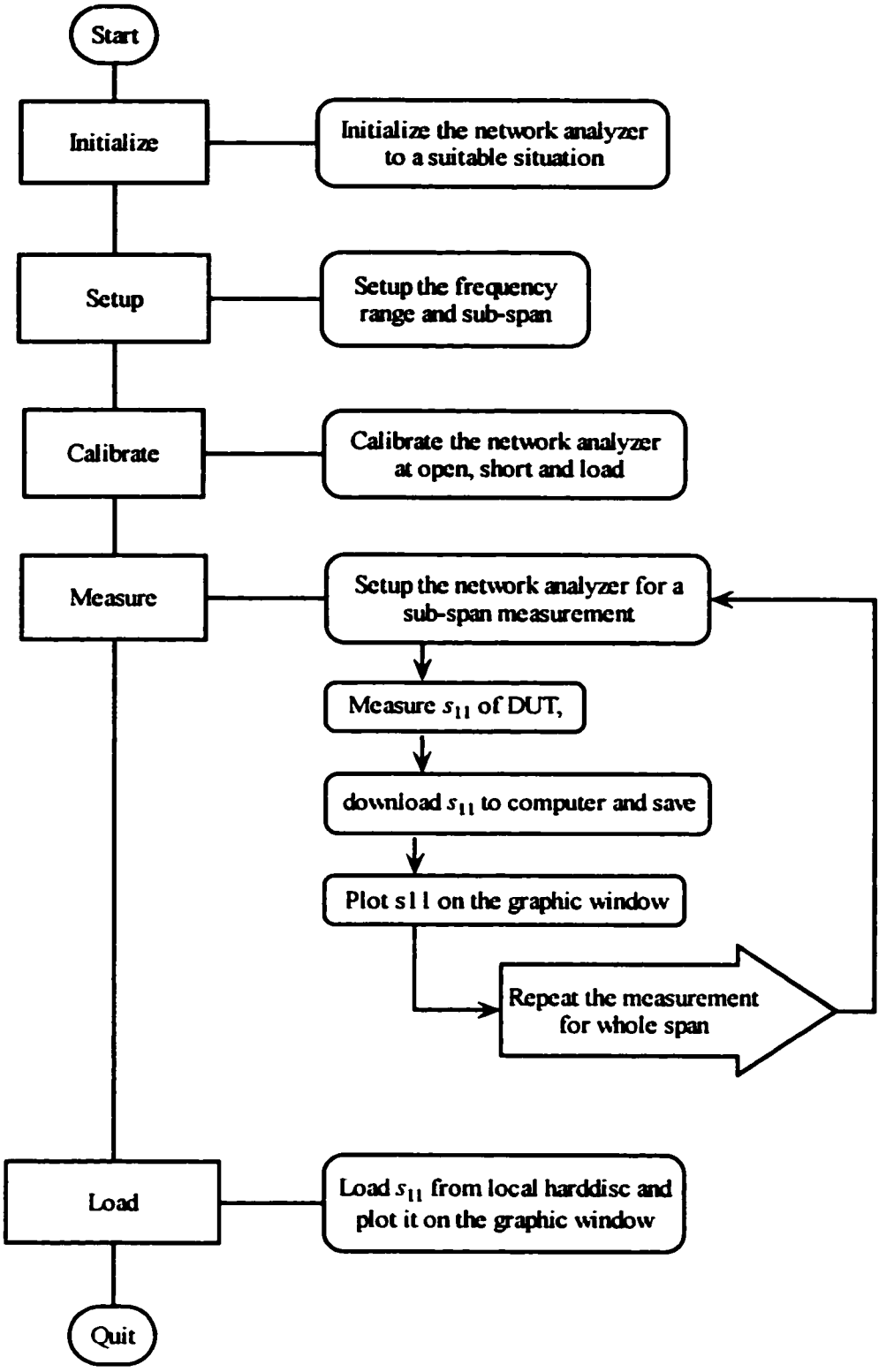

Fig.4.3 *The flowchart of the LabWindow control program*

A few measurement data near a resonant peak are shown in Fig. 4.4. For an 8MHz span, 1601 points measurement, the frequency resolution is merely 5kHz. For 10MHz span, the resolution is even worse. To improve the resolution, an interpolation algorithm was used. The measured s_{11} was converted into impedance Z_{in} and admittance Y_{in} with the equations

$$Z_{in} = R_0 \frac{1+s_{11}}{1-s_{11}} \tag{4.1}$$

$$Y_{in} = \frac{1}{R_0} \frac{1-s_{11}}{1+s_{11}} \tag{4.2}$$

where $R_0 = 50\Omega$ is the system characteristic impedance. Let R_{in} and C_{in} be the real part of Z_{in} and Y_{in}, respectively, *i.e.*, resistance and conductance of the resonator. Near each parallel resonant peak of R_{in} and series resonant peak of C_{in}, a few points were taken for curve fitting by a parabolic function. The maxima of the fitting functions for R_{in} and C_{in} were taken as the parallel and series resonant frequencies, respectively. The fitting results are also shown in Fig.4.4. By repeating the curve fitting process and maximum evaluation for each resonant peak, high accurate resonant spectra were obtained. Sometimes, the maximum of a resonance is just located at the edge of a sub-span measurement, *i.e.*, at point #1, #2 or #1600, #1601. In this set of sub-span data, there are not enough points near the resonant peak for curve fitting. Thus, two sets of data from adjacent sub-span measurement have to be combined first and then curve fitting and maximum extraction can be executed. A *Mathematica*™ program is developed to realize the curve fitting and resonant frequency extraction over the whole span. The program will also plot the *SPRF* and $k_{eff}^2(m)$ *vs.* frequency. Its flow chart is show in Fig. 4.5.

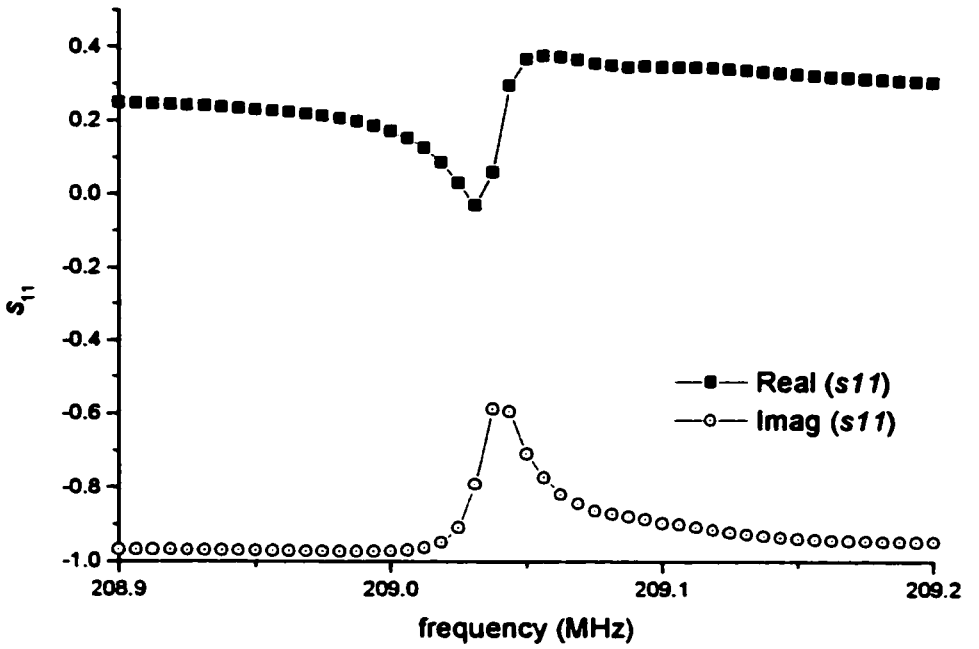

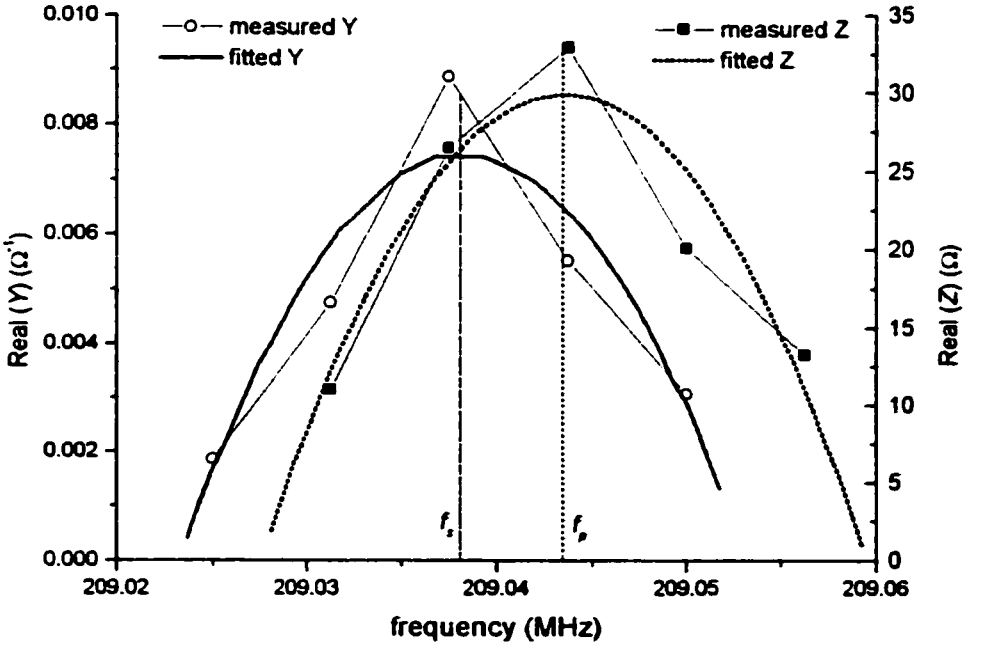

Fig.4.4 *The s_{11} and curve fitting near one resonance*

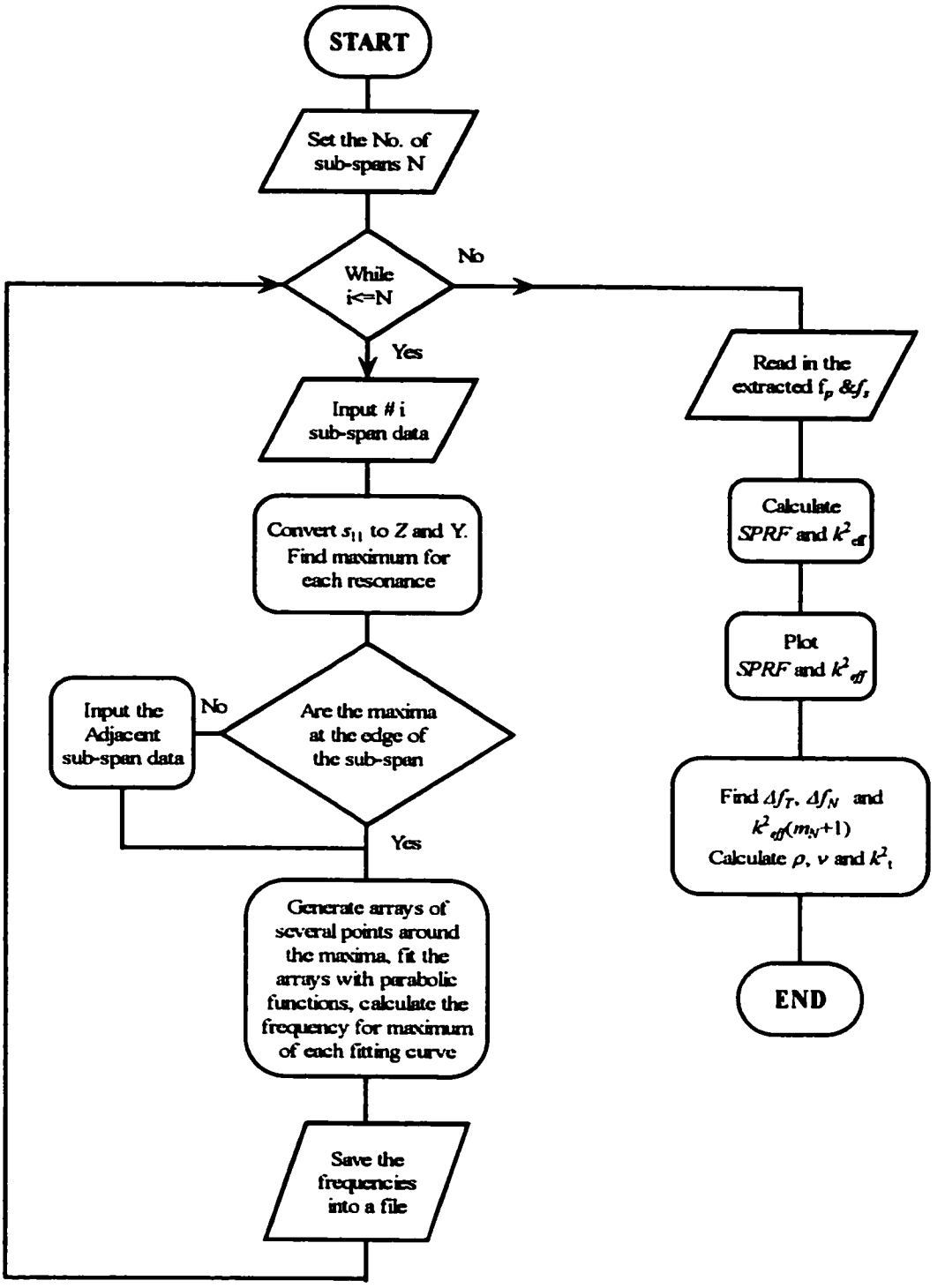

Fig.4.5 *The flow chart of a Mathematica program to extract the resonant spectra and to apply the Resonant Spectrum Method to the experimental data*

4.3 The experimental results

A few ZnO/fused Quartz composite resonator samples with 62mil and 92mil substrate respectively were measured with the method described above. Although there are 4 resonators on each substrate and all of them have been measured, only a few of them are shown here because of their similarity. Fig. 4.6 shows the s_{11} of one resonator on 62mil substrate in one sub-span. From the figure, it can be seen that some other resonant modes exist. Although they are not dominant, they do sometimes cause trouble in determining the frequency of a resonant peak. Fig. 4.7 shows the real and imaginary

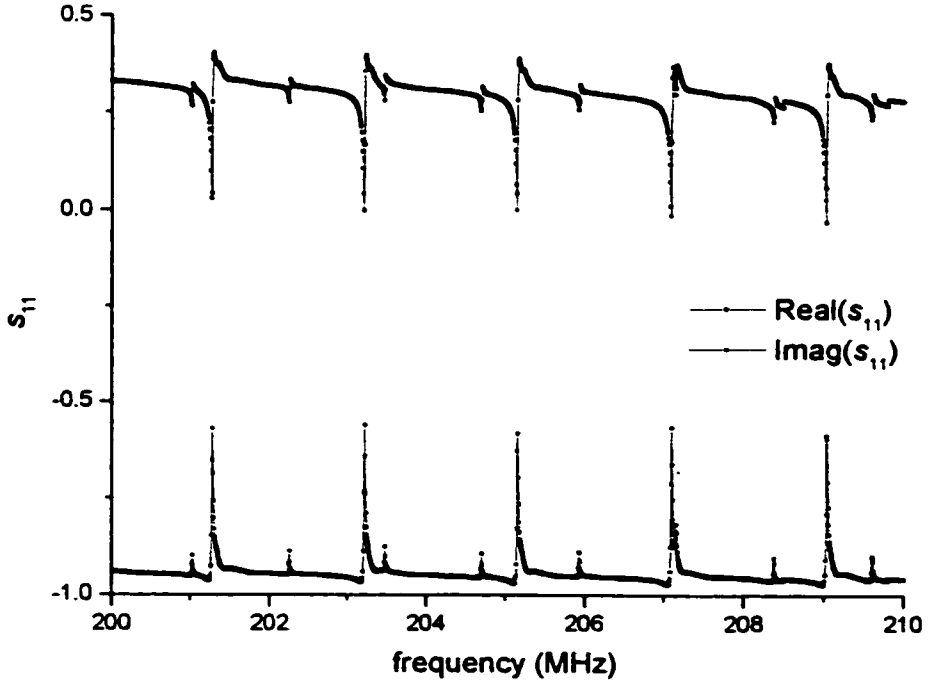

Fig. 4.6 *s_{11} of one sub-span measurement on a ZnO/fused quartz composite resonator*

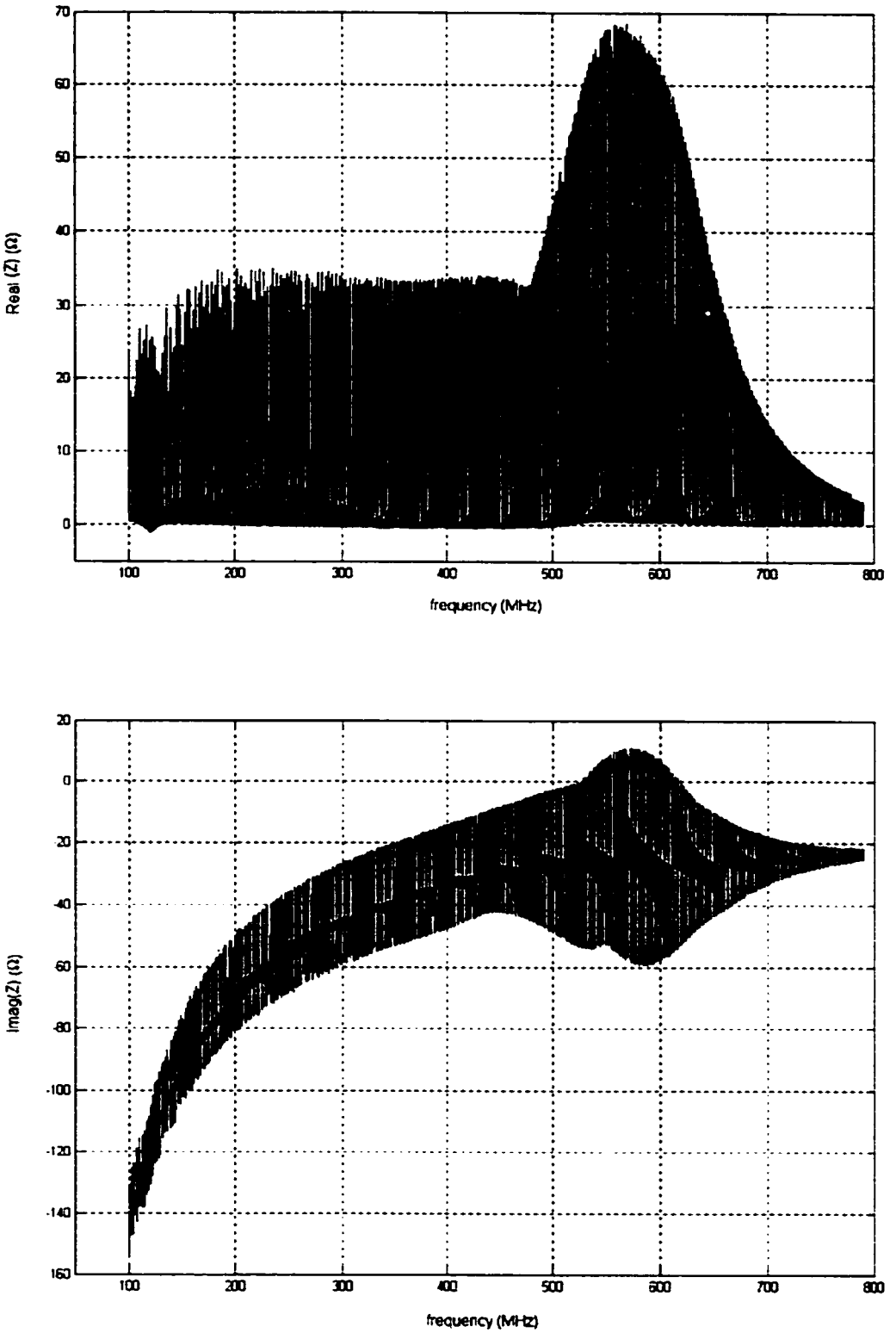

Fig.4.7 *impedance of a ZnO/fused quartz composite resonator*

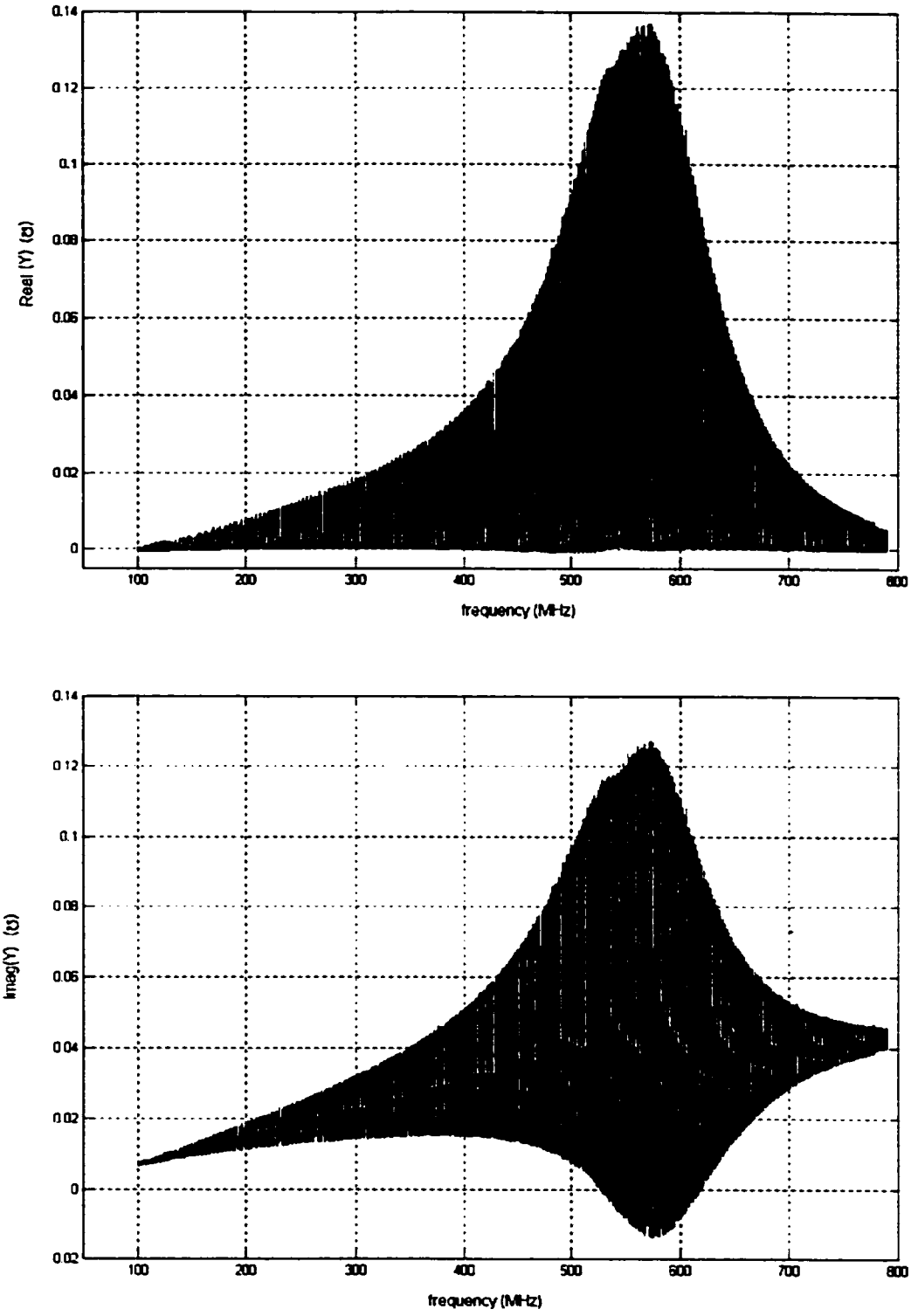

Fig.4.8 *The conductance of a ZnO/fused quartz composite resonator*

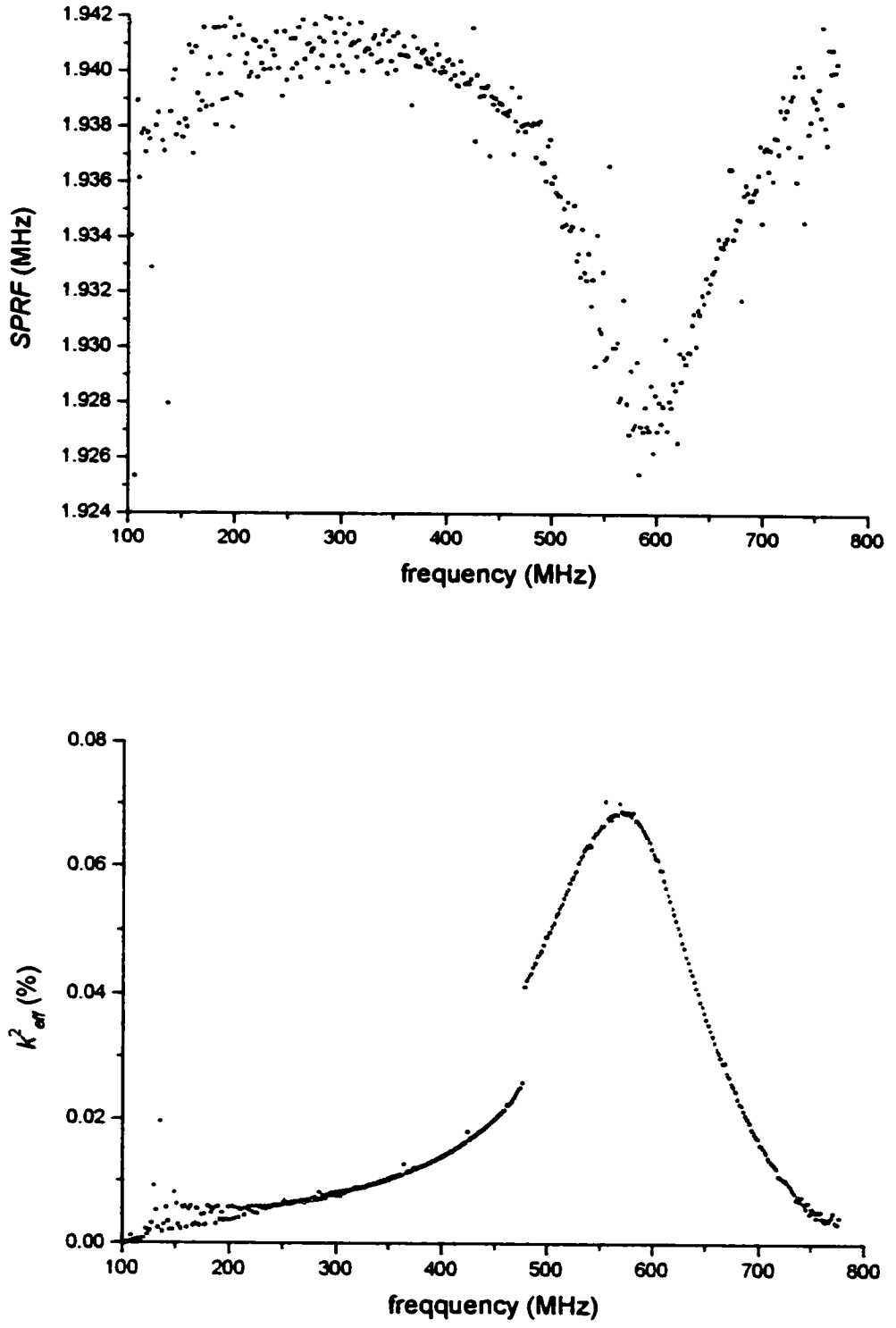

Fig.4.9 *SPRF and k^2_{eff} distributions of sample 1 (62mil substrate)*

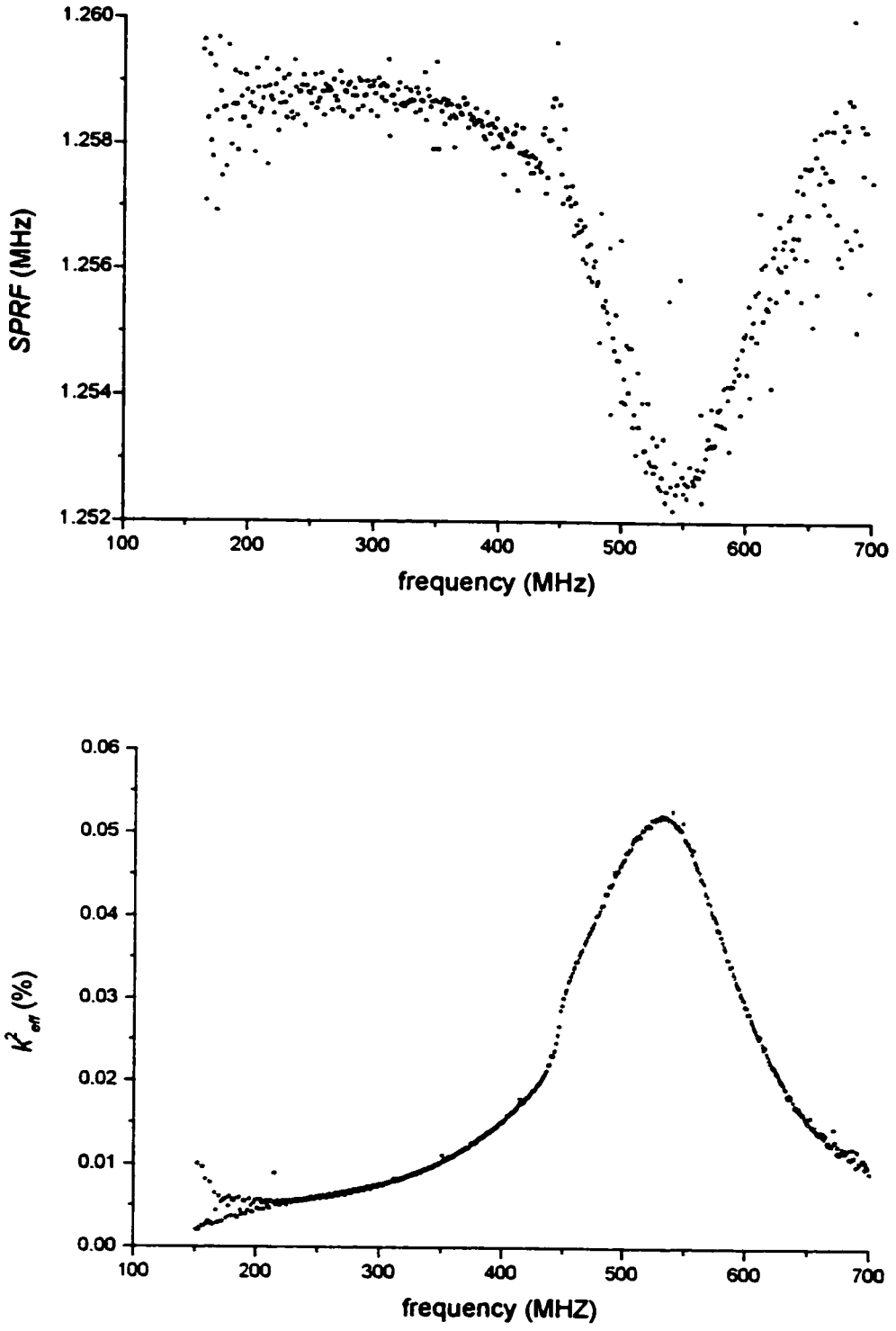

Fig.4.10 *SPRF and k^2_{eff} distributions of sample 3 (92mil substrate)*

part of the impedance of the resonator in whole span, which are converted from s_{11} according to Eq. (4.1), and Fig.4.8 shows the real and imaginary part of the admittance of the resonator converted from s_{11} according to Eq. (4.2). From these figures, the characteristic shape of a composite resonator can be seen clearly, which are described in Chapter 2 as a response of a capacitor with multiple resonant peaks. The resonant peaks are distributed almost evenly over the whole frequency range and have maximum resonance in the first normal region because the sample has a soft substrate. From Fig. 4.7 it can also seen that the minimum resistance is very close to 0, which means the contact resistance or electrode resistance is either very small or well calibrated. This will be discussed in Chapter 5 in more detail.

After further interpolation near each resonant peak with the *Mathematica* program described in last section, the parallel and the series resonant spectra were extracted. The distributions of the *SPRF* and the effective coupling coefficients of the composite resonators were calculated with Eq. (2.11) and Eq. (2.9), and they are shown in Fig.4.9 and Fig.4.10, from which the characteristic frequencies Δf_N, Δf_T and the effective coupling coefficient $k_{eff}^2(m_N+1)$ are measured. For ZnO/fused quartz sample which is the soft substrate case, Δf_N is the minimum and Δf_T is the maximum of *SPRF*, respectively, and $k_{eff}^2(m_N+1)$ is the effective coupling coefficient at the resonant mode corresponding to Δf_N. They are listed in Table 4.1. Our measurements also showed that for the resonators on the same substrate, their impedance responses as well as the characteristic values Δf_N, Δf_T and $k_{eff}^2(m_N+1)$ differ from each other slightly.

It is shown that the data of the *SPRF* are a little dispersive, and the characteristic values, Δf_N and Δf_T are determined by averaging the measurement data around the center of the first normal and transition region, respectively. Even with the dispersion, the periodic shape of the *SPRF* distribution is very regular and the results are fairly sure. It is interesting to note that $k_{eff}^2(m)$ are very smoothly distributed over a wide frequency range and almost no dispersion occurs. As a result, no data averaging or fitting is necessary and the characteristic value of $k_{eff}^2(m_N+1)$ can be evaluated accurately. These experimental results clearly show the practicality of the *Resonant Spectrum Method.*

The density ρ, the longitudinal velocity v, and the electromechanical coupling coefficients k_t^2 of the ZnO film in the samples were then calculated by using the *Resonant Spectrum Method* equations (3.47), (3.48) and (3.49). The elastic constant c_{33}^D was then calculated with Eq.(1.6). They are listed in Table 4.1. As a comparison, the results calculated with the approximate formulas (3.50) are also given in Table 4.1. The difference in these two methods is much less than 1%. The other parameters of the ZnO film and the parameters of the fused quartz substrate and aluminum electrodes used in the calculation are listed as follows [39]:

ZnO film: l = 4.8μm (Sample 1: 62mil substrate);

l = 5.2μm (Sample 2: 92mil substrate);

Fused Quartz: ρ_{sb} = 2200 kg/m^3; V_{sb} =5973.4 m/s;

l_{sb} =1536.5 μm; (Sample 1: 62mil substrate);

l_{sb} =2370.3 μm; (Sample 2: 92mil substrate);

Al electrodes: ρ_e = 2695 kg/m^3; V_e = 6418 m/s; l_e = 0.4 μm.

Table 4.1. Characteristic values and parameters determined by experiment

Sample	Experiment				Parameters calculated with The *Resonant Spectrum Method*				
	Δf_N (MHz)	Δf_T (MHz)	$k_{eff}^2(N)$ (%)	$N=m_N+1$	ρ (kg/m^3)	c_{33}^D (10^{10}N/m^2)	v (m/s)	k_t^2 (%) Eq.(3.52)	k_t^2 (%) Eq.(3.53)
1	1.9271	1.9411	0.0650	308	5665.8	20.83	6063.1	7.27	7.26
2	1.2525	1.2588	0.0505	436	5525.3	20.80	6135.9	8.02	8.00

In Fig. 4.9, there is a small jump on the effective coupling coefficient near 470MHz. By checking the resistance response of the resonator near 470MHz as shown in Fig.4.11a, It is found that there are several small resonant peaks at each mode which we believe is caused by some other resonant modes. The dominant peak shifts from left to right, causing a small discontinuity on the determination of the parallel resonant frequencies. But the conductance response as shown in Fig.4.11b at this frequency range has no such phenomena and there is no jump on the series resonant frequencies. Consequently k_{eff}^2, which is determined by the difference between the parallel and series resonant frequencies, has such a small discontinuity. Since for the *Resonant Spectrum Method*, the electromechanical coupling coefficient k_t^2 is calculated from the effective coupling coefficient k_{eff}^2 at the first normal region or the first transition region, the small discontinuity of k_{eff}^2 at this frequency range has no impact on this method. But if a curve

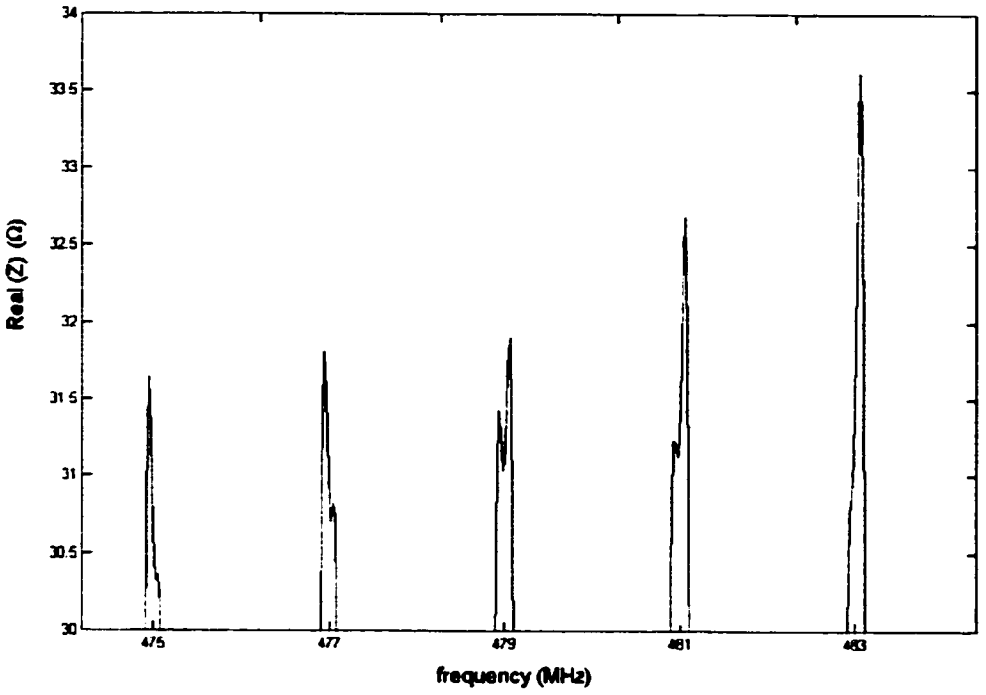

a.

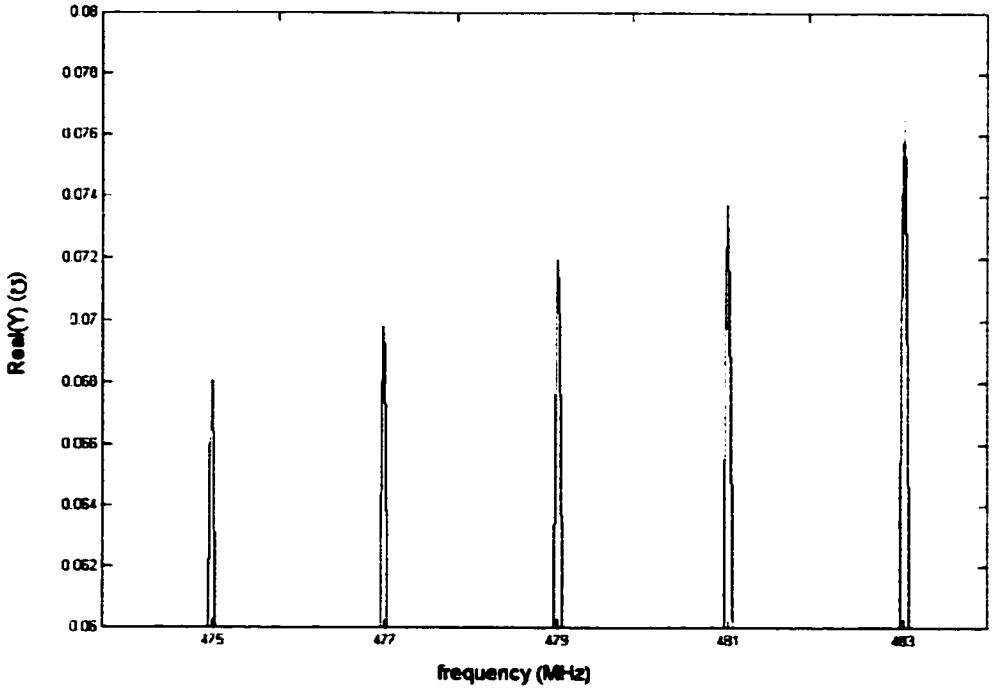

b.

Fig.4.11 *The resistance and admittance of Sample 1 resonator near the "jump"*

fitting method were used to fit the k_{eff}^2 distribution, like the method introduced in Chapter 1 [23], such a discontinuity would have a big impact on the accuracy of data extraction.

4.4 Summary

In this chapter, experiments on measuring ZnO/fused quartz composite resonators have been presented. The measurement setup, control program, and data process have been described in detail. The measurement results of *SPRF* and k_{eff}^2 are pretty good, but it is obvious that k_{eff}^2 has much better regularity than the *SPRF* distributions. An abnormal jump on *SPRF* and k_{eff}^2 distribution near 470MHz has been found and the reason was analyzed. It has no effect on the *Resonant Spectrum Method* calculations, because only the value of k_{eff}^2 at the maximum is of significance.

CHAPTER 5. ACCURACY AND VALIDITY OF THE *RESONANT SPECTRUM METHOD*

Since the ZnO film parameters are process related, there are no standard values to compare with the results we obtained from the experiment. In this chapter, we will investigate the accuracy and validity of the *Resonant Spectra Method* by numerical simulations. Some second order effects on the accuracy of the method, such as the mass loading effect of electrodes, mechanical loss effect, probe contact /electrode resistance effect, will be discussed.

5.1 Simulations with the *Resonant Spectrum Method*

To verify the *Resonant Spectrum Method*, three composite resonators are simulated. The first two are the samples measured in the last chapter, ZnO film on fused quartz substrate with aluminum electrodes, which represent the case where the acoustic impedance of the piezoelectric layer is greater than that of the substrate, *i.e.* soft substrate. The values of the velocity, the density and the coupling coefficient of the ZnO films are the data determined by experiment in the last chapter. In the simulation they are used as the input parameters. The third sample is a porous PZT film on a stainless steel plate [9], which represents the case where the acoustic impedance of the piezoelectric layer is less than that of the substrate, *i.e.* hard substrate. For this sample, the stainless steel is one of

the electrodes and the top electrode is ignored since its thickness is much smaller than the PZT film. The parameters of each layer in the composite resonators used in the simulation are listed in Table 5.1.

The parallel and series resonant frequencies of these composite resonators are calculated by finding the maxima of resistance and conductance of the resonators using Eq.(2.1). Although mathematical software like *Mathematica* provide functions to solve maximization problems, difficulties on convergence occurred very often in the simulation because the resonant peaks are so sharp and the response beside the resonance is almost flat. The convergence is highly dependent on the original value. If the original value is far away from the resonant peak, the minimization function may converge to a false point in the flat part beside the resonant peak. This problem is more serious for the frequency range where the effective coupling coefficient is small and the resonant peaks are small and sharp, for example, the low frequency range in the ZnO/quartz composite resonator samples. To avoid this difficulty, a *Mathematica* program was developed using the Newton method to solve the maximization problem for sharp resonance. The convergence coefficient was adjusted for different frequency range to achieve best convergence. Even so, the program sometimes converges to points other than the maximum points. Thus, much attention has to be paid to the false convergence problem.

The distributions of the *SPRF* and $k_{eff}^2(m)$ *vs.* frequency of Sample-I and Sample-II are shown in Fig.5.1 and Fig.5.2 by solid dots. The experimental data are also shown in these figures as a comparison. For Sample-III, they are shown in Fig.5.3. The simulated characteristic values of Δf_N, Δf_T and $k_{eff}^2(m_N + 1)$ are obtained from these figures. Using

Table 5.1. The parameters of composite resonators used in simulation

Sample	Piezoelectric film				Substrate				Electrode				R
	ρ (kg/m^3)	v (m/s)	k_t^2 (%)	l (μm)	ρ_{sb} (kg/m^3)	v_{sb} (m/s)	l_{sb} (μm)	z_{sb}	ρ_e (kg/m^3)	v_e (m/s)	l_e (μm)	z_e	
I	5665.8	6063.1	7.27	4.8	2200	5973.4	1536.5	0.38	2695	6418	0.4	0.51	306.7
II	5525.3	6135.9	8.02	5.3	2200	5973.4	2370.3	0.39	2695	6418	0.4	0.51	435.4
III	7000.0	2400	4.0	50	7800	5900	2400	2.74			0		19.5

Table 5.2. Simulation results

Sample	ρ		c_{33}^D		v		k_t^2 (exact eqs.)		k_t^2 (approximate eqs.)	
	(kg/m^3)	error	(10^{10}N/m^2)	error	(m/s)	error	(%)	error	(%)	error
I	5544.2	-2.1%	20.67	-0.8%	6106.1	0.7%	7.05	-3.0%	7.12	-2.1%
II	5422.5	-1.9%	20.63	-0.8%	6167.9	0.5%	7.75	-3.4%	7.79	-3.0%
III	7011.8	0.2%	4.10	1.6%	2419.2	0.8%	3.98	-0.4%	4.24	6.0%

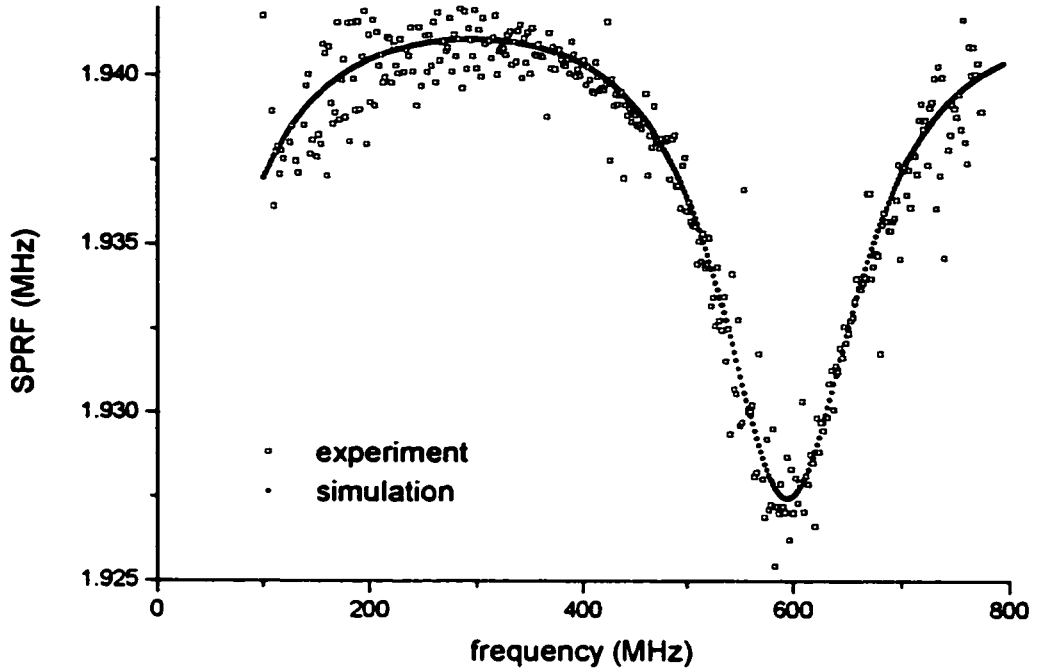

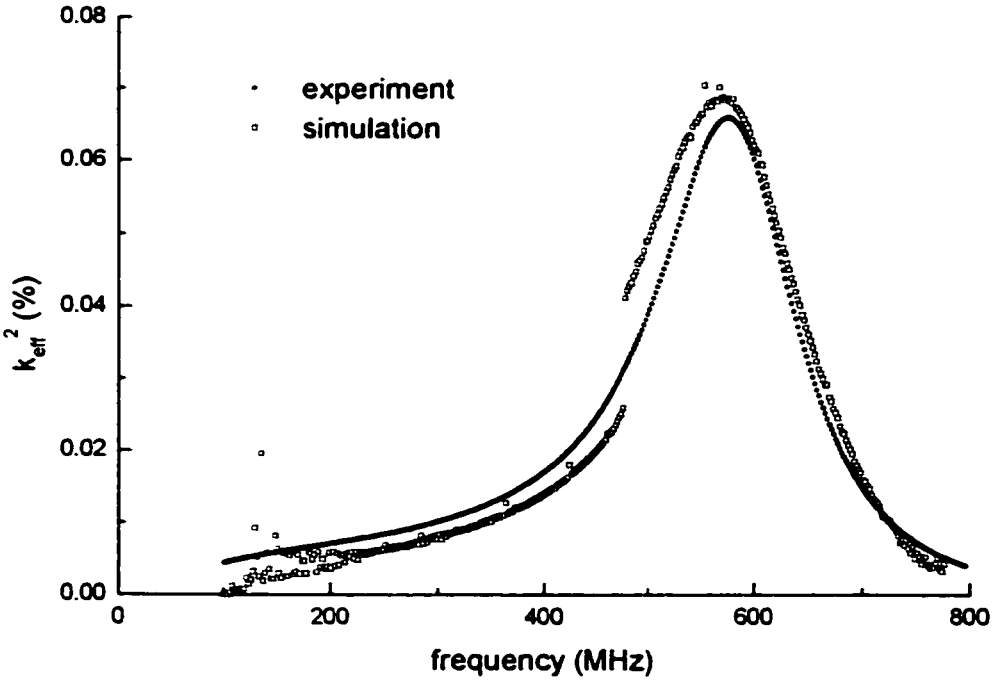

Fig.5.1 *SPRF and* k_{eff}^2 *distribution of Sample I (62mil resonator)*

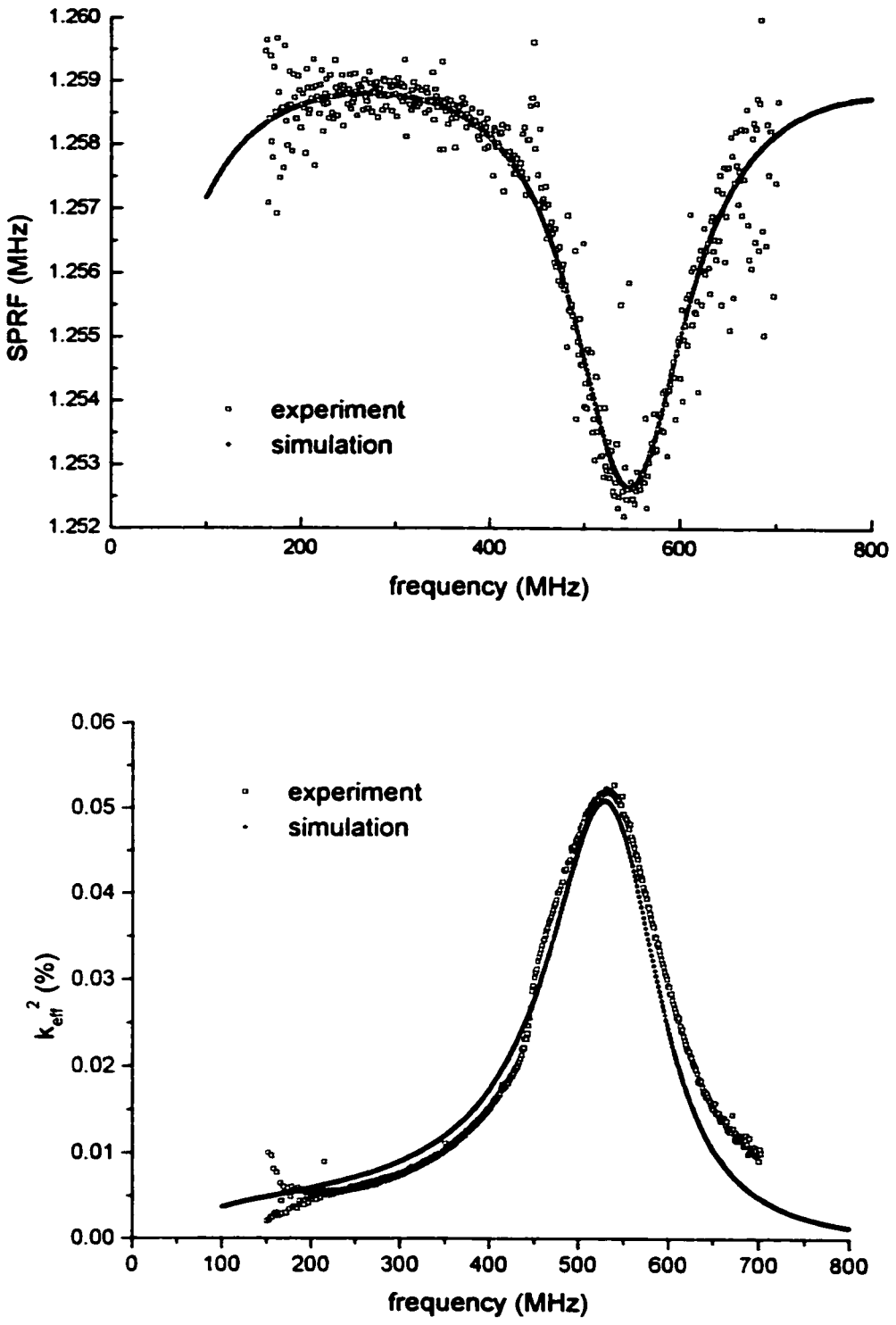

Fig.5.2 *SPRF and* k_{eff}^2 *distribution of Sample II (92mil thick resonator)*

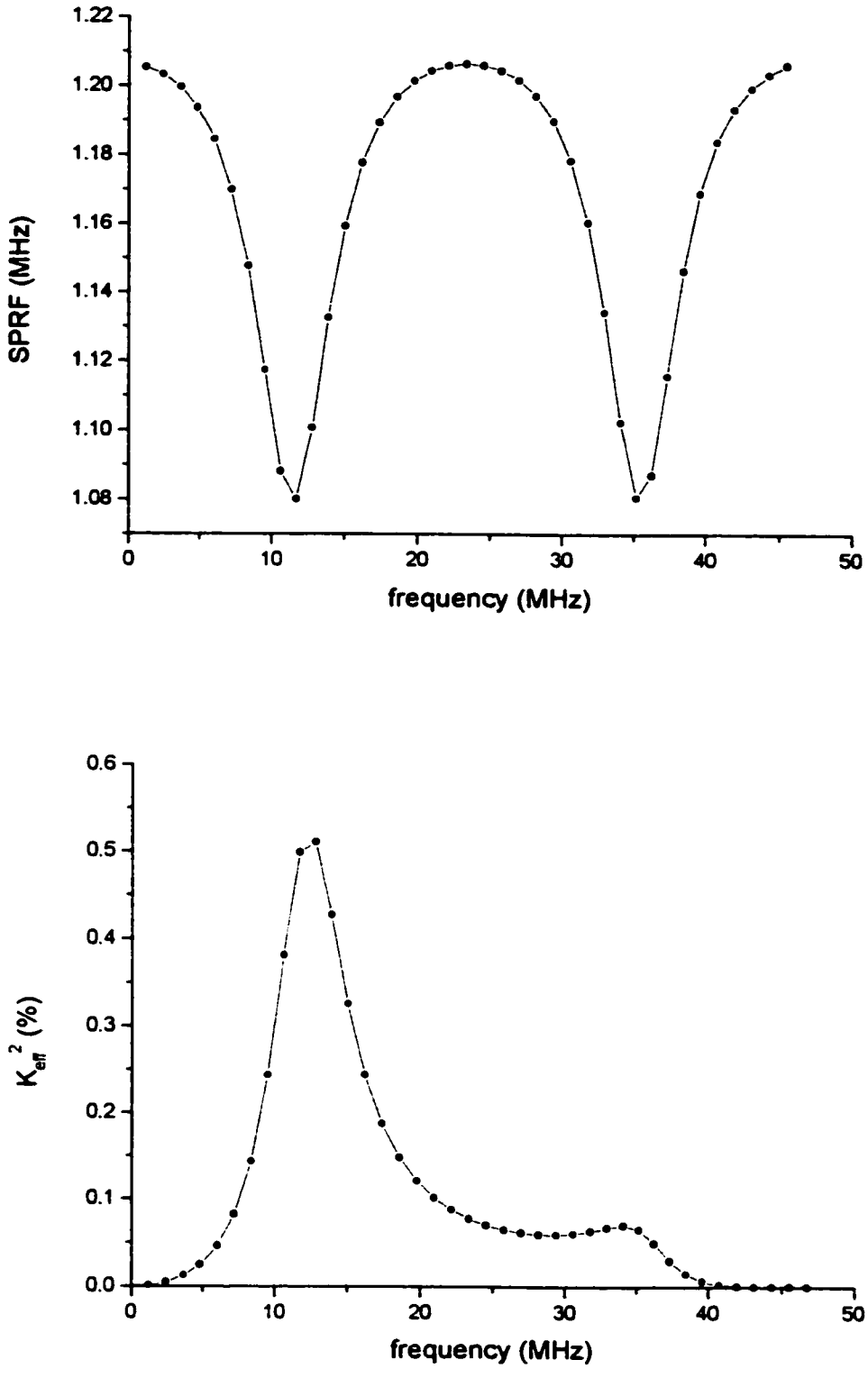

Fig.5.3 *SPRF* and $k_{eff}^2(m)$ *distribution of Sample III*

the equations of the *Resonant Spectrum Method* in Chapter 3 and the material parameters in Table 5.1, we obtained the simulation output of three parameters of the piezoelectric films as well as the elastic constant. The results are listed in Table 5.2. The errors listed are with reference to the input data shown in Table 5.1. Small imaginary parts were introduced into the velocities of both the piezoelectric film and the substrate to avoid singularities in the simulation. The imaginary parts of the velocities stand for the mechanical loss of the acoustic wave and have little effect on the distribution of the *SPRF* and the effective coupling coefficients. This will be discussed in section 5.3.

It is shown in Table 5.2 that the difference between the output values and input values are within 3.5% for all three parameters calculated with the *Resonant Spectrum Method*, as well as c_{33}^{D} which is calculated with Eq.(1.6). Assuming the data evaluated from the experiment (given in Table 4.1 and listed in Table 5.1 as the input parameters) are the "true" values for Sample-I and -II, the values determined by this method are accurate to 3.5% for the samples used here. For such high frequency devices, a few percent errors are quite acceptable.

The approximate Eq.(3.53) also works very well for Sample I and II, where the resonant mode order in the first normal region is very high. But for Sample III where the mode order in the first transition region is very small, the error is quite large. This is in agreement with the analysis in Chapter 3 that only when R is large or is close to an integer (for Eq.(3.53)) or a half integer (for Eq. (3.55)), the approximate equations are valid.

The main sources of the error are some approximations used in the derivation of the *Resonant Spectrum Method*, most important among them are the thin electrode

approximation and lossless material approximation. The impact of these two approximations on the accuracy of the method will be discussed in the following sections.

5.2. Effect of the electrodes

In our early work [26][27], the mechanical effect of electrode was ignored by putting the thickness of the electrodes equal to zero. In the later work [28]~[30], the *Resonant Spectrum Method* was extended to a four layer composite resonator by taking two electrodes into account. In the derivation of the *Resonant Spectrum Method* formulae for the four layer case, a thin electrode approximation has been used. The errors caused by this approximation may be significant for high frequency resonators where the thickness of the electrodes is comparable with the thickness of the piezoelectric film. It is therefore necessary to investigate the valid range of the electrode thickness for the method and the errors caused by the electrodes. Fig.5.4 shows the *SPRF* and $k_{eff}^2(m)$ distributions for various electrode thicknesses in a ZnO/fused quartz composite resonator as Sample-I. It can be seen that the thicker the electrode, the greater the $k_{eff}^2(m)$. These results are qualitatively in agreement with the formula (3.15). Table 5.3 lists the simulation results on ρ, v and k_t^2 for various electrode thicknesses. It is shown that the errors of the three parameters increase with the increase of the electrode thickness. When the thickness of the aluminum electrodes is within 10% of the ZnO film, the error is less than 5%, which is quite acceptable.

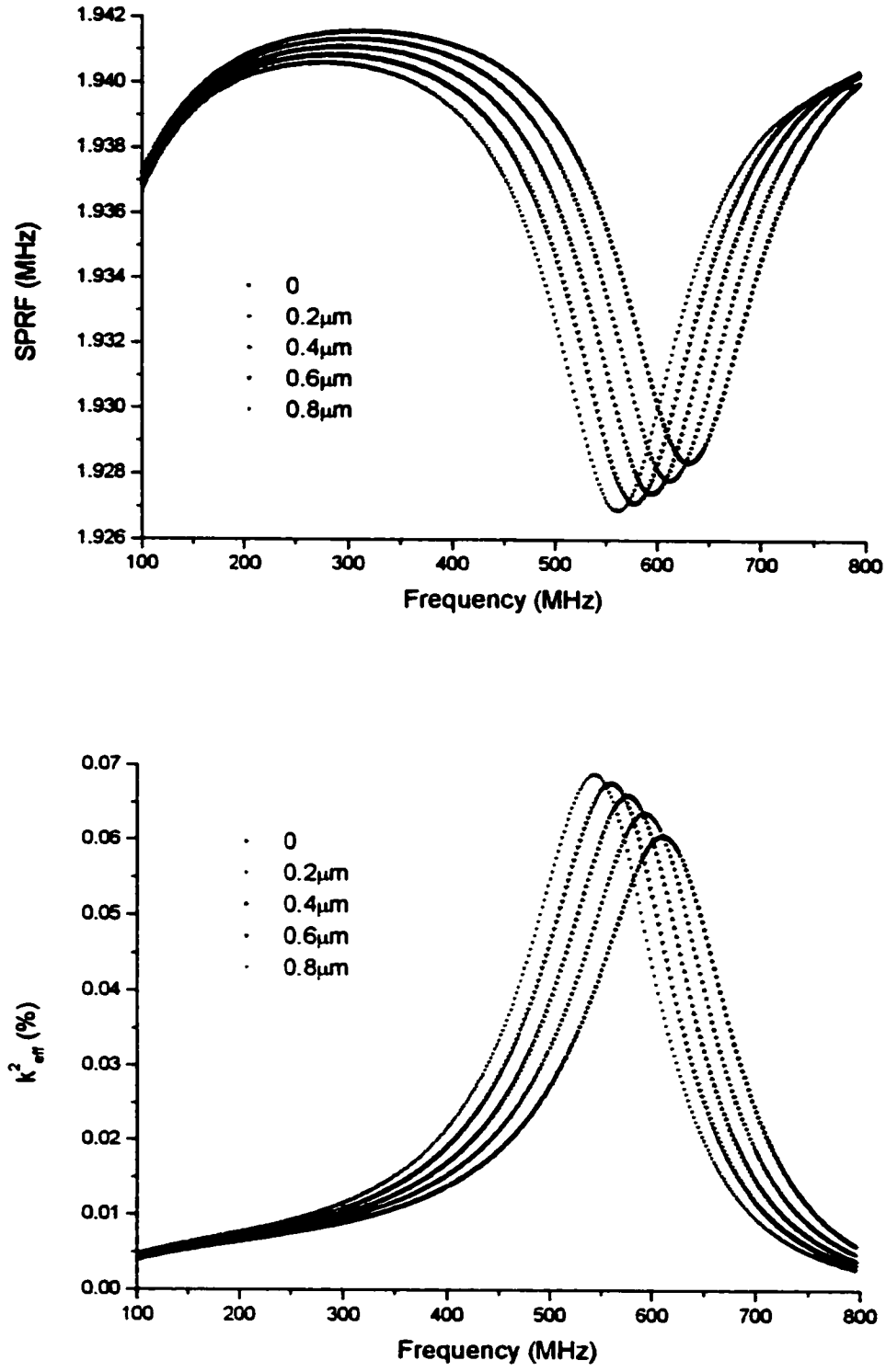

Fig.5.4 *SPRF and k^2_{eff} distribution for various electrode thicknesses*

As a comparison, we use the *Resonant Spectrum Method* formulae with the electrode effect ignored. Putting $l_{e1} = l_{e2} = 0$, Eq.(3.53) becomes Eq.(2.63)

$$k_t^2 = \left(1 + \frac{\rho_{sb} l_{sb}}{\rho l}\right) \cdot k_{eff}^2 (m_N + 1) \tag{5.1}$$

In the 0.4μm electrode case in Table 5.3, the above equation results in a k_t^2 of 7.83% and an error of 7.74% when other parameters are the input value in Table 5.1. If the velocity and density are the simulation results in Table 5.3, above equation of k_t^2 will result an error of 10%. When taking the electrode effect into account and using Eq.(3.53), it can be found in Table 5.3 that the error of k_t^2 is only 2.1%. The result shows clearly that the effects of the electrode have to be compensated pretty well and our modified formulae are effective.

The reason for the error has a clear mathematical interpretation. As given in (3.13), an approximation

$$\tan \gamma_e \approx \gamma_e \tag{5.2}$$

is used in deriving the *Resonant Spectrum Method*, which means the electrodes can be considered as a mass loading. For a ZnO/quartz composite resonator with aluminum electrodes as simulated here, v_e is close to v. When the electrode thickness is one tenth of the piezoelectric film thickness,

$$\gamma_e \sim \gamma / 10 \approx \pi / 10 \tag{5.3}$$

in the first normal region. The use of approximation (5.2) gives an error of 3.4%. Furthermore, Eq.(3.10) has to be modified to include the phase delays in the electrodes.

Assuming the middle electrode is split half-half into top resonator and composite substrate, then

$$\gamma \approx \pi - \gamma_e - 0.5\gamma_e \sim 0.85\pi \tag{5.4}$$

$$\gamma_{sb} \approx \pi - 0.5\gamma_e \sim (m_N - 0.05)\pi \tag{5.5}$$

The approximations of (2.12) will bring 8.1% error to γ and 0.8% error to γ_{sb}. With contributions from other approximations, the overall error is around 5%. The condition for the electrode thickness being one tenth of the piezoelectric film thickness can be used as a rough criterion for the *Resonant Spectrum Method* to achieve good accuracy.

The data given in Table 5.3 shows that the results obtained from approximate equations (5.53) seem better than those from equation (5.52). This may be caused by the approximation of m_N introducing an opposite error which cancels out part of the error from equation (5.52).

Table 5.3. Method error for various electrode thicknesses

Electrode	ρ		v		c_{33}^D		k_t^2 (Eq.3.52)		k_t^2 (Eq.3.35)	
Thickness	(kg/m^3)	error	(m/s)	error	($10^{10}N/m^2$)	error	(%)	error	(%)	error
0	5654.5	-0.2%	6072.6	0.2%	20.85	0.1%	7.19	-1.1%	7.21	-0.8%
0.2μm	5625.1	0.7%	6080.6	0.3%	20.80	-0.1%	7.15	-1.7%	7.17	-1.4%
0.4μm	5544.2	-2.1%	6106.1	0.7%	20.67	-0.8%	7.05	-3.0%	7.12	-2.1%
0.6μm	5430.2	-4.2%	6154.7	1.5%	20.57	-1.2%	6.88	-5.4%	7.05	-3.0%
0.8μm	5290.4	-6.6%	6212.2	2.5%	20.42	-2.0%	6.64	-8.7%	6.89	-5.2%

Further investigation on the effect of the electrodes reveals that the top electrode and the middle electrode have different contributions to the degradation of the accuracy. The top electrode can be understood as a mass loading to the resonator if the approximation (5.2) is valid. It can be taken as part of the piezoelectric film, which decreases the resonant frequency of the piezoelectric film and lowers the frequencies corresponding to the first transition and normal region. The *SPRF* in the first normal region, Δf_N, decreases with the increase of the mass of the top electrode and the k_{eff}^2 in the first normal region increases with the increase of the mass of the top electrode. Fig.5.5 shows the variation of *SPRF* and k_{eff}^2 with different top electrode thickness while the middle electrode thickness keeps a constant 0.4μm. The figure demonstrates that the variation of *SPRF* and k_{eff}^2 has little to do with the acoustic impedance of the top electrode. A gold top electrode, with acoustic impedance 3.65 times that of an aluminum electrode, has almost the same effect on *SPRF* and k_{eff}^2 if its mass is the same as the aluminum electrode. To do this, we choose the gold electrode thickness in the simulation as

$$l_{el,Gold} = \frac{\rho_{el,Al}}{\rho_{el,Gold}} l_{el,Al} \tag{5.6}$$

Thus, only the mass of the top electrode effects the distribution of *SPRF* and k_{eff}^2, and it is pretty well compensated in the *Resonant Spectrum Method*.

The middle electrode, however, acts more or less as a coupling layer between the piezoelectric film (working as a transducer) and the substrate. Physical intuition indicates that the effect of the middle electrode must relate to the acoustic impedances of the

piezoelectric film, the middle electrode and the substrate. If the impedance of the middle electrode is between the impedances of the film and the substrate, it works like an acoustic coupler. If the impedance of the middle electrode differs very much from the impedances of the film and the substrate, it works like a mismatch layer. An extreme example is when the middle electrode has exactly the same acoustic properties as the piezoelectric film and then can be taken as part of the piezoelectric film. Thus the effect of the middle electrode is similar to the top electrode as a mass loading as described above. But when the middle electrode has the same acoustic properties as the substrate, it can be taken as part of the substrate. Thus, the *SPRF* will change significantly but the central frequency of the piezoelectric film will not change very much. Fig.5.6 ~5.8 show the effect of the middle electrode on the *SPRF* and k_{eff}^2 for different electrode thickness and impedance when the top electrode is aluminum and its thickness is kept constant at 0.4μm.

In Fig.5.6, the middle electrode is assumed to be Titanium, which has an acoustic impedance close to the ZnO piezoelectric film. The effect of this electrode is similar to the top electrode as a mass load. In Fig.5.7, the middle electrode is aluminum, which has an acoustic impedance close to the quartz substrate. The effect of this electrode is quite different from that of the Ti electrode. While Δf_T doesn't change very much for the Ti electrode, Δf_N changes. For the Al electrode case it looks like the whole SPRF curve shifts up with the increase of the electrode thickness. This can be explained as in Eq.(3.20), f_0 should take the effect of the middle electrode into account since its acoustic properties are very close to those of the substrate and thus it is equivalent to an increase of the substrate thickness. The *Resonant Spectrum Method*, however, treats the effect of

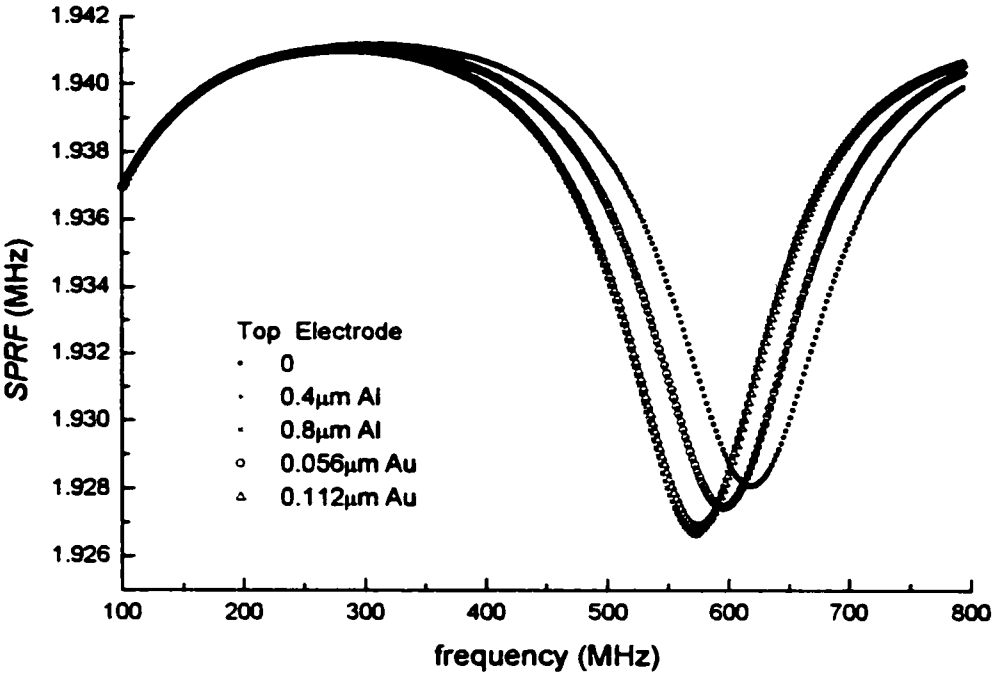

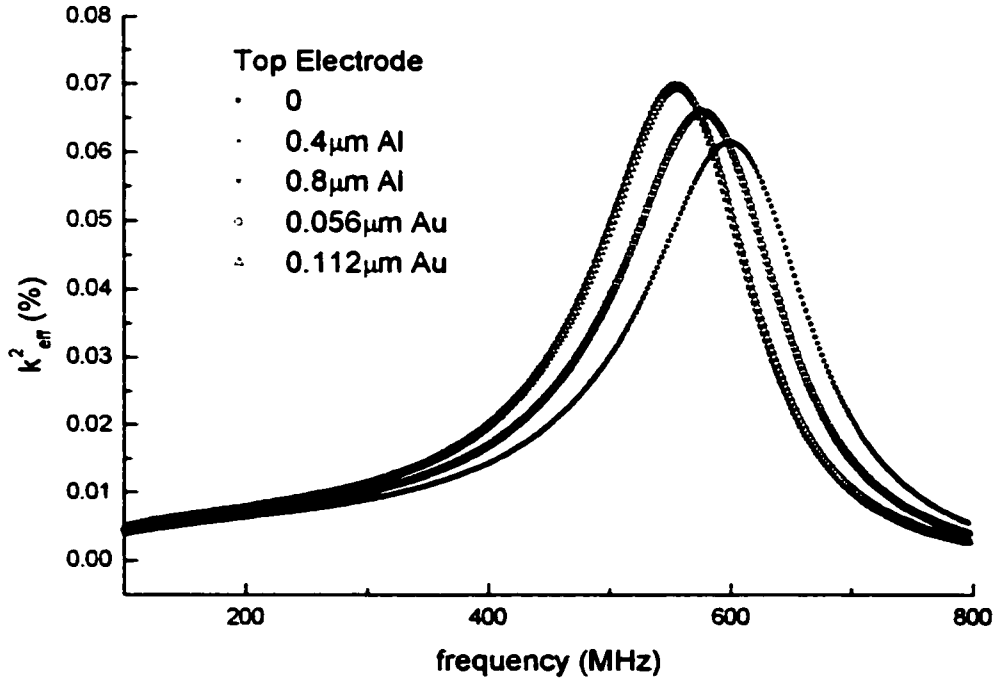

Fig.5.5 *SPRF and k^2_{eff} distribution for various top electrodes*

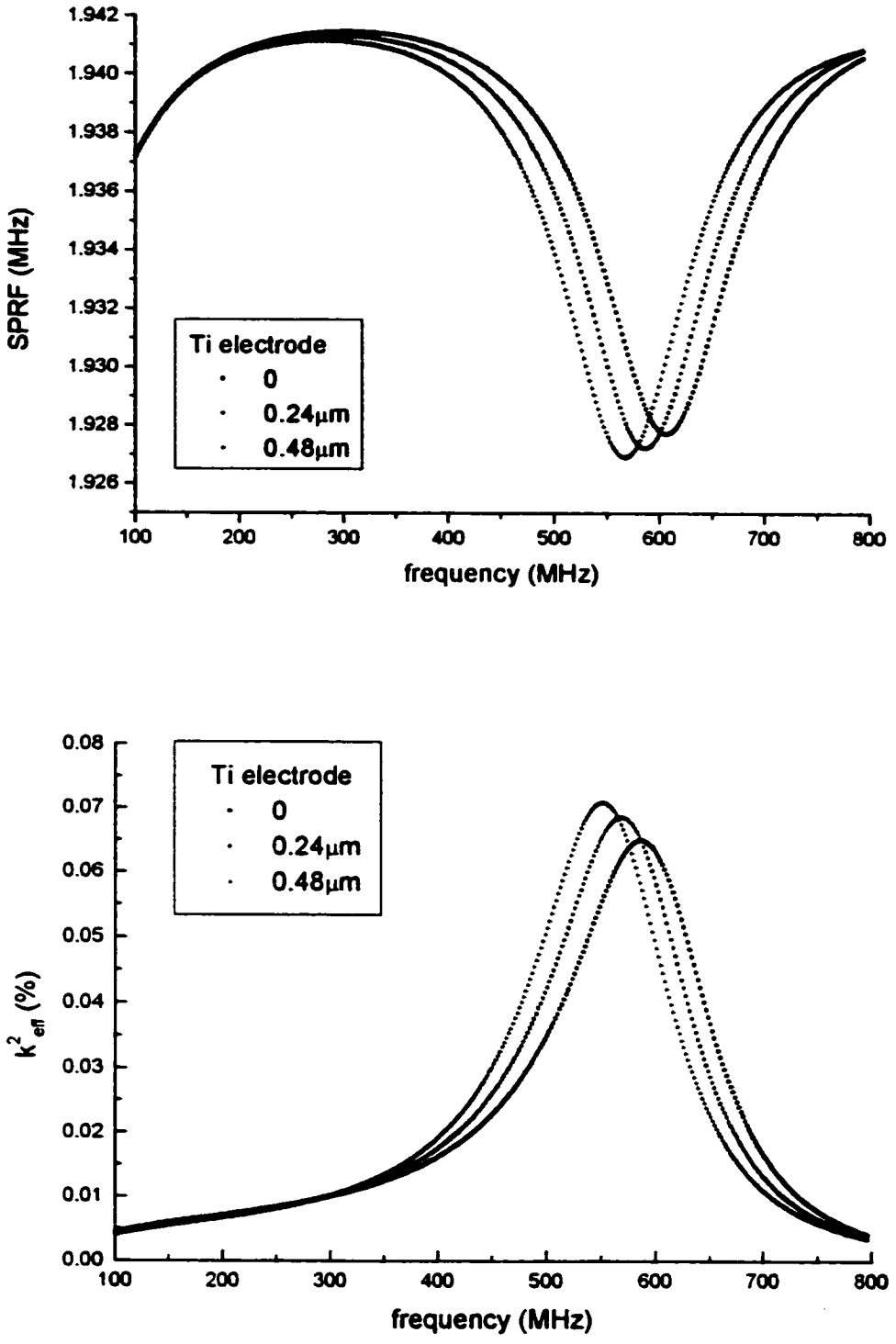

Fig.5.6 *SPRF and* $k^2_{eff}(m)$ *for titanium middle electrode with different thickness*

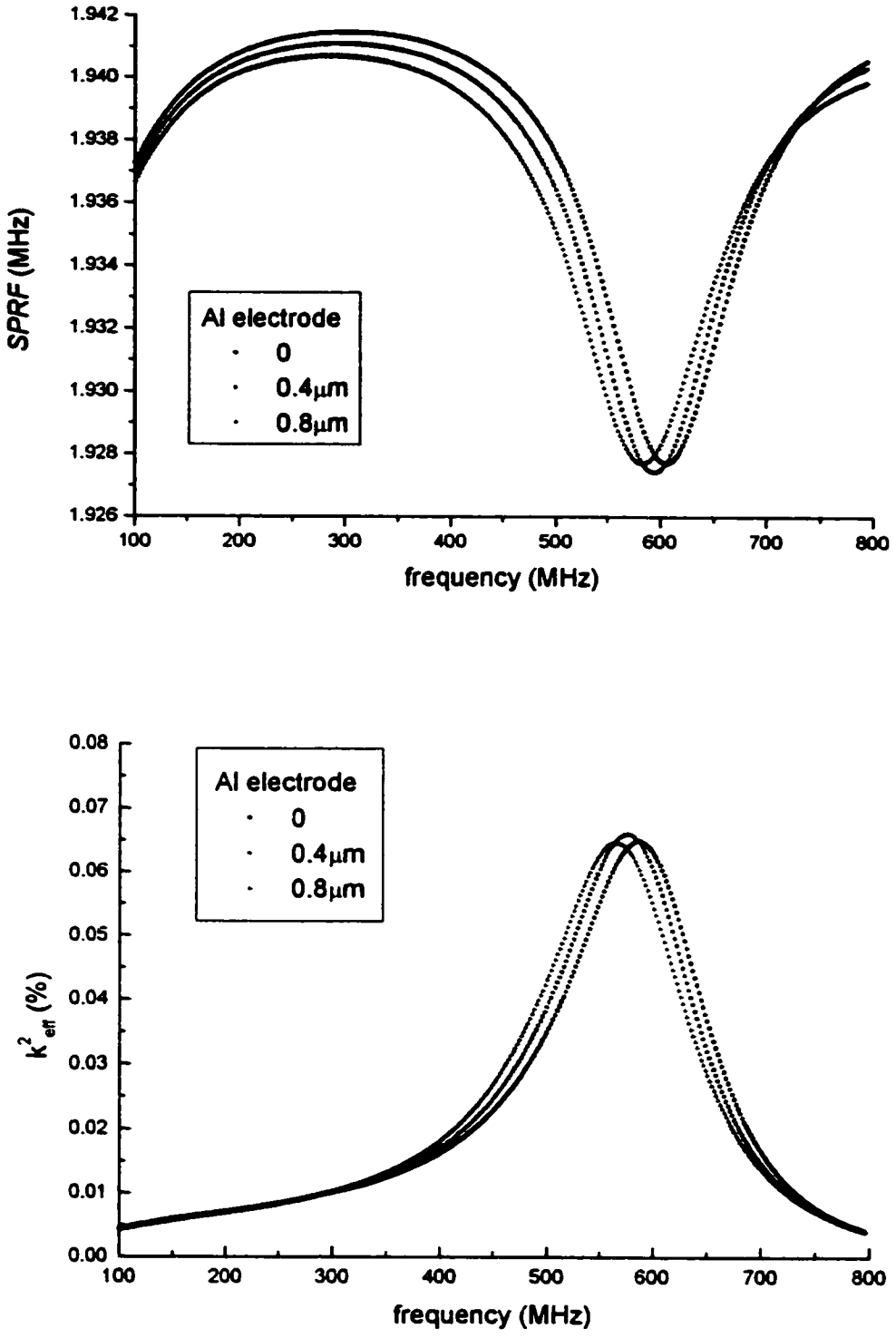

Fig.5.7 *SPRF and* $k_{eff}^2(m)$ *for aluminum middle electrode with different thickness*

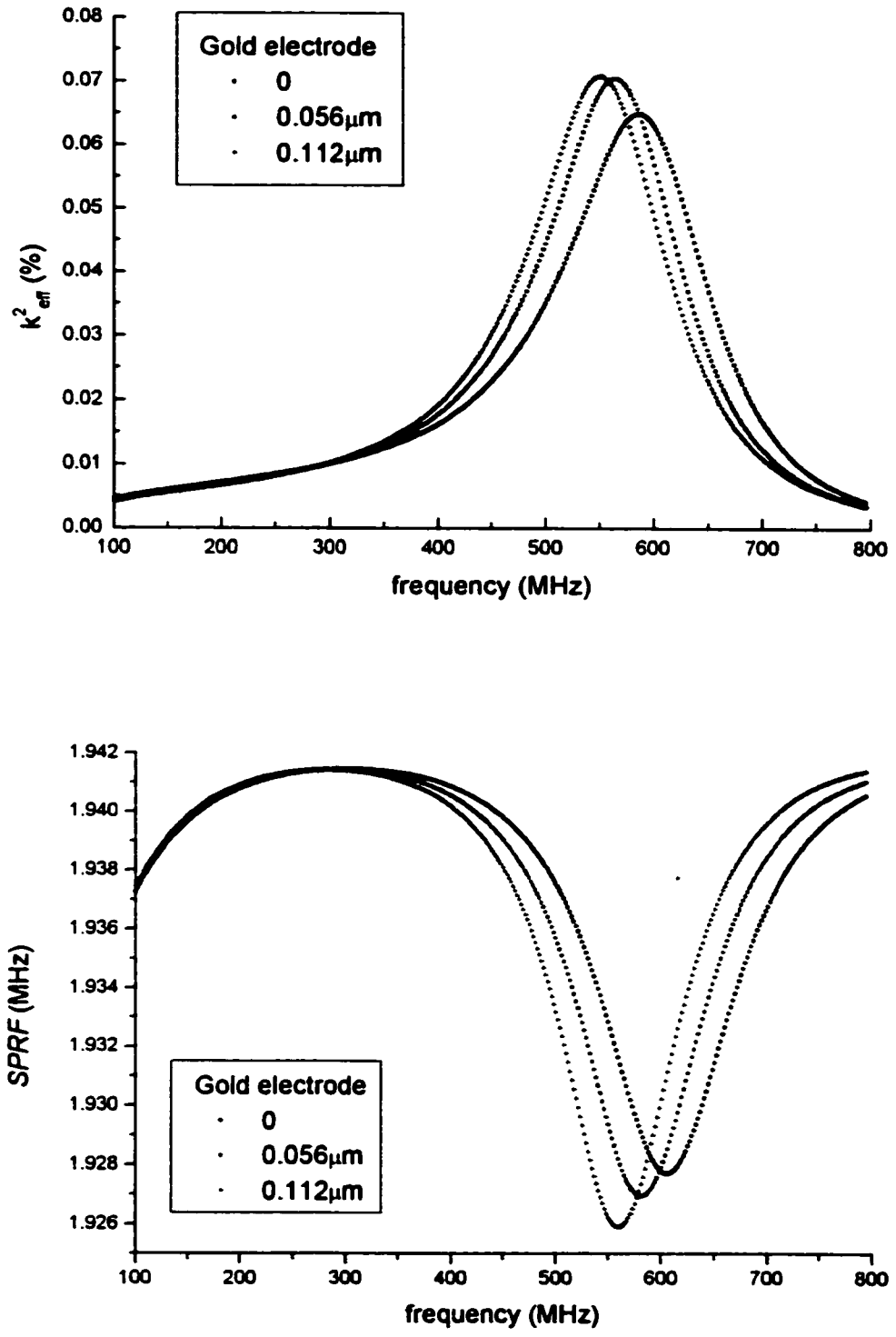

Fig.5.8 *SPRF and* $k^2_{eff}(m)$ *for gold middle electrode with different thickness*

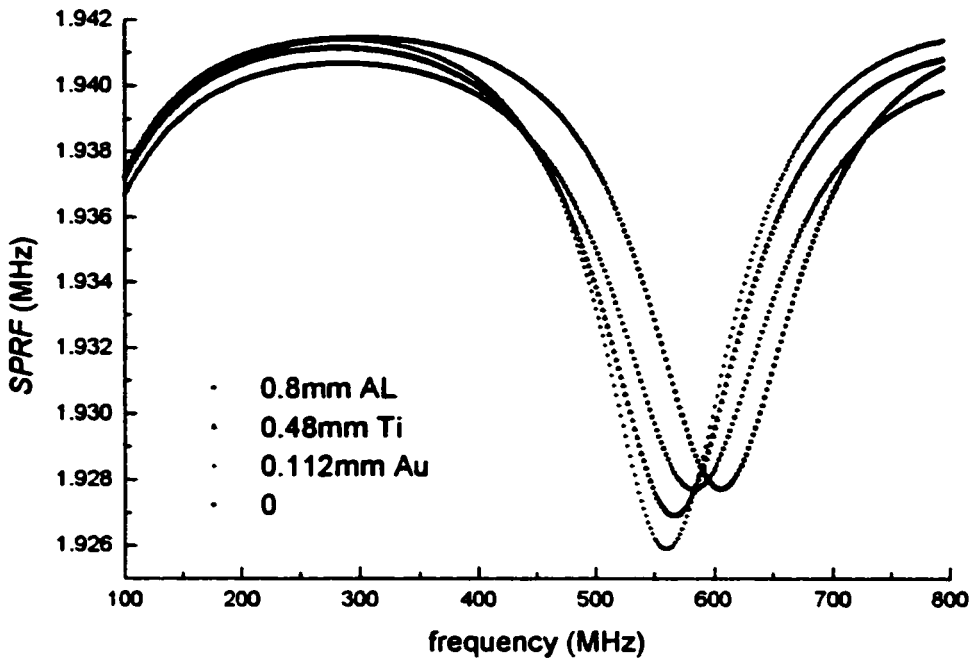

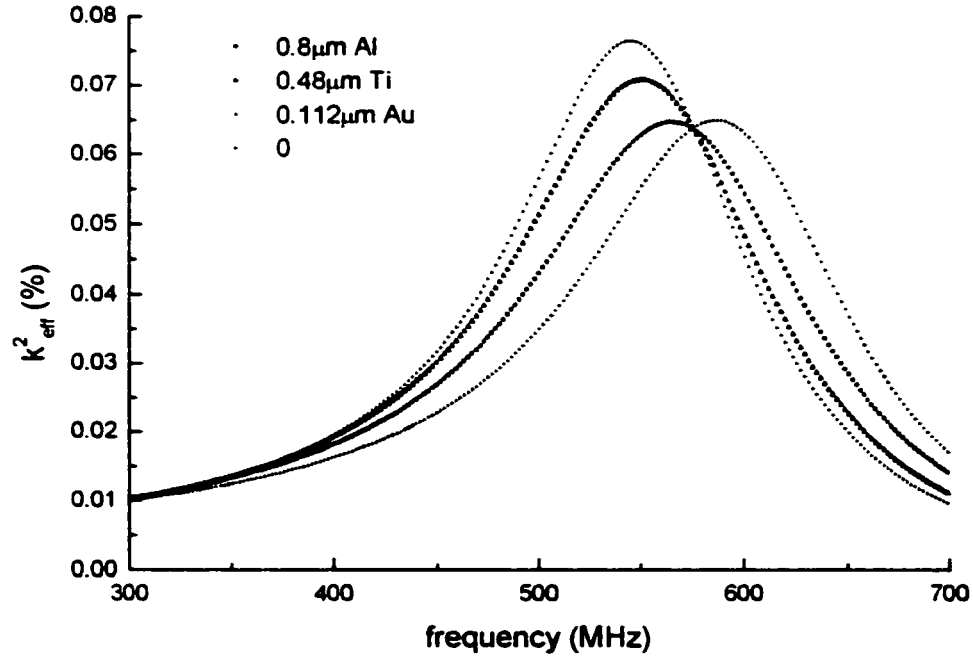

Fig.5.9 *Comparison of SPRF and* $k^2_{eff}(m)$ *for different middle electrode material*

the middle electrode more like mass loading and is not very accurate when the electrode properties are close to those of the substrate. We also find that the frequency of the first normal region does not change with different electrode thickness as much as for the Ti electrode case. This is in agreement with our qualitative analyses above. In Fig.5.8, the middle electrode is gold, which has an acoustic impedance much higher than that of ZnO and quartz. Fig.5.9 shows a comparison of the *SPRF* and the k_{eff}^2 with different material middle electrode having a mass equal to 0.8μm Al. Contrary to the top electrode effect, the middle electrode effect heavily depends on the acoustic impedance of the electrode material, not only the electrode mass.

5.3. Effect of mechanical loss

In deriving equation (2.6) and (2.7) to determine the parallel and series resonant frequencies, from which the k_t^2 evaluating formulae are derived, all the material parameters are assumed to be real. This means that all materials are assumed lossless. For high frequency devices or porous piezoelectric ceramics, however, the losses are significant and they are important for the determination of the impedance of a resonator, from which the resonant frequencies are calculated. The IEEE standard [21] also states that for a single piezoelectric plate resonator with lossy material, the parallel resonant frequency of the resonator, which is defined as the frequency of maximum resistance in this standard, can be used in Eq.(1.8) to determine k_t^2 only when Q is high. Therefore it is

necessary to investigate the validity of the *Resonant Spectrum Method* when the materials are lossy, *i.e.*, whether Eq.(2.62) and (2.64) are valid when the resonant frequencies are derived at the lossless case from their determination equations (2.6) and (2.7).

The effect of the mechanical losses on evaluating *SPRF* and k_t^2 is investigated with numerical simulation by taking the velocities of the piezoelectric film and the substrate as complex values. The imaginary parts stand for propagation loss of the acoustic wave. The ratio of the real to the imaginary part of velocity is referred to as the material Q value. Taking different Q values for the piezoelectric film and the substrate, and directly calculating the resonant frequency spectra from the impedance of the composite resonator, we evaluated the corresponding *SPRF* and $k_{eff}^2(m_N+1)$. Because k_t^2 is definitely determined by $k_{eff}^2(m_N+1)$ or $k_{eff}^2(m_T+1)$ when other material parameters are taken as constants, only the $k_{eff}^2(m)$ distribution is necessary to be simulated for different losses.

Fig.5.10 shows the input impedance of the ZnO/SiO_2 composite resonators with different material Q values. In Fig.5.10b, the Q values of the two materials are chosen such that the impedance is close to the experimental result (Fig.5.10a). Fig.5.10c and Fig.5.10d are the cases where the material Q values are much higher and much lower, respectively. In the high Q case, the imaginary parts of the velocities of the piezoelectric film and the substrate decrease to 1/10 and 1/2 from the nominal values in Fig.5.10b, respectively. In the low Q case, the imaginary parts increase by 5 times and twice, respectively. It is shown that the resonant amplitude changes significantly. The smaller the propagation losses, the higher the resonant peaks, and *vice versa*.

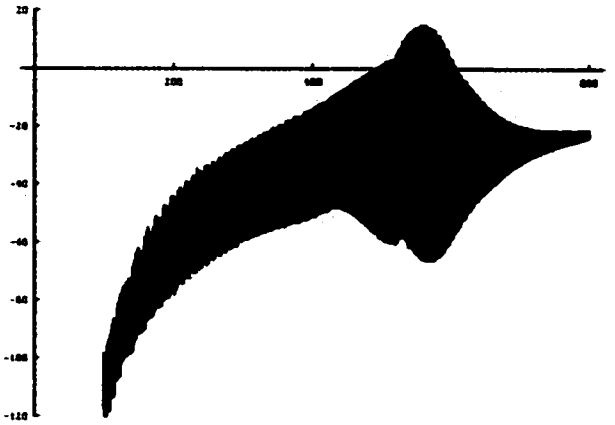

a. experiment

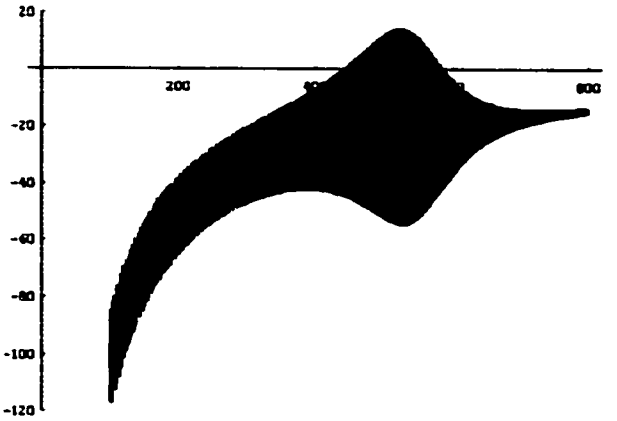

b. simulation: v = 6330(1+0.004j)

v_{sb}*=5960(1+0.00006j)*

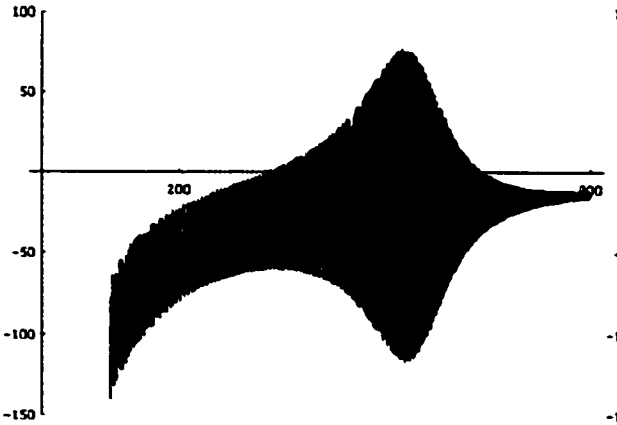

c. simulation: v = 6330(1+0.0004j)

v_{sb} *=5960 (1+0.00003j)*

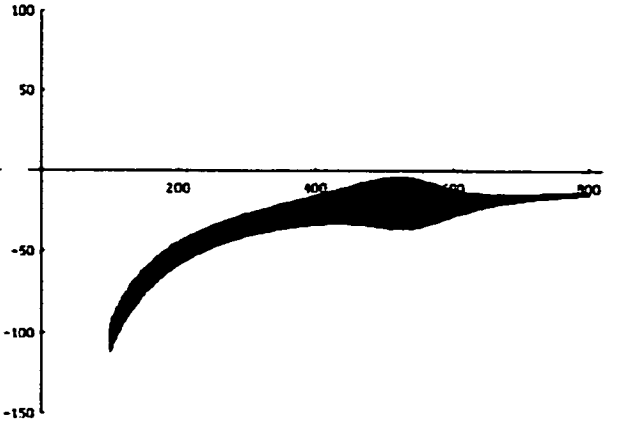

d. simulation: v = 6330(1+0.02j)

v_{sb} *=5960 (1+0.00012j)*

Fig.5.10 *Imaginary part impedances of 4-layer composite resonators*

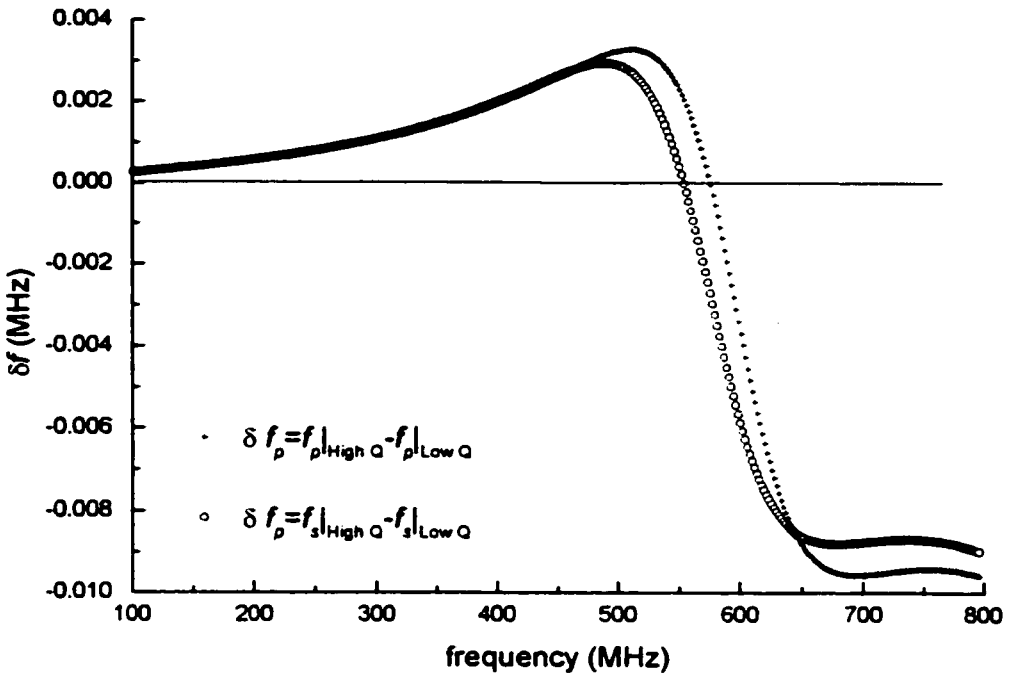

Fig.5.11 *Difference between the resonant frequencies of high Q and low Q resonators.*

Fig.5.11 shows the difference between the resonant frequencies of the high Q and the low Q resonators, δf *vs.* frequency. In the low frequency range, the resonant frequency difference increases with frequency up to a certain frequency near the first normal region. Then the resonant frequencies difference begins to decrease with frequency until another turnover frequency. Beyond that the difference will remain almost constant. Although the reason for the distribution shape is not clear, we can, however, find some useful information from these curves. At low frequencies where k_{eff}^2 is small, δf_p and δf_s vary with frequency in the same way, so that k_{eff}^2 is almost exactly the same for the high and

the low Q resonators. Around the first normal region where k_{eff}^2 is relatively large, δf_p and δf_s behave differently. Therefore, k_{eff}^2 will not be the same for the high and the low Q resonators in this frequency range. In other words, the mechanical loss will have some effect on the accuracy of the *Resonant Spectrum Method*.

Fig.5.12 shows the distributions of *SPRF* and $k_{eff}^2(m)$ for high Q and low Q cases. Since both *SPRF* and $k_{eff}^2(m)$ are relative quantities, their differences between the high Q and the low Q resonators should not be as significant as the resonant frequencies themselves. This can be seen from Fig.5.12. Although the mechanical losses in the piezoelectric film and the substrate have been changed by a factor of 50 and 4 respectively, the distributions of *SPRF* and $k_{eff}^2(m)$ have no significant variation. The values of *SPRF* and $k_{eff}^2(m)$ in the first normal region, Δf_N and $k_{eff}^2(m_N+1)$, change by only 0.3kHz and 0.001%, respectively. The value of *SPRF* in the first transition region, Δf_T, has no measurable difference. The acoustic properties of the piezoelectric films evaluated from the high Q and the low Q resonators with the *Resonant Spectrum Method* have only a few percent difference, as listed in Table 5.4. Thus, it can be concluded that the *Resonant Spectrum Method* is valid for lossy material. The parameters determined by this method are insensitive to the mechanical loss. This behavior is in accordance with IEEE standard [21] and Naik, *etc.* [23].

In practice, the substrate of a composite resonator is usually made out of high quality materials such as fused quartz or silicon, substrate acoustic loss is fairly small and constant and it won't reach the variation range in the simulation of Fig.5.12. Fig.5.13

shows the *SPRF* and $k_{eff}^2(m)$ when the loss in the substrate is taken as the nominal value as in Fig.5.12b and only the Q of the piezoelectric film changes from one tenth to 5 times of the nominal value. The variation of the loss in the piezoelectric film by a factor of 50 leads to a trivial difference in *SPRF* and $k_{eff}^2(m)$. This is in accordance with the physical nature of a composite resonator that the acoustic wave travels mainly in the substrate and the loss of the piezoelectric film has little effect. Therefore, the effect of mechanical loss in the piezoelectric film for practical resonator samples may be much less than what has been shown in the simulation Fig.5.12. This feature gives further advantages to the validity of the *Resonant Spectrum Method* for a wide range of practical piezoelectric films, even for high loss materials.

Table 5.4 Simulation results for different Q of the piezoelectric film and the substrate

Q of Piezofilm	Q of Substrate	ρ		v		c_{33}^D		k_t^2	
		(kg/m^3)	error	(m/s)	error	($10^{10}N/m^2$)	error	(%)	error
high	high	5555.2	-1.95%	6107.0	0.72%	20.72	-0.54%	0.0704	-3.16%
low	low	5446.5	-3.87%	6154.4	1.50%	20.62	-0.98%	0.0696	-4.26%
high	nominal	5554.9	-1.96%	6107.0	0.72%	20.72	-0.54%	0.0702	-3.44%
low	nominal	5490.0	-3.1%	6137.2	1.22%	20.68	-0.74%	0.0705	-3.03%

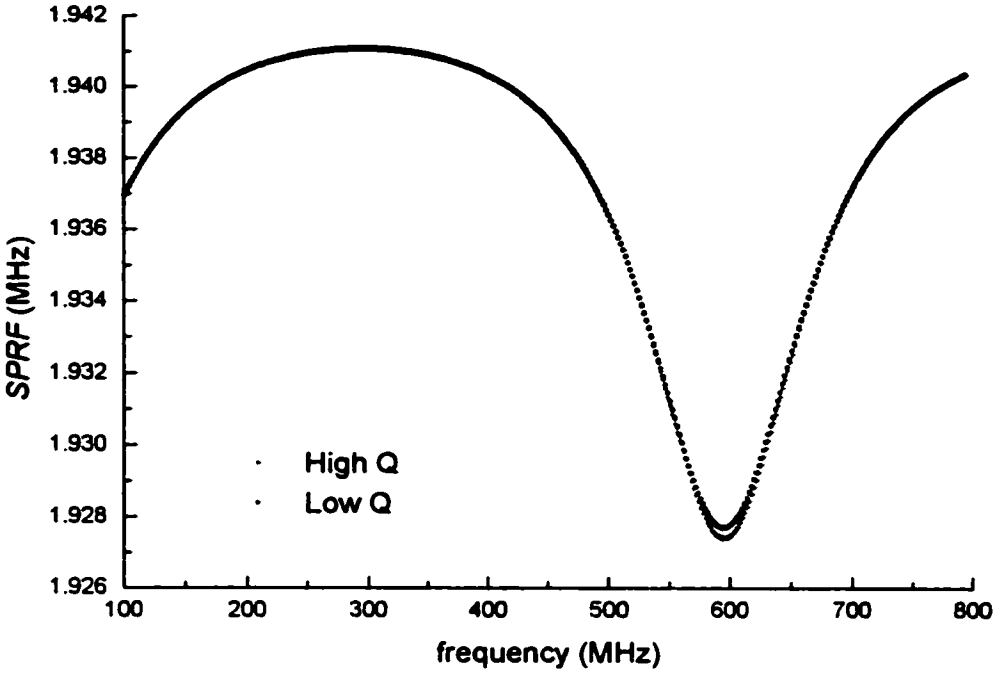

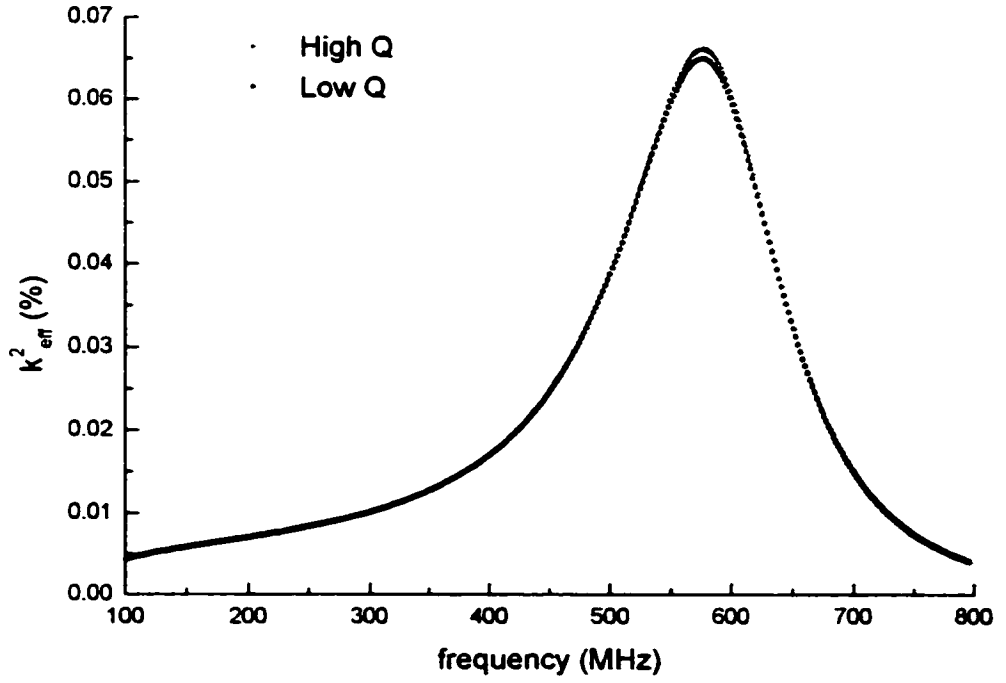

Fig.5.12 *SPRF and* $k^2_{eff}(m)$ *for high Q and low Q composite resonator*

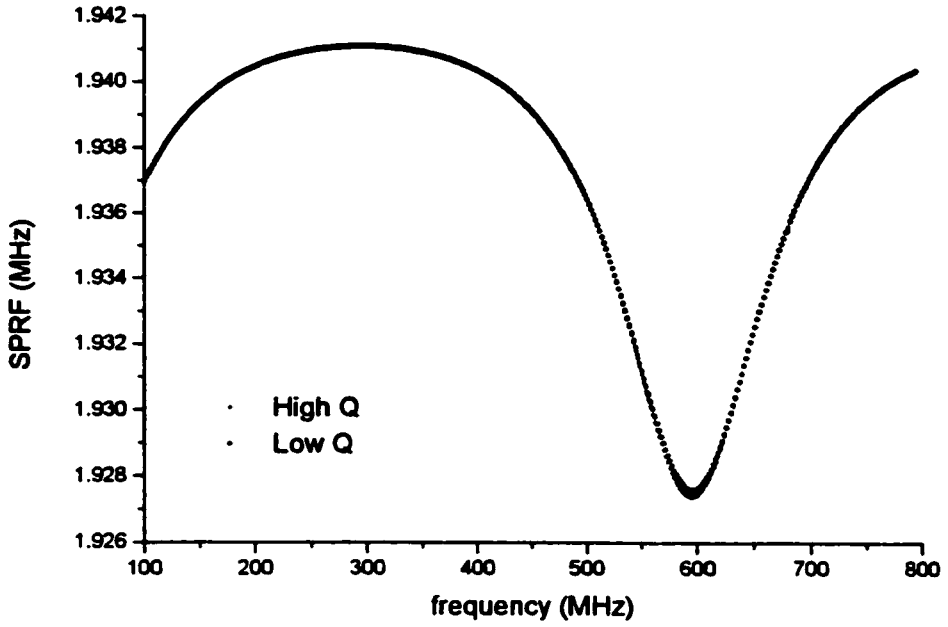

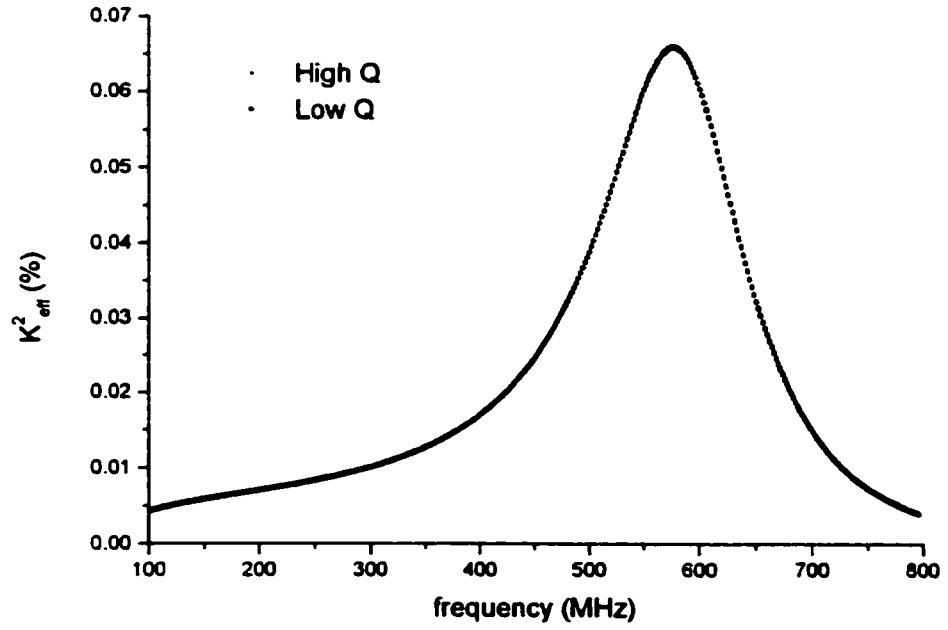

Fig.5.13 *SPRF and* $k^2_{eff}(m)$ *for high Q and low Q ZnO film*

while the loss in the substrate is constant

5.4 Probe contact resistance and electrode resistance

In our experiment, the contact resistance was included in the calibration. During the measurement of the samples, equal contact pressure was kept to ensure roughly equal contact resistance in each measurement. Thus, the effect of the difference in contact resistances was not taken into account. But in practice, it may be difficult to keep the same contact resistance during the measurement for different samples. Besides the contact resistance, the resistance of electrodes cannot be calibrated either. Since it is in series with the contact resistance, both of them together will simply be referred to as contact resistance.

The equivalent circuit of a single plate piezoelectric resonator with an extra contact resistance is shown in Fig.5.14. Since its impedance approximates that of a composite resonator near a resonance, the result for a simple resonator is also valid for a composite resonator. The impedance of a simple resonator with contact resistance is simply

$$Z = R_c + R_e + jX_e \tag{5.5}$$

Assuming the contact resistance is a constant, independent of frequency, then the frequency of the maximum of the real part of Z is only determined by R_e, has nothing to

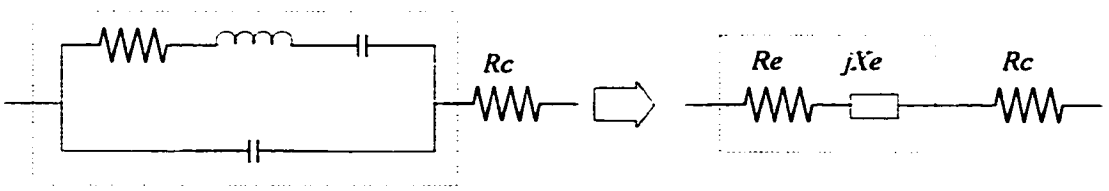

Fig.5.14 *Equivalent circuit for a simple resonator with contact resistance*

do with R_c. It is concluded that the parallel resonant frequency and furthermore the *SPRF* are not affected by the contact resistance. The admittance of such a resonator is

$$Y = 1/(R_c + R_e + jX_e) \tag{5.6}$$

The conductance is the real part of Y, which is

$$\mathrm{Re}(Y) = \frac{R_c + R_e}{(R_c + R_e)^2 + X_e^2} \tag{5.7}$$

Based on Eq.(5.7), the contribution of R_c is no longer independent of frequency. Thus, the series resonant frequency is affected by the contact resistance. Since the effective coupling factor is determined by the difference between the parallel and series

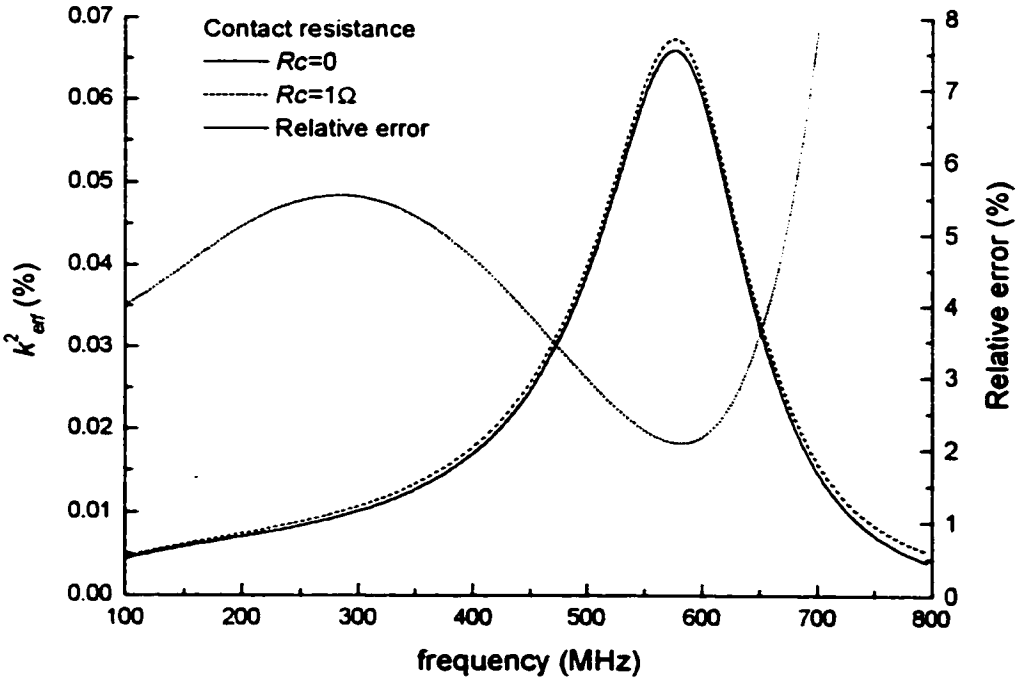

Fig.5.15 $k^2_{eff}(m)$ *for different contact resistance*

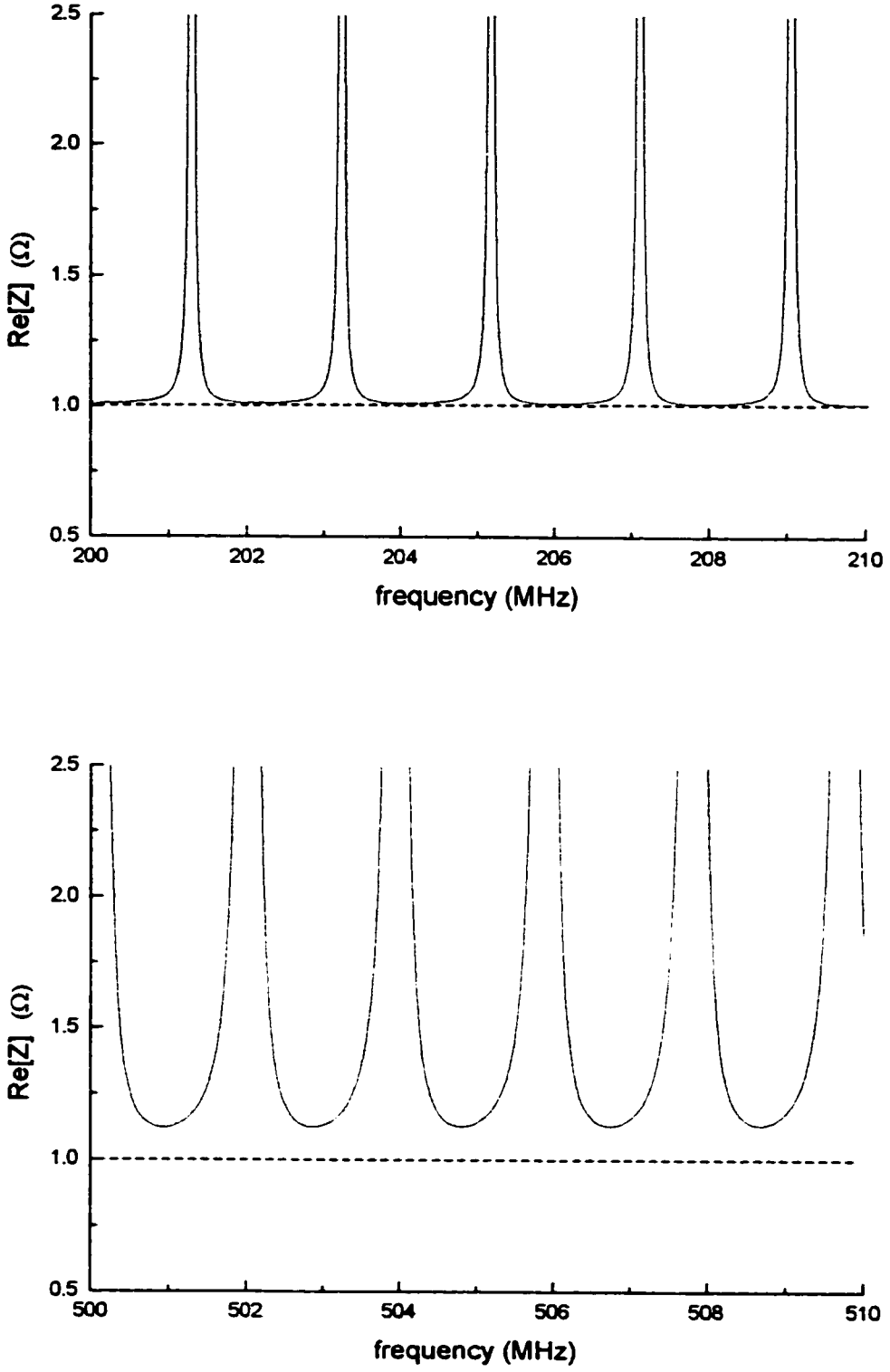

Fig.5.16 *The resistance of a Sample I resonator with 1Ω contact resistance*

frequencies, it is also affected by the contact resistance. Fig.5.15 shows the k_{eff}^2 of sample I in Table 5.1 with 1Ω contact resistance. It can be seen that the existence of the contact resistance increases k_{eff}^2. When the *Resonant Spectrum Method* equations are used to calculate k_t^2 of the ZnO film in Sample I, a 1Ω contact resistance will cause a positive error of the order of 2%.

In practice, the contact resistance can be extracted from the impedance response of the composite resonator and can then be subtracted from the admittance response so that a more accurate series resonant spectrum can be obtained. In this way, the effect of contact resistance can be eliminated to a certain degree.

If the contact resistance is frequency independent (this is true as a first-order approximation), we can determine from the resistance response of a composite resonator, as shown in Fig.5.16, that the minimum resistance is very close to the contact resistance. It should be noted that the contact resistance must be obtained from the frequency far away from where k_{eff}^2 has maximum. This is especially important for the case where the substrate is very thick and k_{eff}^2 is large. In this case, the resonant peaks of the composite resonator are very close to each other. In the region where k_{eff}^2 is maximum, the resonance is very strong and the impedance response will not return to zero. This is evident in Fig.5.16 which shows the resistance of sample I with a 1Ω contact resistance. Sample I has the maximum k_{eff}^2 in the first normal region, around 580MHz. Around 200MHz, the resonances are much weaker and the resonant peaks are narrow. The minimum resistance is very close to the contact resistance. But around 500MHz, the resonances are much

stronger and the minimum of the resistance is larger than the contact resistance. Therefore, for this sample, the contact resistance is more easily extracted from the impedance response near 200MHz. It is obvious that the contact resistance cannot be easily extracted from the admittance response, where the behavior of the contact resistance is frequency dependent. With the contact resistance extracted from the resistance response, the series resonant frequencies and consequently k_{eff}^2 can be calculated more accurately.

5.5 Summary

In this chapter, analyses and simulations have been performed to verify the accuracy of the *Resonant Spectrum Method*.

1. The accuracy of the method on ZnO and PZT composite resonators is better than 3.5%, which is quite acceptable.

2. The electrode will introduce errors in this method. For ZnO/quartz resonator, the error can be controlled under 5% when the thickness of the Al electrodes is within 10% of the thickness of the ZnO film.

3. The *Resonant Spectrum Method* is not sensitive to the mechanical loss in the piezoelectric film.

4. The contact/electrode resistance may cause some extra error for the *Resonant Spectrum Method*. A correction method has been suggested.

CHAPTER 6. APPLICATIONS OF THE *RESONANT SPECTRUM METHOD*

The *Resonant Spectrum Method* provides several formulae relating the resonant frequencies, their spacing and effective coupling coefficients with material parameters of a composite resonator. In this chapter, we will discuss the application of the *Resonant Spectrum Method* in characterization of piezoelectric films and design of resonator filters.

6.1 Characterization of the piezoelectric film in a composite resonator

The *Resonant Spectrum Method* has been used in Chapter 4 to characterize ZnO film in ZnO/fused quartz composite resonators. In this section, we will summarize the procedure to apply the method in the characterization of piezoelectric films, as well as methods to improve the accuracy.

1. Measure the parallel and series resonant spectra of the composite resonator.

The resonant spectra can be extracted from impedance measurement, as was performed in Chapter 4, or with any other valid method. If a network analyzer is used to measure the impedance, interpolation of measurement data may be needed to extract highly accurate resonant spectra.

If the central frequencies of the first transition region and the first normal region are known in advance, for example in mass production after initial work, only a few

resonances in both regions need to be measured so that the measurement time can be largely reduced.

2. Evaluate the characteristic value Δf_T, Δf_N and k_{eff}^2.

From the calculation of the *SPRF* and k_{eff}^2 distribution near the first transition region and the first normal region using the measured resonant spectra, Δf_T, Δf_N and k_{eff}^2 can be evaluated. If the *SPRF* or k_{eff}^2 is dispersive, some averaging or curve fitting may be necessary.

3. Calculate the parameters of the piezoelectric film.

With the *Resonant Spectrum Method*, two parameters of the piezoelectric film, e.g. the elastic constant c_{33}^D and the density ρ, as well as the electromechanical coupling coefficient k_t^2 can be calculated directly. If the composite resonator has a soft substrate, the k_{eff}^2 value in the first normal region and Eq.(3.49) or Eq.(3.50) should be used to calculate k_t^2. If the composite resonator has a hard substrate, the k_{eff}^2 value in the first transition region and Eq.(3.51) or Eq.(3.52) should be used.

6.2 Applications in resonator filter design

Piezoelectric resonators have been used in filter design for many years. Initially, the resonators were mainly single crystal resonators and the filters had narrow bandwidth and only worked under 100MHz. With the development of piezoelectric film technology, high

Q resonators can be achieved at microwave frequency in the forms of composite resonators or FBARs (film bulk acoustic resonator). FBARs have attracted much interest recently, with Agilent Technology having successfully produced these resonators for PCS duplexers [40][41]. The theoretical foundation for FBAR is simple, as introduced in Chapter 1, but its manufacture is much difficult and complicated. Composite resonator filters, however, are easier to manufacture and compatible with most semiconductor processing. But composite resonator filters also have their inherent drawbacks, such as multi modes, thus limiting the composite resonator filters in certain applications.

Although the *Resonant Spectrum Method* is developed to characterize piezoelectric films, its formulae can also help to design a composite resonator filter.

The composite resonators can be used to realize a bandpass filter in a ladder configuration. In such a configuration, two resonators are connected in series and parallel respectively, as shown in Fig.6.1. The series resonator has a series resonant frequency equal to the parallel resonant frequency of the parallel resonator. The bandwidth of such a filter is mainly determined by the difference between the parallel and series resonant frequencies, which is in fact determined by the electromechanical coupling coefficient of the resonator. For composite resonators, it is the effective coupling coefficient that determined the difference between the parallel and series resonant frequencies, which can be calculated directly with the formulae of the *Resonant Spectrum Method*. The parallel and series resonant frequencies of a composite resonator can also be calculated with the *Resonant Spectrum Method*. In this section, we will give an example of designing a ladder filter with the *Resonant Spectrum Method* formulae.

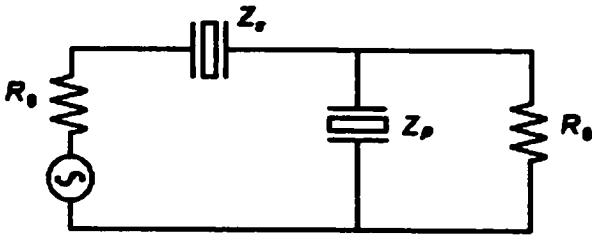

Fig.6.1 *Resonator filter in ladder configuration*

First, we will simulate a ladder filter composed of two ideal resonators. An ideal resonator can be represented with a lumped element equivalent circuit as shown in Fig.1.4 and hereafter will be referred to as LE resonator. The parallel capacitors in both resonators determine the impedance and the stopband rejection of the filter. The impedance of a ladder filter is approximately given by [42]

$$R_0 = \frac{1}{4\pi^2 f_0^2 C_{2s} C_{2p}} \tag{6.1}$$

where f_0 is the center frequency of the filter, C_{2s} and C_{2p} are the parallel capacitors of the series and parallel resonators, respectively. As in most applications, the filter impedance is designed to be 50Ω and for simplicity, we set $C_{2s} = C_{2p}$. Assuming the filter has a center frequency at 600MHz, then

$$C_{2s} = C_{2p} = 5.30515\text{pF} \tag{6.2}$$

Assuming the resonators have Q = 4500 and k_{eff}^2=0.1%, according to the BVD model of an LE resonator in Chapter 1, the parameters for both resonators are:

Parallel resonator: f_{pp}=600MHz, f_{sp} = 599.757MHz, C_{1p}=4.21052fF. (6.3)

Series resonator: f_{ps}=600.243MHz, f_{ss} = 600MHz, C_{1s}=4.22495fF. (6.4)

where the second subscript p and s represent the parallel and series resonator, respectively. Thus, the impedances of the parallel resonator Z_p and the impedance of the series resonator Z_s can be calculated using the BVD model Eq.(1.13), and are shown in Fig.6.2. The frequency response of a ladder filter is given by [7]

$$s_{21} = \frac{2}{2 + \frac{Z_s}{Z_p} + \frac{Z_s}{R_0} + \frac{R_0}{Z_p}} \tag{6.5}$$

Fig.6.3 shows the s_{21} of the filter composed of the above resonators. It is noted that the passband response is not flat due to the limited Q, and the 2dB bandwidth of 258kHz is close to the difference between the parallel and series resonant frequencies of each resonator, 243kHz.

Next, two ZnO/fused quartz composite resonators will be designed to replace the LE resonators in the above filter. The parameters to be determined are the thicknesses of the ZnO films and the fused quartz substrates, and the area of the electrodes. They can be calculated from the effective coupling coefficient and the parallel resonant frequency which are known from the simulation of the LC resonator filter above. The other parameters used in the design are the same as in Table 5.1 and the propagation losses in ZnO film and quartz substrate are the same as the nominal value in section 5.3. The aluminum electrodes are assumed the same as in section 5.2, *i.e.* 0.4μm. The detailed steps to complete the design are described below.

1. Calculate m_N for the parallel resonator

To calculate the parallel resonant frequency using Eq. (3.17) and the effective coupling coefficient using (3.23), the mode order m_N must be known. It can be approximated as the ratio of the resonant frequency of the top resonator to the resonant

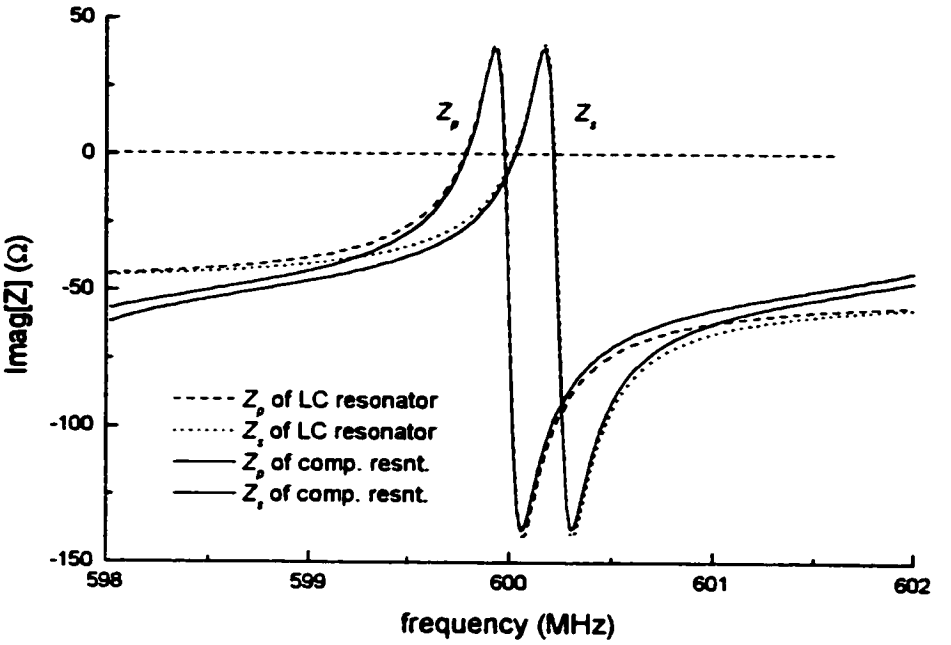

Fig.6.2 *Imaginary part of resonator impedance*

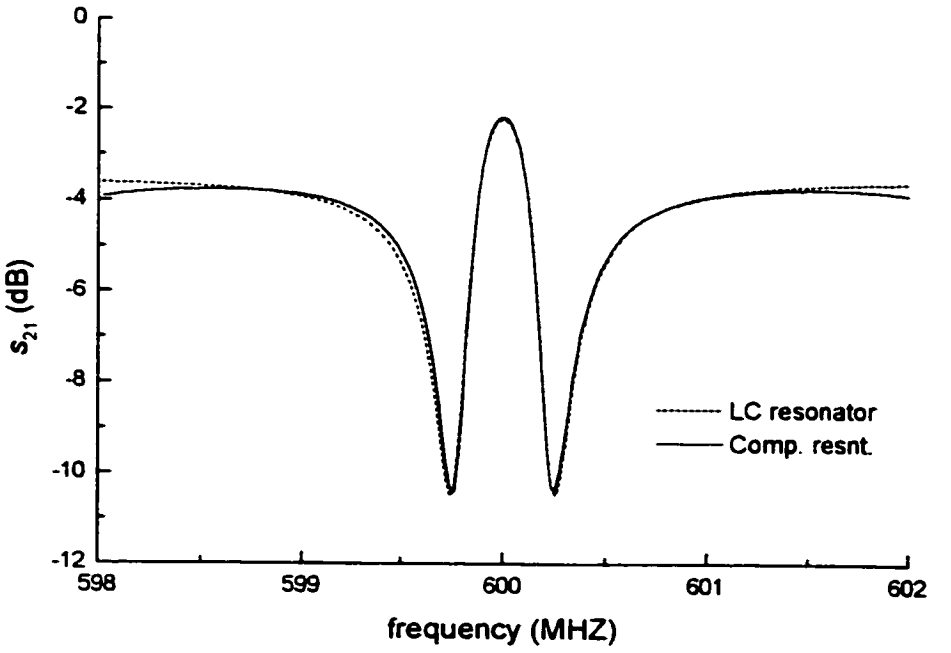

Fig.6.3 *Frequency responses of ladder filters composed of LC or composite resonators*

frequency of the composite substrate as discussed in Chapter 3. The resonant frequency of the top resonator should be located at the center frequency of the filter for best Q value, therefore f_c = 600MHz. From Eq.(3.26), we can derive an approximate value of the thickness of the ZnO film:

$$l=4.76719\mu m. \tag{6.6}$$

Inserting this value into Eq. (3.31) and letting $k_{eff}^2(m_N+1)=0.1\%$, an approximate value of thickness of the substrate is calculated as

$$l_{sb}=986.608\mu m. \tag{6.7}$$

Thus, using Eq. (3.28), the mode order at the center frequency of the filter is obtained as

$$m_N = 198. \tag{6.8}$$

2. Calculate the thicknesses of the ZnO film and the substrate and the area of electrode of the parallel resonator.

Having determined m_N, we can calculate l and l_p by solving the accurate equations (3.17) and (3.23) simultaneously. The results are:

$$l = 4.77311\mu m, \qquad l_{sb} = 985.351\mu m. \tag{6.9}$$

Check the mode order again and we get m_N = 198.

The area of the electrode is determined by C_{2p} in Eq. (6.2) and the thickness of the piezoelectric film,

$$S = \frac{l}{\varepsilon}C_{2p}=0.325\text{mm}^2 \tag{6.10}$$

3. Calculate m_N for the series resonator

Since the series resonant frequency of the series resonator f_s = 600MHz, the parallel resonant frequency of this resonator can be calculated with the effective coupling

coefficient definition Eq. (2.30), which is $f_p = 600.243$MHz. Repeating the procedures in Step 1, the approximate values for the series resonator are

$$l = 4.76541\mu m, \qquad l_{sb} = 985.351\mu m, \tag{6.11}$$

and the mode order

$$m_N = 198. \tag{6.12}$$

Generally, if the bandwidth of the designed filter is small, the difference between the parallel resonant frequencies of two resonators is also small and m_N should be the same.

4. Calculate the thicknesses of the ZnO film and the substrate and the area of the electrode of the series resonator.

Repeating the procedures in Step 2 for the series resonator results in

$$l = 4.77118\mu m, \qquad l_{sb} = 984.951\mu m \tag{6.13}$$

and the electrode area

$$S = 0.324857 mm^2 \tag{6.14}$$

5. Calculate the frequency response of the resonator filter.

Putting the thicknesses of the ZnO film and the substrate and the electrode areas into Eq.(3.8), the impedances of both parallel and series resonators can be calculated, and are shown in Fig.6.2 as the solid lines. Then with Eq.(6.5), the frequency response s_{21} of the filter can be calculated. It is shown in Fig.6.3 as the solid line. It can be seen from these figures that the response of the composite resonator filter is very similar to the response of the LE resonator filter.

It is shown that in this filter the passband is not flat. To improve passband response, the resonance of the series resonator can be shifted a little higher or the resonance of the parallel resonator a little lower, or both. For example in the above filter, if the series

resonant frequency of the series resonator is shifted to 600.4MHz, instead of 600MHz, the filter response achieved is shown in Fig.6.4. The 2dB bandwidth has been increased to 625kHz and the insertion loss remains 1.6dB. These results are very much alike the results of the filter composed of LE resonators, whose response is shown in Fig.6.4 as the dashed line. The rejection of the composite resonator filter looks even better than the LC one, but actually, it is caused by other modes of the resonators. A wide frequency range response of the composite resonator filter is shown in Fig.6.5, where the multi passband is clearly shown.

In our simulation, we have assumed the resonator having a relatively low Q value of 4500. Actually, Q > 10,000 is achievable for composite resonators in the microwave frequency range [3]. Higher Q value resonators in a ladder filter will improve the filter response, *i.e.* lower insertion loss and sharp transition band. Fig.6.6 shows the comparison of the frequency responses of filters composed of different Q value resonators. The Q value of the high Q resonators is around 10,000, which are realized by reducing the imaginary part of acoustic wave velocity in the ZnO to 25% and in the quartz substrate to 50% of their nominal values used for the low Q resonators.

In the filter design above, the substrate thickness of the parallel and the series resonators are different. It brings more difficulty and uncertainty in the fabrication procedure. This shortcoming can be avoided by using the same thickness substrate for both resonators. In the design example above, in Step 3 we simply use the same value $m_N = 198$ for the series resonator. In Step 4, since the thickness of the substrate is known as 985.351μm, the thickness of the ZnO film can be calculated with Eq.(3.17) alone and it gives

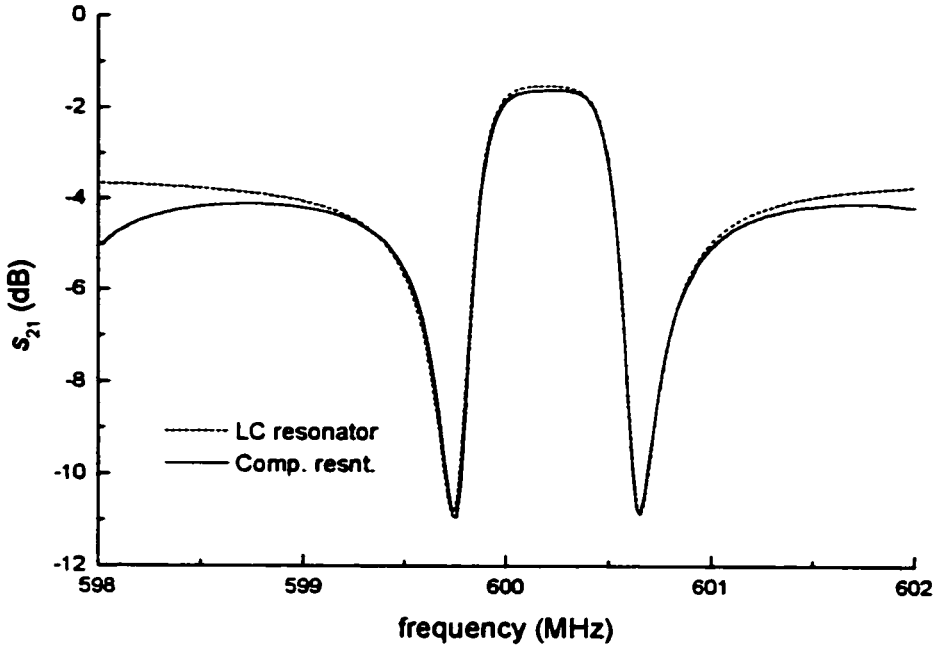

Fig.6.4 *Frequency responses of wide passband ladder filters*

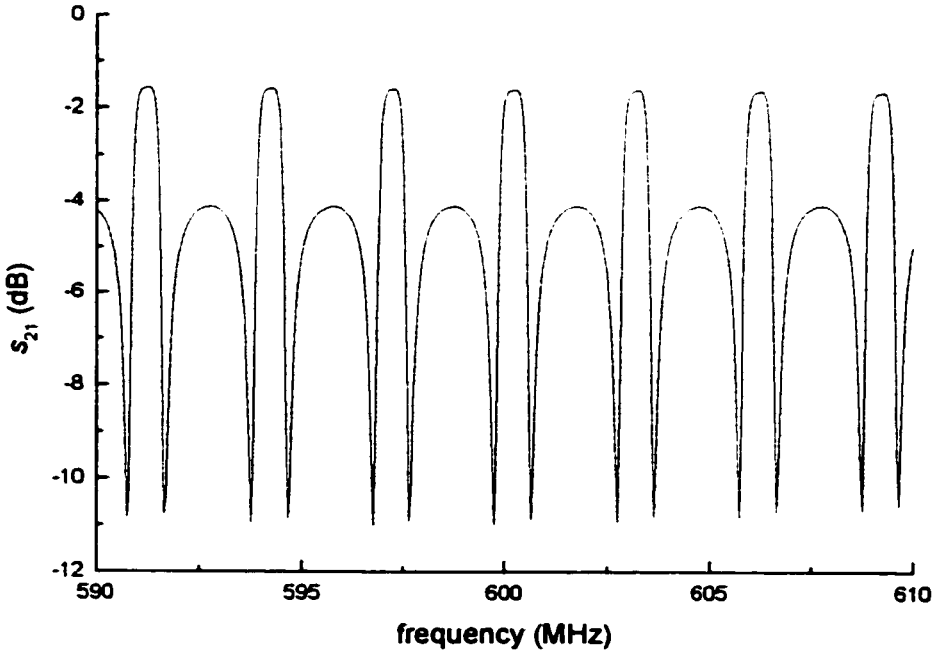

Fig.6.5 *Wide range frequency responses of wide passband ladder filters*

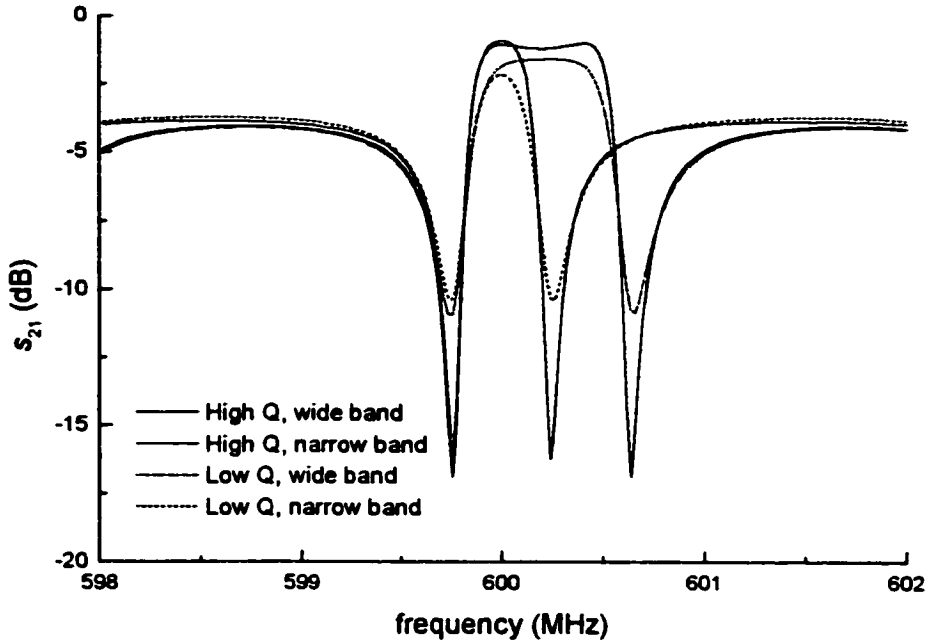

Fig. 6.6 *Frequency responses of high Q and low Q composite resonator filters*

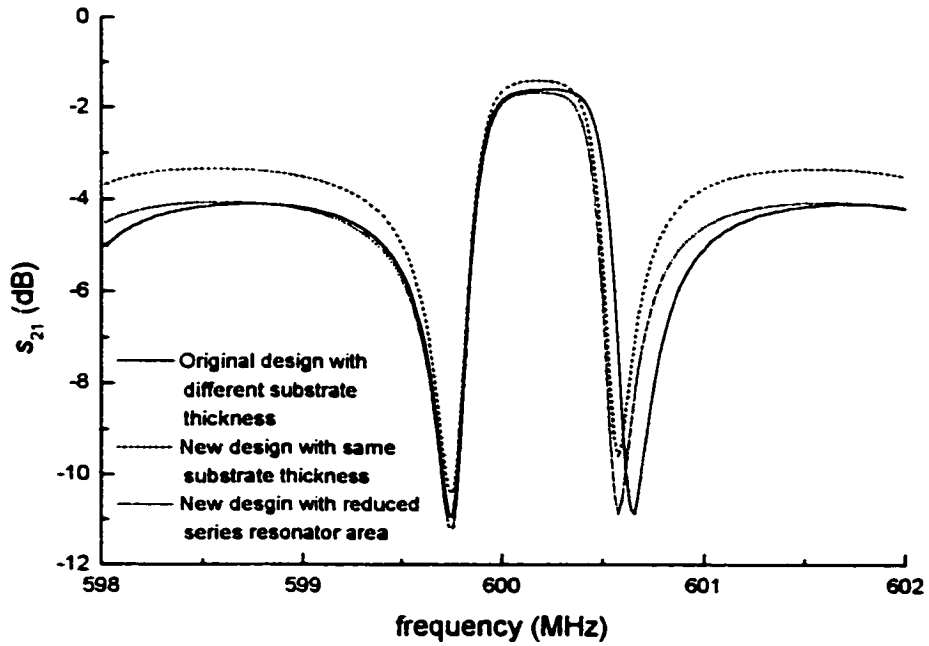

Fig. 6.7 *Frequency responses of filters with resonators of same substrate thickness*

$l = 4.35791\mu m$.

When we calculate f_c and m_N with this ZnO thickness value, it is found that

$f_c = 652.886MHz, \quad m_N = 215$.

This means that the first normal region of the series resonator is at higher frequency range and therefore, the resonances at 600MHz have lower Q values. If the Q value of the resonator is high, the difference in Q value between the parallel and the series resonators won't be a problem. For Q = 4500 or 10000, the lower Q of the series resonator reduces the filter bandwidth and rejection level, as shown in Fig.6.7. The reduction of the stopband rejection can be compensated by reducing the resonator electrode area of the series resonator. Fig.6.7 shows when the electrode area of the series resonator is reduced by 90%, the rejection levels of the two filters are very close as well as the insertion losses.

To achieve a better stopband rejection, several of such filters can be cascaded together, or connected in a Π or T configuration. This topic is beyond the scope of the thesis and will not be discussed in detail.

6.3 Summary

In this chapter, we reviewed the steps of applying the *Resonant Spectrum Method* to characterize a piezoelectric film in a composite resonator and introduced a design routine for composite resonator filters. To characterize a piezoelectric film, one should consider following steps.

1. Measure the parallel and series resonant spectra of the composite resonator.

2. Evaluate the characteristic value Δf_T, Δf_N and k_{eff}^2.

3. Calculate the parameters of the piezoelectric film.

To design a composite resonator filter, one should consider following steps.

1. Calculate m_N for the parallel resonator

2. Calculate the thicknesses of the ZnO film and the substrate and the electrode area of the parallel resonator.

3. Calculate m_N for the series resonator

4. Calculate the thickness of the ZnO film and the substrate and the electrode area of the series resonator.

5. Calculate the frequency response of the resonator filter.

CHAPTER 7. CONCLUSION

The *Resonant Spectrum Method* is a direct method to characterize a piezoelectric film deposited on a substrate to form a composite resonator. Different from the other piezoelectric film characterization methods reviewed in Chapter 1, which are all based on curve fitting techniques, the *Resonant Spectrum Method* provides a set of explicit formulae. After knowing the parallel and series resonant spectra of a composite resonator and acquiring two characteristic value Δf_N and Δf_T of *SPRF* and corresponding effective coupling coefficient from the resonant spectra, three major parameters of piezoelectric films, *i.e.* the electromechanical coupling coefficient, the elastic constant and the density can be calculated directly from the explicit formulae.

Chapter 2 and 3 presented the derivation of the *Resonant Spectrum Method* for two layer and four layer composite resonators, respectively. The *Resonant Spectrum Method* for each case has four basic equations of *SPRF* and k_{eff}^2 in the first normal region and first transition region, and two approximate equations of k_{eff}^2 in both regions. These equations are related to the material and geometric parameters of the composite resonator.

It has been found that the acoustic impedance ratio of the piezoelectric film and the substrate dominates the shapes of *SPRF* and k_{eff}^2 distributions. For the soft substrate case, the *SPRF* has a minimum in the first normal region and a maximum in the first transition region. k_{eff}^2 has its maximum in the first normal region and the equations of k_{eff}^2 at this region should be used to calculate the k_t^2. Conversely, for the hard substrate case, the *SPRF* has a maximum in the first normal region and a minimum in the first transition

region. k_{eff}^2 has its maximum in the first transition region and the equations of k_{eff}^2 in the first transition region should be used to calculate the k_t^2.

Measurement on a few samples of ZnO/fused quartz resonators was presented in Chapter 4. A program to control a network analyzer to measure the s_{11} of a composite resonator and a program to interpolate the data and extract the parallel and series resonant spectra have been developed to acquire *SPRF* and k_{eff}^2 of the composite resonator. The results of the *Resonant Spectrum Method* from the measurement agree with the results from simulation very well and the errors for the density, the velocity and the electromechanical coupling coefficient are within 3.5% for the samples measured here.

Simulations and discussions on the validity and accuracy of the *Resonant Spectrum Method* were presented in Chapter 5. Studies on the electrode effect show that the existence of electrodes is a major source of error for the *Resonant Spectrum Method*, although this has been significantly reduced when the electrodes are taken into account in four layer composite resonators. Keeping the Al electrode thickness within 10% of the thickness of the ZnO film in a ZnO/fused quartz composite resonator will keep the error within 5%. The existence of electrodes will also decrease the frequencies corresponding to the first normal and transition regions, but increase the effective coupling coefficient. Further studies revealed that the top and middle electrode affect the resonant spectra in different ways. The top electrode affects the resonator as a mass loading. The effect of the middle electrode is more complicated and is related to its impedance.

The *Resonant Spectrum Method* is not sensitive to the mechanical loss of the materials in a composite resonator. The simulations show that when the mechanical loss

changes over a large range, the *SPRF* and k_{eff}^2, and consequently the parameters calculated with the *Resonant Spectrum Method* equations do not change significantly. This feature gives the *Resonant Spectrum Method* more practicability in characterization applications.

The contact resistance and electrode resistance also introduce some extra errors to the *Resonant Spectrum Method* for k_t^2 calculation. A method to subtract their effect is suggested if the resistance can be considered as a constant.

The *Resonant Spectrum Method* can find wide applications in piezoelectric film characterization. An obvious advantage of this method is its "directness". The explicit equations also give more physical interpretation on the relationship between the *SPRF* and k_{eff}^2 and resonator parameters. Another advantage of the method is that only the distributions of resonant frequencies are of interest. Therefore, the calibration of the measurement system is not critical, even though the accuracy of the calibration makes a great difference in the measurement of electrical impedance. This feature is convenient for some applications where accurate calibration is difficult.

The equations of the *Resonant Spectrum Method* are also useful in designing resonator filters. A design example was given in Chapter 6. The thicknesses of the piezoelectric film and substrate, and the areas of the resonators in the filter can be calculated with the *Resonant Spectrum Method* equations to meet filter specifications on bandwidth, stopband rejection and impedance. High Q value resonators will help to achieve better filter performances in insertion loss and shape factor.

Future work on the *Resonant Spectrum Method* could be done on the improvement of the accuracy for the electrode effect. In our derivation in Chapter 3, the electrodes are assumed much thinner than the piezoelectric film so that in the determination of the first normal region center Eq.(3.10) and the first transition region center Eq.(3.34), the electrodes are ignored. This assumption causes some significant errors when the electrodes are thick. An improvement may be achieved by including the electrode effect into these two equations. Besides, in the derivation, all the approximations are used in first order, higher order terms are ignored. A study on the validity of these approximations will help us to understand better on the error source of the method.

Furthermore, some analysis could be done on the impact of the inaccuracy of other resonator parameters involved in the *Resonant Spectrum Method*, such as the thickness of the piezoelectric film and the thickness, the density and the elastic constant of the substrate. The errors of these parameters will be directly transferred into the result of the *Resonant Spectrum Method*. This study will provide a guidance for the requirement of the accuracy of these parameters and therefore help for successfully application of the *Resonant Spectrum Method*.

BIBLIOGRAPHY

[1] V. M. Ristic, "Chapter 5: Piezoelectric bulk wave transducers", *Principles of Acoustic Devices*, Wiley, New York, 1983

[2] K. M. Lakin, G. R. Kline and K. T. McCarron, "Thin film bulk acoustic wave filters for GPS", *1992 Ultrosonics Symposium Proc.*, pp. 471-476.

[3] K. M. Lakin, G. R. Kline and K. T. McCarron, "High-Q microwave acoustic resonators and filters", *IEEE Trans. MTT*, Vol. 41 (12), pp. 2139-2146, 1993

[4] K. M. Lakin, "Development of miniature filters for wireless applications", *IEEE Trans. MTT*, Vol. 43, pp. 2933-2939, 1995

[5]Y. Shibata, N. Kuze, K, Kaya, M. Matsui, M. Kanai and T. Kawai, "Piezoelectric LiNbO3 and LiTaO3 films for SAW device applications", *1996 Ultrasonics Symposium Proc.*, pp. 247-254

[6] S. Fujii, Y. Seki, K, Yoshida, H. Nakahata, K. Higaki, H Kitabayashi and S. Shikata, "Diamond wafer for SAW application", *1997 Ultrasonics Symposium Proc.*, pp. 183-186

[7] Qing-Xin Su, Paul Kirby, Eiju Komuro, Masaaki Imura, Qi Zhang, and Roger Whatmore, "Thin-film bulk acoustic resonators and filters using ZnO and lead–zirconium–titanate thin films", *IEEE Trans. MTT*, Vol. 49 (4), pp.769-778, 2001

[8] R.M Malbon, D. J. Walsh and D.K Winslow, "Zinc-oxide film microwave acoustic transducers", *Appl. Phys. Lett.*, Vol. 10 (1), pp. 9-10, 1967

[9] L. Zuo, M. Sayer and C-K. Jen, "Sol-gel fabricated thick piezoelectric ultrasonic transducers for potential applications in industrial material processes", *1997 Ultrasonics Symposium Proc.*, pp.

[10] A. Schroth, M. Ichiki, J. Akedo, M. Tanaka and R. Maeda, "Properties and application of jet printed piezoelectric PZT film for actuation purposes", *Proc. of the 1997 International Symposium on Micromechatronics and Human Science*, pp. 67 -72

[11] H. P. Lobl, M. Klee, O. Wunnicke, R. Kiewitt, R. Dekker, E. V. Pelt, "Piezoelectric AlN and PCT films for micro-electronic applications", *1999 Ultrasonics Symposium Proc.*, pp. 1031-1036

[12] Jiun-Ting Lee, Neil Little, Thomas Rabson and Marc Robert, "Thin film Lithium Noibate on diamond-coated silicon substrates for surface acoustic wave applications", *1999 Ultrasonics Symposium Proc.*, pp. 269-272

[13] M. Kadota, "Combination of ZnO film and quartz to realize large coupling factor and excellent temperature coefficient for SAW devices", *1997 Ultrasonics Symposium Proc.*, pp. 261-266

[14] T. E. Parker and H. Wichansky, "Temperature-compensated surface-acoustic-wave devices with SiO_2 overlays", *J. App. Phys.*, Vol. 50, pp. 1360-1369, 1979

[15] F. S. Hickernell, H. D. Knuth, R. C. Dablemont and T. S. Hickernell, " The surface acoustic wave propagation characteristics of 64° Y-X $LiNbO_3$ and 36° Y-X $LiTaO_3$ Substrates with thin-film SiO_2", *1995 Ultrasonics Symposium Proc.*, pp. 345-348

[16] K. Yamanouchi, H. Odagawa, T. Kojima, A. Onoe, A. Yoshida and K. Chikuma, "Piezoelectric KnbO3 films for SAW device applications", *Electronics Letters*, Vol. 34 (7), pp. 702-703, 1998

[17] D. Cushman, K. F. Lau, E. M. Garber,K. A. Mai, A. K. Oki, K. W. Kobayashi, "SBAR filter monolithically integrated with HBT amplifier", *1990 Ultrasonics Symposium Proc.*, pp. 519 -524

[18] S.V. Krishnaswamy, J.F. Rosenbaum, S. Howits and R.A.Moore, "Film bulk acoustic wave resonator technology", *1990 Ultrasonics Symposium Proc.*, pp. 529-536

[19] G. Yoon, J. D. Park and H. D. Park, "Characterization of ZnO-based FBAR devices for RF application", *2nd International Conference on Microwave and Millimeter Wave Technology Proceedings*, pp. 192-195, 2000

[20] E. A. Gerber and L. F. Koerner, "Methods of measurement of the parameters of piezoelectric vibrators", *Proc. IRE*, pp. 1731-1739, 1958

[21] "IEEE Standard on Piezoelectricity (ANSI/IEEE Std. 176-1987)", *IEEE Trans. on UFFC*, Vol. 43 (5), 1996.

[22] F. S. Hickernell, "Measurement techniques for evaluating piezoelectric thin films", *1996 Ultrasonics Symposium Proc.*, pp. 235-241

[23] B.S. Naik, J. J. Lutsky, R. Rief and C. D. Sodini, "Electromechanical coupling constant extraction of thin-film piezoelectric materials using a bulk acoustic wave resonator", *IEEE Trans. UFFC*, Vol. 45(1), pp. 257-263, 1998.

[24] A. J. Bahr and I. N. Court, " Determination of the electromechanical coupling coefficient of thin-film Cadmium Sulphide", *J. of Appl. Phys.*, Vol. 39 (6), pp. 2863-2868, 1968

[25] A. H. Meitzler and E. K. Sittig, "Characterization of piezoelectric transducers used in ultrasonic devices about 0.1GHz", *J. of Appl. Phys.*, Vol. 40 (11), pp. 4341-4352, 1969

[26] J. D. N. Cheeke, Y. Zhang, Z. Wang, M. Lukacs, and M. Sayer, "Characterization for piezoelectric films using composite resonators", *1998 Ultrasonics Symposium Proc.*, pp. 1125 -1128

[27] Z. Wang, Y. Zhang, and J.D.N. Cheeke, "Characterization of electromechanical coupling coefficient of piezoelectric film using composite resonators", *IEEE Trans. UFFC*, Vol. 46 (5), pp. 1327-1330, 1999

[28] Y. Zhang, Z. Wang, J.D.N Cheeke and F.S. Hickernell, "Direct characterization of ZnO films in composite resonators with the resonance spectrum method", *Proc. 1999 IEEE Ultrasonic Symposium*, pp. 991-994

[29] Y. Zhang, Z. Wang, and J.D.N. Cheeke, "Simulation of electromechanical coupling coefficient by modified modal frequency spectrum method including the electrode effect", *Ultrasonics*, Vol.38, pp. 114-117, 2000

[30] Y. Zhang, Z. Wang and J. D. N. Cheeke, "Resonant spectrum method to characterize piezoelectric film in composite resonator", submitted to *IEEE Trans. UFFC*.

[31] K. M. Lakin, "Fundamental properties of thin film resonators", *1991 Frequency Control Symposium Proc.*, pp. 201-206

[32] E. K. Sittig, "Effects of bonding and electrode layers on the transmission parameters of piezoelectric transducers used in ultrasonic digital delay lines", *IEEE Trans. Sonics and Ultrasonics*, Vol. 16 (1), pp. 2-10, 1969

[33] E.K. Sittig, "Design and technology of piezoelectric transducers for frequencies above 100 MHz", *Physical Acoustics, Vol. IX*, Edts. W.P. Mason and R.N. Thurston, pp. 221-275, Academic Press, New York, 1972

[34] P-C. Xu, K-E. Lindenschmidt and S. A. Meguid, "A new high frequency analysis of coating using leaky Lamb-waves", *J. Acoust. Soc. Am.*, Vol. 94, pp. 2954-2962, 1993

[35] Z. Wang, C. K. Jen and J. D. N. Cheeke, "Material characterization using leaky Lamb-waves", *1994 IEEE Ultrasonic Symposium Proc.*, pp. 1227-1232

[36] Z. Wang, X. Li and D. N. Ckeeke, "A modified modal frequency spacing method for coating characterization", *J. Acoust. Soc. Am.*, Vol. 104 (5), pp. 3199-3122, 1998

[37] Z. Wang and J. D. N. Cheeke, "Characterizing unpoled piezoelectric ceramic films by Lamb waves", *IEEE Trans. UFFC*, Vol. 46 (5), pp. 1094-1100, 1999

[38] F. S. Hickernell, Private communication

[39] B. A. Auld, "Appendix 2: Properties of materials", *Acoustic fields and waves in solids*, Vol. 1, Wiley, New York, 1973

[40] J. Larson III, R. Ruby, P. Bradley and Y. Oshmyansky, "A BAW Antenna Duplexer for the 1900 MHz PCS Band", *1999 Ultrasonics Symposium Proc.*, pp.887-890

[41] D. Figueredo, R. Ruby, P. Bradley, E. Ong, D. Feld, J. Phillibet, W. Lim, F. Babbitt, G. Singh, R. Silva, J. Larson, Y. Oshmyansky, S. Wartenberg, R. Waugh, L. Ooi, R. Liew and J. Choy, "Manufacturing and Performance Considerations for Thin Film Bulk Acoustic Resonator (FBAR) USPCS band duplexers", Agilent Technology internal report

[42] O. Ikata, T. Miyashita, T. Matsuda and Y. Satoh, " Development of low-loss band-pass filters using SAW resonator for portable telephones", *1992 IEEE Ultrasonics Symposium Proc.*, pp. 111~115